

FINAL REPORT

Evaluation of Corrosion Inhibiting Materials Applied by Impregnation (Pressure Injection) Methods to Prevent Corrosion of Post-Tensioned Tendons

FDOT Contract Number: BDV25-977-35

USF Contract Number: 2104 1265 00

Continuing FDOT Project Manager: Matthew Duncan

Initiating FDOT Project Manager: Ivan Lasa (Retired)

Continuing PI: Christopher L. Alexander, University of South Florida, Tampa, FL.

Initiating PI: Alberto Sagüés (Retired).

Report Prepared by:

Justin Silnutzer

Hesham Mraied

Gray Mullins

Alberto Sagüés

Christopher L. Alexander

Department of Civil and Environmental Engineering



**UNIVERSITY OF
SOUTH FLORIDA**

Tampa, FL 33620

July 2020

DISCLAIMER

The opinions, findings, and conclusions expressed in this publication are those of the authors and not necessarily those of the Florida Department of Transportation.

The contents of this report reflect the views of the authors, who are responsible for the facts and the accuracy of the information presented herein. This document is disseminated under the sponsorship of the Department of Transportation's University Transportation Centers Program, in the interest of information exchange. The U.S. Government assumes no liability of the contents or use thereof.

UNIVERSAL CONVERSION TABLE

SI* (MODERN METRIC) CONVERSION FACTORS									
APPROXIMATE CONVERSIONS TO SI UNITS					APPROXIMATE CONVERSIONS FROM SI UNITS				
SYMBOL	WHEN YOU KNOW	MULTIPLY BY	TO FIND	SYMBOL	SYMBOL	WHEN YOU KNOW	MULTIPLY BY	TO FIND	SYMBOL
LENGTH					LENGTH				
in	inches	25.4	millimeters	mm	mm	millimeters	0.039	inches	in
ft	feet	0.305	meters	m	m	meters	3.28	feet	ft
yd	yards	0.914	meters	m	m	meters	1.09	yards	yd
mi	miles	1.61	kilometers	km	km	kilometers	0.621	miles	mi
AREA					AREA				
in ²	square inches	645.2	square millimeters	mm ²	mm ²	square millimeters	0.0016	square inches	in ²
ft ²	square feet	0.093	square meters	m ²	m ²	square meters	10.764	square feet	ft ²
yd ²	square yard	0.836	square meters	m ²	m ²	square meters	1.195	square yards	yd ²
ac	acres	0.405	hectares	ha	ha	hectares	2.47	acres	ac
mi ²	square miles	2.59	square kilometers	km ²	km ²	square kilometers	0.386	square miles	mi ²
VOLUME					VOLUME				
fl oz	fluid ounces	29.57	milliliters	mL	mL	milliliters	0.034	fluid ounces	fl oz
gal	gallons	3.785	liters	L	L	liters	0.264	gallons	gal
ft ³	cubic feet	0.028	cubic meters	m ³	m ³	cubic meters	35.314	cubic feet	ft ³
yd ³	cubic yards	0.765	cubic meters	m ³	m ³	cubic meters	1.307	cubic yards	yd ³
NOTE: volumes greater than 1000 L shall be shown in m ³									
MASS					MASS				
oz	ounces	28.35	grams	g	g	grams	0.035	ounces	oz
lb	pounds	0.454	kilograms	kg	kg	kilograms	2.202	pounds	lb
T	short tons (2000 lb)	0.907	megagrams (or "metric ton")	Mg (or "t")	Mg (or "t")	megagrams (or "metric ton")	1.103	short tons (2000 lb)	T
TEMPERATURE (exact degrees)					TEMPERATURE (exact degrees)				
°F	Fahrenheit	5 (F-32)/9 or (F-32)/1.8	Celsius	°C	°C	Celsius	1.8C+32	Fahrenheit	°F
ILLUMINATION					ILLUMINATION				
fc	foot-candles	10.76	lux	lx	lx	lux	0.0929	foot-candles	fc
fl	foot-Lamberts	3.426	candela/m ²	cd/m ²	cd/m ²	candela/m ²	0.2919	foot-Lamberts	fl
FORCE and PRESSURE or STRESS					FORCE and PRESSURE or STRESS				
lbf	poundforce	4.45	newtons	N	N	newtons	0.225	poundforce	lbf
lbf/in ²	poundforce per square inch	6.89	kilopascals	kPa	kPa	kilopascals	0.145	poundforce per square inch	lbf/in ²

*SI is the symbol for the International System of Units. Appropriate rounding should be made to comply with Section 4 of ASTM E380.

(Revised March 2003)

TECHNICAL REPORT DOCUMENTATION PAGE

1. Report No.	2. Government Accession No.	3. Recipient's Catalog No.	
4. Title and Subtitle: Evaluation of Corrosion Inhibiting Materials Applied by Impregnation (Pressure Injection) Methods to Prevent Corrosion of Post-Tensioned Tendons		Report Date: August, 2020	
		Performing Organization Code	
Author(s): Justin Silnutzer, Hesham Mraied, Gray Mullins, Alberto Sagüés, Christopher L. Alexander		Performing Organization Report No.	
Performing Organization Name and Address: Department of Civil and Environmental Engineering University of South Florida (USF) Tampa, FL 33620		Work Unit No. (TR AIS)	
		Contract or Grant No. BDV25-977-35	
Sponsoring Agency Name and Address Florida Department of Transportation 605 Suwannee St. MS 30 Tallahassee, Florida 32399 (850)414-4615		Type of Report and Period Covered Draft Final Report 12/15/16 – 9/30/20	
		Sponsoring Agency Code	
Supplementary Notes			
<p>Abstract: Tendon impregnation has been proposed as a potential method to prevent and arrest corrosion in post-tensioned tendons. This technology uses the interstitial spaces between the tendon wires to inject a corrosion-mitigating fluid into the tendon. This project was performed to evaluate the long-term effectiveness and the service life of the material(s) used for impregnation of tendons and identify other materials that could produce better end results. In addition, the effects of the impregnation methods on the physical characteristics of the tendon system were evaluated to determine applicability to bonded tendons. Alternative fluids and Vector Corrosion Technologies' proprietary fluid were tested. It was found that the alternative fluid provided temporary corrosion mitigation (several months) prior to requiring re-impregnation. The proprietary fluid was effective in arresting corrosion for at least twice as long, provided adequate application, as indicated by fluid removed at the end of the targeted application. Tendon failure forecasts showed that the proprietary fluid has the potential to extend tendon service life if fluid application is adequate and assuming reimpregnation is not required beyond the testing period of this work. The corrosion-mitigating capabilities may however be compromised by chloride-containing water intrusion. Additionally, pullout testing showed that the proprietary fluid causes a substantial reduction in the steel-to-grout bond strength, suggesting that the proprietary fluid would not be suitable for bonded tendon application in which load transfer is expected.</p>			
Key Words: bond strength; electrochemical testing; damage forecast		Distribution Statement: No restrictions	
Security Classif. (of this report) Unclassified.	Security Classif. (of this page) Unclassified.	No. of Pages: 138	Price

ACKNOWLEDGEMENTS

The authors acknowledge David Whitmore and Martin Beaudette of Vector Corrosion Technologies who provided the proprietary fluid and performed the proprietary fluid impregnation of the mock-up post-tensioned tendons and pile specimens.

EXECUTIVE SUMMARY

Structures incorporating post-tensioned tendons (PTT) are expected to have a service life of many decades but often need rehabilitation within several years of service due to corrosion. Corrosion in many cases has occurred in regions of grout deficiencies in the form of voids formed by bleed water accumulation and subsequent reabsorption or evaporation through incomplete anchorage sealing. Other possible causes of corrosion include intrusion of external chloride and water through anchorages or defects in the high-density polyethylene (HDPE) and possible adverse galvanic coupling between anchorage components and the strand. As a result, a corrosion control method, marketed by Vector Corrosion Technologies, Inc. (Vector), under the name Post-Tech® PTI Impregnation System, has emerged recently. The impregnation material is pressure-injected into the tendon duct through either an intermediate port or anchor position and propagates along the entire length of the PTT, ultimately saturating voids and grout deficiencies while creating a corrosion-protective barrier on the surface of the reinforcement. The impregnation material is intended to provide cost-effective protection with otherwise minimal disruption. This project was conducted to evaluate the long-term effectiveness and the service life of the material(s) used for impregnation of tendons and to evaluate the effects of the impregnation methods on the physical characteristics of the tendon system to determine applicability to bonded tendons.

Experiments were performed on mock-up PTT specimens constructed with either sound grout or grout with deficiencies in the form of admixed sodium chloride or an excessive water-to-grout mix ratio. Selected specimens were impregnated with either the Vector proprietary fluid (VPF) or an alternative fluid penetrant with a low viscosity. Electrochemical testing of these mock-up specimens yielded good initial prognosis for successful corrosion abatement by impregnating post-tensioned tendons with the impregnation materials delivered via the interwire channels. However, the effective service period for the alternative fluid was only several months while the service period of the VPF is at least twice as much. The experimental results of an alternative fluid suggested that the initial corrosion protection mechanism associated with impregnation was activation control of the cathodic component of the corrosion reaction. Additional control by polarization of the anodic component was indicated to take place as well as time proceeded. Direct testing of the VPF indicated that the corrosion inhibiting mechanism is the formation of a barrier coating that reduces the rate of both anodic and cathodic reactions.

Autopsies were performed on selected mock-up PTT specimens injected with the VPF to directly assess the distribution of fluid and its ability to prevent further corrosion damage. A uniform coating of the impregnation fluid was observed on the steel strands of the sound grouted specimens, indicating effective delivery of the proprietary fluid in the interstitial space between the steel and the grout. For PTT specimens constructed with admixed chlorides in the grout, the impregnation fluid was unevenly distributed along the steel strands and preferentially coated regions of minimal corrosion products. Despite this, 3D corrosion damage analysis showed that the proprietary fluid resulted in a substantial reduction (35%–70%) in the maximum corrosion penetration compared to untreated tendons. This quantitative information was used to calculate tendon failure forecasts that estimate that tendon impregnation has the potential to extend the time until the first strand failure by almost a factor of 3 when adequately applied and assuming long-term effectiveness. Possible limitations that may compromise the performance of the proprietary fluid include grout voids and chloride containing water intrusion.

In the process of evaluating the effect of pressurized penetrants on strand-to-grout bond, numerous specimens were prepared using ½-in Grade 270, 7-wire strands grouted into cored concrete ducts in prestressed concrete pile segments. The bonded length (12 in) was selected such that the strand-grout bond was tested to failure without premature strand breakage. Pullout tests of both impregnated and unimpregnated specimens were conducted. Strands treated with alternative fluids (WD-40 or PB Blaster) after the grout was fully cured indicated no discernible effect from the presence or use of either penetrant material when compared to unimpregnated samples. However, tendon samples impregnated with the VPF product showed marked reductions in pullout capacity. While this may have less effect on grouted externally post-tensioned tendon applications, it can have dire consequences for internal tendon applications where load transfer between the strand and surrounding grout and concrete is expected.

In summary, the Vector proprietary fluid shows promising corrosion control capabilities upon implementation and after several months of service if adequately applied. Appropriate delivery of the impregnation fluid relied on adequate interwire space which was facilitated by multiple steel strands and lack of pre-existing corrosion products. Lastly, VPF notably reduced the bond strength of the steel and the surrounding grout compared to alternative impregnation materials (WD-40 and PB Blaster).

TABLE OF CONTENTS

DISCLAIMER	II
UNIVERSAL CONVERSION TABLE.....	III
TECHNICAL REPORT DOCUMENTATION PAGE.....	IV
ACKNOWLEDGEMENTS	V
EXECUTIVE SUMMARY.....	VI
LIST OF FIGURES.....	X
LIST OF TABLES.....	XV
CHAPTER 1 INTRODUCTION.....	1
1.1 Project Objectives and Tasks.....	2
CHAPTER 2 LITERATURE REVIEW.....	4
2.1 Summary.....	13
CHAPTER 3 EXPOSURE AND ELECTROCHEMICAL TESTING	15
3.1 Section A: Alternative Fluid Testing	15
3.1.1 Results and Discussion.....	17
3.1.2 Findings and Implications	26
3.2 Section B: Vector Proprietary Fluid	27
3.2.1 Results and Discussion.....	31
3.2.1.1 1ft Tendons	31
3.2.1.2 3ft Tendons	33
3.2.2 Findings AND Implications.....	36
3.3 Section C: Predictive corrosion Modeling.....	37
3.3.1 Data Aquisition.....	37
3.3.2 Results and discussion	41
3.3.3 Findings AND Implications.....	48
CHAPTER 4 BOND STRENGTH TESTING.....	49
4.1 Section A: Alternative Fluids	49
4.1.1 Concrete Specimen Testing.....	49
4.1.1.1 Construction of Concrete Specimen 1.....	49
4.1.1.2 Construction of Concrete Specimen 2.....	52
4.1.1.3 Construction of Concrete Specimens 3-8.....	55
4.1.1.4 Alternative Fluid Injection for Concrete Specimens 4-8.....	56
4.1.1.5 Construction of Concrete Specimen 9.....	56
4.1.1.6 Alternative Fluid Injection for Concrete Specimen 9.....	57
4.1.1.7 Construction of Concrete Specimens 10-24.....	59
4.1.1.8 Alternative Fluid Injection for Concrete Specimens 15-19.....	60
4.1.1.9 PB Blaster injection for concrete Specimens 20-24.....	62
4.1.2 Results and Discussion.....	63
4.1.2.1 Pullout test results for Concrete Specimens 1-5.....	64
4.1.2.2 Pullout test results for Concrete Specimens 6-24.....	66
4.1.3 Findings and Implications	82
4.2 Section B: Vector Proprietary Fluid	88
4.2.1 Results and Discussion.....	93
4.2.2 Summary	95
CHAPTER 5 POSSIBLE LIMITATIONS AND SERVICE LIFE FORECASTING	96

5.1	Degradation mechanisms	96
5.1.1	Results and Discussion.....	97
5.1.2	Findings and implications.....	100
5.2	Autopsy and Failure Forecast	102
5.2.1	Results and discussion	106
5.2.2	Finding and implications	108
5.3	Failure forecasting.....	110
5.3.1	Summary	113
CHAPTER 6 CONCLUSIONS AND RECOMMENDATIONS		114
6.1	Alternative Fluid Performance	114
6.2	vector proprietary Fluid performance	114
6.3	modeling - Influence of parameters on corrosion rates Model	115
6.4	recommendations.....	115
REFERENCES.....		116
APPENDIX.....		123

LIST OF FIGURES

Figure 2-1: Schematic of application of impregnation fluid ⁴⁶	6
Figure 2-2: Corrosion protection effect of impregnation fluid applied on a steel plate exposed to salt spray test. Compare with untreated upper left portion. ⁴⁷	7
Figure 2-3: Impregnation fluid reported to successfully displacing moisture from a tendon end opposite to the injection end. ⁴⁷	8
Figure 2-4: Impregnation material seep out of the far end of a >250ft long tendon. ⁴⁷	9
Figure 2-5: Projected time required for the impregnation fluid to seep out of the far end of 256ft tendon.....	11
Figure 2-6: Projected time for the impregnation fluid to fill a void present at the indicated distance from the injection point.....	12
Figure 3-1: Sample Preparation Schematic.....	16
Figure 3-2: Sample of Electrochemical Testing	16
Figure 3-3: Evolution of grout resistivity. Stages designated by Roman numerals. Results from 5 replicate specimens.	18
Figure 3-4: Evolution of EOC. Results from 3 replicate specimens.....	19
Figure 3-5: Typical evolution of EIS behavior for (a) as-cast, (b) during corrosion, and (c) following impregnation. The last figures in the legends indicate days since casting.	20
Figure 3-6: The evolution of magnitudes derived from EIS tests (a) R_s (b) R_p (c) Y_0 and (d) n as a function of time. The legends indicate replicate specimen designations.....	21
Figure 3-7: Evolution of (a) i_{corr} from EIS and (b) grout resistivity measured by EIS and FWAP	22
Figure 3-8: Evolution of (a) PD curves – typical. Solid lines: as-cast; Dotted lines: after chloride exposure and before impregnation; Dashed lines: after impregnation and (b) i_{corr} – all results. ..	23
Figure 3-9: PD curves before and after IR-drop correction	24
Figure 3-10: Relationship between Eoc and i_{corr}	25
Figure 3-11: Long-term evolution of corrosion rate in control and impregnated tendons.	26
Figure 3-12: The construct of a 3ft tendon after the curing process	27
Figure 3-13: The Voigt electrical equivalent circuit model used in the regression software.	29
Figure 3-14: The calibration curve of polarization resistances multiplied by the relative grout conductivities	31
Figure 3-15: Corrosion rate as a function of time prior to and following impregnation of 1 ft tendons: a) Chloride-free; b) Chloride-contaminated	32
Figure 3-16: The ohmic resistance of the grout contained within the 1ft tendons before and after impregnation: a) Chloride-free; b) Chloride-contaminated	33
Figure 3-17: Corrosion rate as a function of time prior to and following impregnation of 3 ft tendons: a) Chloride-free; b) Chloride-contaminated	34
Figure 3-18: The ohmic resistance of the grout contained within the 31ft tendons before and after impregnation: a) Chloride-free; b) Chloride-contaminated	35
Figure 3-19: Results over time for a 3ft tendon made with a high water to cement ratio: a) Corrosion rate; b) Ohmic resistance	36
Figure 3-20: Concrete column schematic diagram	37
Figure 3-21: Grout resistivity effect on oxygen concentration maps after 100 days for (a-base) $\rho=1000 \Omega.m$, (b) $\rho=500 \Omega.m$, and (c) $\rho=5000 \Omega.m$	42

Figure 3-22: Oxygen diffusivity effect on oxygen concentration maps after 100 days for (a-base) $D_o=1E-8$ m ² /s, (b) $D_o=1E-9$ m ² /s, and (c) $D_o=1E-10$ m ² /s.....	42
Figure 3-23: Cathodic exchange current density effect on oxygen concentration maps after 100 days for (a-base) $i_{oc}=3E-5$ A/m ² , (b) $i_{oc}=3E-5$ A/m ² , and (c) $i_{oc}=3E-5$ A/m ²	43
Figure 3-24: Anodic exchange current density effect on oxygen concentration maps after 100 days for (a-base) $i_{oc}=3E-4$ A/m ² , (b) $i_{oc}=3E-5$ A/m ² , (c) $i_{oa}=3E-6$ A/m ²	43
Figure 3-25: Local radius loss at day 40 for varying (a) i_{oc} , (b) i_{oa} , and (c) both i_{oc} and i_{oa} . The green profile corresponds to baseline conditions. All variations are for an active zone of 20% of the strand length.....	45
Figure 3-26: Local radius loss at day 40 for varying (a) grout resistivity, (b) oxygen diffusivity. The green profile corresponds to baseline conditions. All variations are for an active zone of 20% of the strand length.....	46
Figure 3-27: Local radius loss at day 40 for varying active anodic size. Baseline conditions. 100% corresponds to the entire central 5-cm long region being active.	47
Figure 3-28: (a) Evolution with time of oxygen concentration and nominal radius loss averaged over the anode. (b) Decay of percentage of remaining nominal strand cross sectional area with and without, oxygen replenishment. Calculations for base condition anode on 20% of the strand length.	48
Figure 4-1: Cutting 14-inch square pile for concrete specimens and coring simulate duct corridors into 1ft concrete segments	49
Figure 4-2: Concrete specimen 1 completely setup before grout installation	50
Figure 4-3: Feeding flexible hose into tendon for water injection (top left); Mixing grout in 4x8 concrete cylinder (top right); Pouring grout into funnel to prevent grout spillage (middle left); Removing steel brick to place concrete specimen horizontal and injecting water into tendon (middle right); Extracting flexible hose from tendon (bottom left); Water wicking out of the strand from water injection (bottom right).	51
Figure 4-4: Cutting of the back of the duct extensions (left); cutting off part of the elbow for clearance (right).	52
Figure 4-5: Tendon 1 with no water injection (top left); Tendon 2 with 10cc water injection (top right); Tendon 3 with 25cc water injection (bottom left); Tendon 4 with 50cc water injection (bottom right).	52
Figure 4-6: Predrilling holes into the concrete face (top left); Silicon applied to the bottom of the metal flanges (top right); Anchoring the metal flanges to the concrete face (bottom left); All flanges anchored and silicon placed around the flanges (right).	53
Figure 4-7: Concrete specimen 2 back (left) and front (right).....	53
Figure 4-8: Water filled syringe with flexible hose in the tendon (left); Back of the specimen with the standpipes and adapters (right).	54
Figure 4-9: Removal of PVC fittings leaving grouted strands exposed.	55
Figure 4-10: Specimen pressurized with WD-40 (left); WD-40 traveling along strand (right). ..	56
Figure 4-11: Concrete Specimen 9 before grout installation.	57
Figure 4-12: Concrete specimen 9 prepared for WD-40 injection for 24-hrs. Concrete specimen 9 with PVC manifold (lower left); specimen 9 WD-40 injection (lower right).....	58
Figure 4-13: Strand coated in WD-40 (left) and extracted strand after WD-40 injection (right). ..	58
Figure 4-14: Concrete specimens 10-24.	59
Figure 4-15: The property of thixotropic grout.....	60

Figure 4-16: Concrete Specimen 15 before WD-40 injection.	61
Figure 4-17: Manifold attached to the back of the specimen (left); Clear tubing filled with WD-40 (right).	62
Figure 4-18: Concrete Specimen 24 after 24-hrs of PB Blaster injection.	62
Figure 4-19: Pullout test setup for concrete specimen 9.	63
Figure 4-20: Results from specimen 1 load (lbs) vs. time (sec).	65
Figure 4-21: Results from specimen 2 load (lbs) vs. time (sec).	65
Figure 4-22: Results from specimen 3 load (lbs) vs. time (sec).	65
Figure 4-23: Results from specimen 4 load (lbs) vs. time (sec).	66
Figure 4-24: Results from specimen 5 load (lbs) vs. time (sec).	66
Figure 4-25: Results from specimen 6 load (lbs) vs. time (sec).	69
Figure 4-26: Results from specimen 7 load (lbs) vs. time (sec).	69
Figure 4-27: Results from specimen 8 load (lbs) vs. time (sec).	70
Figure 4-28: Results from specimen 9 load (lbs) vs. time (sec).	70
Figure 4-29: Results from specimen 10 load (lbs) vs. time (sec).	71
Figure 4-30: Results from specimen 11 load (lbs) vs. time (sec).	71
Figure 4-31: Results from specimen 12 load (lbs) vs. time (sec).	71
Figure 4-32: Results from specimen 13 load (lbs) vs. time (sec).	71
Figure 4-33: Results from specimen 14 load (lbs) vs. time (sec).	72
Figure 4-34: Results from specimen 15 load (lbs) vs. time (sec).	72
Figure 4-35: Results from specimen 16 load (lbs) vs. time (sec).	72
Figure 4-36: Results from specimen 17 load (lbs) vs. time (sec).	73
Figure 4-37: Results from specimen 18 load (lbs) vs. time (sec).	73
Figure 4-38: Results from specimen 19 load (lbs) vs. time (sec).	73
Figure 4-39: Results from specimen 20 load (lbs) vs. time (sec).	74
Figure 4-40: Results from specimen 21 load (lbs) vs. time (sec).	74
Figure 4-41: Results from specimen 22 load (lbs) vs. time (sec).	74
Figure 4-42: Results from specimen 23 load (lbs) vs. time (sec).	75
Figure 4-43: Results from specimen 24 load (lbs) vs. time (sec).	75
Figure 4-44: Rubber plug installed into the front face of concrete specimen 1 (left); water injection into vacated duct (right).	76
Figure 4-45: Full ½-in strand (left); trimmed version of the ½-in strand to calculate the interstitial spaces (right).	80
Figure 4-46: Results from pullout capacity (lbs) vs. void volume (cc)	83
Figure 4-47: Explanation of data scatter shown by the effects of void volume (workmanship). .	84
Figure 4-48: Sample 1-1 (none) lowest void perfect grout distribution.	85
Figure 4-49: Sample 1-2 (none) 40-cc grout on only one side 2061-lb pullout capacity.	85
Figure 4-50: Sample 2-2 fully bonded strand, highest pullout load, 20-cc void volume.	85
Figure 4-51: Sample 12-2 highest void volume, partial bond near bottom, 8729-lb pullout capacity.	85
Figure 4-52: Sample 17-2 (WD-40) full bond where strand slipped free.	85
Figure 4-53: Sample 15-4 (WD-40) lowest bond 73-cc void volume, partial bond near bottom.	86
Figure 4-54: Penetration rates for the two penetrants (time / 12-in).	86
Figure 4-55: Pile segments complete with pipe flanges, barbed hose fittings, and high-pressure hoses to simulate a longer length duct.	88

Figure 4-56: Grouting to be performed on all four duct assemblies at once via looped grout hoses on each end.	89
Figure 4-57: Grouting: grout plant (top left); grout hose connected to bottom duct, strand 3 (top right); grout in bottom two ducts but not yet in top two (bottom left); grout exiting four-duct system (bottom right).	90
Figure 4-58: Removal of hoses (top); breaking grout off the strands (bottom) before installing new hoses and valves on both ends of the entire 8 specimen assembly.	91
Figure 4-59: Connecting hoses removed showing residual impregnation product.	92
Figure 4-60: Strands extending from specimens (left); flush cut on backside (right).	92
Figure 4-61: Pullout testing (left); flange displaced upward 2in (right)	93
Figure 4-62: Pullout resistance for concrete specimen five (upper left), six (upper right), seven (lower left), and eight (lower right).	94
Figure 5-1: A schematic of the experiment for EIS testing on king strands.	96
Figure 5-2: Electrochemical impedance in Nyquist format of king strand coated in 3 layers of the impregnation fluid: a) saturated calcium hydroxide, pH ~12.5; b) Calcium hydroxide with chlorides, pH~12.3.	98
Figure 5-3: a: Corrosion rate data calculated for the king strands with no impregnation material, 1 layer of impregnation material, and 3 layers of impregnation material immersed in SatCaOH and 0.6M NaCl in equal volumetric amounts; b: king strands immersed in Sat.CaOH and NaCl. The non-impregnated king strand is on the left, the 1-layer coated wire is in the middle, and the 3-layer coted wire is on the right.	99
Figure 5-4: Potentiodynamic scan obtained at a scan rate of 0.167 mV/s of 3-layer coated wire (green) and a bare wire (yellow) immersed in a saturated calcium hydroxide and NaCl solution.	99
Figure 5-5: The surface topography of steel after immersion in a 0.6M NaCl solution a) bare wire for 24 hours; b) 3-layer coated wire for 48 hours.	100
Figure 5-6: The autopsy of the 3ft normal tendon showing the grout surface after impregnation.	102
Figure 5-7: The outer surface of the impregnated grout showing the presence of impregnation material in an unsaturated amount.	103
Figure 5-8: Images of the interior pores and voids contained in the 3ft chloride contaminated grout with impregnation material.	104
Figure 5-9: The reinforcement extracted from the 1ft normal tendons. The reinforcement on the top is from the control group and the reinforcement on the bottom is from the impregnated group.	105
Figure 5-10: An image of the reinforcement extracted for the 1ft chloride contaminated tendons. The top image is the control tendon and the bottom image is the impregnated tendon.	105
Figure 5-11: Steel strands after corrosion product removal extracted from 1 ft tendons: a) not impregnated; b) impregnated.	106
Figure 5-12: Steel strands after corrosion product removal extracted from 3 ft tendons: a) not impregnated; b) impregnated.	106
Figure 5-13: The maximum penetration calculation performed on a strand extracted from the 3ft chloride contaminated tendon without impregnation material. The image at the top left is the surface topography, the image at the top right contains a blue line which represent the cross-section where depth was calculated, and the bottom image contains the maximum penetration.	107

Figure 5-14: Average and maximum corrosion rates of strands extracted from 1ft and 3ft chloride contaminated tendons with and without impregnation. 108

Figure 5-15: Steel strand wire cross section showing corrosion damage morphology..... 110

Figure 5-16: Corrosion rate distribution example based upon a sample size of 21,384 with a mean of 110.95 and standard deviation of 128.8. Values correspond to the 3ft tendon without impregnation 111

Figure 5-17: Wire failure percentage as a function of time obtained from corrosion data presented in Figure 5-14. Values shown in red correspond to time in which 20% of the wires have failed. 112

Figure 5-18: Strand failure percentage as a function of time obtained from corrosion data presented in Figure 5-14..... 112

LIST OF TABLES

Table 3-1: Grouting conditions for all of the laboratory specimens	28
Table 3-2: Parameters/Variables with Descriptions and Values.....	39
Table 3-3: List of Scenarios Modeled and Parameters Used.....	40
Table 4-1: Concrete Specimen 1 material weights and water injections with ½-in strands.	50
Table 4-2: Concrete Specimen 2 material weights and water injections with ½-in strands.	54
Table 4-3: Concrete Specimen 3 material weights and water injections with ½-in strands.	55
Table 4-4: Concrete Specimen 4 material weights and water injections with ½-in strands.	55
Table 4-5: Concrete Specimen 5 material weights and water injections with ½-in strands.	55
Table 4-6: Concrete Specimen 6-8 material weights and water injections with ½-in strands.....	56
Table 4-7: Concrete Specimen 9 material weights and water injections with ½-in strands.	57
Table 4-8: Concrete Specimen 10-24 material weights and water injections with ½-in strands..	60
Table 4-9: Pullout loads for concrete specimens 1-5.....	64
Table 4-10: Pullout load for concrete specimens 6 to 24.....	66
Table 4-11: Pullout capacity statistics for impregnated and un-impregnated specimens.	75
Table 4-12: Measured and calculated values for true void in the tendons specimens 1-24.....	76
Table 4-13: Concrete specimen 15-19 oiled with WD-40 at 10-psi.	80
Table 4-14: Concrete specimen 20-24 oiled with PB Blaster at 10-psi.....	81
Table 4-15: Variations in average capacity for different grouting and impregnation conditions.	82
Table 4-16: Peak pullout force and the percent reduction compared to the control.	94
Table 5-1: The grouping of the king strands for testing	97

CHAPTER 1 INTRODUCTION

Hundreds of FDOT bridges use tendons made of high strength steel (ultimate tensile strength of 1.86 GPa (270 ksi)), holding the structure together allowing the use of longer spans with less deflection, thinner sections, heavier load capacities, shorter construction periods, and ultimately reducing the cost of construction when compared to the conventional reinforced structures¹. In external tendons, the steel is in the form of multiple (e.g., ≥ 19) seven-wire strands placed inside HDPE ducts, which prevent the intrusion of water and aggressive chemicals, filled with chloride-free cement grout, which protects the steel from corrosion by maintaining an alkaline environment, hence promoting steel passivation. The grout transfers some of the forces between the strand and the anchorage in case of strand damage or loosening. Variations of that situation exist in internal tendons as well¹.

While grouting technology is usually reliable, severe corrosion distress and even complete failure of PTT has been identified overseas starting in 1980². In Florida, corrosion damage instances were first noted at the Niles Channel Bridge in 1999, followed by Mid Bay Bridge in 2000 and Sunshine Skyway Bridge in 2002³⁻⁷. Comparable situations or deficiencies potentially leading to failure were found elsewhere around that time, including the Sidney Lanier cable-stayed bridge in Georgia, in the Boston Central Artery structures, and in the Varina-Enon Bridge in Virginia⁸⁻¹⁰. The observed failures were attributed to local grout deficiencies in the form of voids due to bleed water accumulation during grouting at the high points of the tendon and subsequent reabsorption by the grout or evaporation through incomplete anchorage sealing, intrusion of external chloride and water through anchorages or defects in the HDPE, possibly aggravated by carbonation of the grout and subsequent alkalinity decrease, as well as possible adverse galvanic coupling between anchorage components and the strand. Investigations leading to that understanding have been discussed and widely reported elsewhere^{3-5, 7-13} and will not be addressed further in this report.

As a result of the aforementioned incidents and investigation of PTT, practice for new structures was modified for greater corrosion control, including development of and specification of the use of pre-packed low-bleed grout materials^{4,8-9,14}. Despite those improvements, corrosion failures were found to take place in a Florida bridge after only eight years of service in a bridge constructed using the new specifications¹⁵⁻¹⁸. Examinations of those new instances revealed grout deficiencies in the form of regions with variously porous, chalky, or soft grouts, some with high moisture content. Although pore solution pH was found to be high, high sulfate concentrations were identified as well. The corrosion mechanism itself for this new type of incident is still not sufficiently known, which is a concern because comparable PTT grout deficiencies were found in other bridges being constructed elsewhere¹⁹. A separate issue, affecting one of the improved tendon grout formulations, was the discovery of unintended chloride ion contamination in some batches of the bagged grout material that was used in various PTT construction projects to an extent that was difficult to assess after the fact²⁰. That finding raises concern about the possibility of premature corrosion developing in the future in other structures.

The historical and more recent findings noted above highlight the present need for effective control of corrosion in PTT systems. Future need for corrosion control is apparent as well, and damage predictive models are already being developed to quantify the need for corrosion control management^{13,21-22}. Immediate repair of any tendons found to be undergoing corrosion is essential as these are critical structural components where the integrity of the bridges depends on the large tensile load concentration by the tendon¹. Advanced corrosion

damage to the extent that one or more strands have been lost will normally require replacement of the entire tendon. However, moderate corrosion damage, or indications of grout deficiencies that have not yet translated into strand corrosion, may be amenable to repair to stop or prevent corrosion development. Such repair could be feasible in some limited, relatively accessible places as immediately within the anchor. However, topical repairs elsewhere by traditional methods may involve extensive intrusive treatments, which are likely impractical or not cost effective compared with tendon replacement. Alternative corrosion control procedures are highly desirable.

A potential corrosion control alternative, marketed by Vector Corrosion Technologies, Inc. under the name Post-Tech® PTI Impregnation System²³ has emerged recently, based on tendon impregnation with a proprietary fluid. The fluid comprises a hydrocarbon and silicon-based material that's purpose is to impregnate and saturate the surrounding grout within a duct. Once the tendon is impregnated, the impregnation material forms a protective film on the strands that is designed to mitigate corrosion. Impregnation is started at a convenient injection point at the anchor or at intermediate positions. The fluid propagates along the entire length and is intended to provide cost-effective protection with otherwise minimal disruption. The technology has been adopted by FDOT as the current method available for corrosion control under circumstances that do not require tendon replacement. However, the long-term effectiveness and whether the fluid has any influence on the physical characteristics of the tendon system is unclear. Therefore, the project objectives and tasks are outlined as follows:

1.1 PROJECT OBJECTIVES AND TASKS

- a) To evaluate the long-term effectiveness and the service life of the material(s) used for impregnation of tendons and identify other materials that could produce better end results.
- b) Evaluate the effects of the impregnation methods on the physical characteristics of the tendon system to determine applicability to bonded tendons.

Task 1: Literature Review

Task 2: Exposure and Electrochemical Testing:

- a) Conduct exposure and electrochemical testing to characterize the ability of the proprietary and other identified alternative tendon impregnation material(s) to prevent or delay the onset of corrosion on new and in-service tendons using proper size laboratory specimen of impregnated tendons.
- b) Evaluate the ability of the tendon impregnation material(s) to arrest already existing corrosion of in-service tendons.

Task 3: Physical Property Testing:

- a) This task shall identify the effects of the impregnation material on the physical properties of the tendon system, and its suitability for use on internal and external tendon systems. Evaluate the physical characteristics of the impregnation material(s) as needed to make the material injectable including the effect of the material regarding the bond of the strand to surrounding protective grout.

Task 4: Service Life Determination:

- a) Conduct laboratory experimentation to determine the effective service period of the proprietary and identified alternative tendon impregnation material(s) and the degradation mechanisms. Based on the results, identify the effects and procedures for future re-impregnation on tendons should this be necessary to ensure the service life of the tendons.

The progression of the report will be sectioned into chapters which will address each task as listed above.

CHAPTER 2 LITERATURE REVIEW

The impregnation system introduced above relies primarily on the injection of a corrosion control fluid via the interstitial spaces between the wires of a tendon's strands. A thorough review of the existing literature did not reveal any directly comparable system of injection for PTT corrosion protection. However, some systems that treat the internal condition of tendons to mitigate corrosion and influence the bond properties were identified and are described next.

Because the system to be investigated relies in part on interactions with the hardened grout in the tendon, it is worthwhile to mention the application of similar products albeit used primarily on freely exposed reinforced concrete. There the ingress of water, chloride ions and other aggressive species into reinforced structures can be limited by the application of concrete sealers, which can be classified into surface-penetrating and crack sealers²⁴. Surface-penetrating sealers, typically silanes, siloxanes and silicates, prevent the ingress of water and chloride ions into the concrete matrix by decreasing capillary action near the surface²⁵. Those agents wet the surface of the concrete and penetrate into pores near the surface, thus resulting in pore plugging and limiting the penetration of water and chloride ions into the structure interior. Silicates react with some of the components of the concrete to form precipitates to seal the pores²⁶. Crack sealers such as High Molecular Weight Methacrylate (HMWM), polyurethane-based and low viscosity epoxy-based materials are used to fill or seal the cracks of concrete to prevent the intrusion of corrosive species into the interior of reinforced structures via crack flow²⁶. Because of their low viscosity, crack sealants can rely on gravity to fill the cracks²⁷. Commercially available penetrants of the types mentioned above will be examined later on in the project for possible application as an alternative impregnating medium.

For PTT applications inhibitors are used for protection of strands before or at the construction site. For the former, it is common practice to apply a corrosion inhibitor (vapor phase or emulsifiable oils) to packaged strands to protect them from weathering and atmospheric humidity after manufacturing and during shipping²⁸⁻²⁹. For the latter, corrosion inhibitors are used sometimes inside PTT ducts prior to grouting, to avoid deterioration of the strand during the interval between strand placement and tensioning, and the moment of grouting. For example, the specification for grouting of post-tensioned structures by the Post-Tensioning Institute (PTI) 30 indicated the time limit between stressing the pre-stressed steel and grouting as follows; 7 days in very damp atmosphere or salt water (humidity > 70%), 20 days in moderate atmosphere (40% < Humidity < 70%), and 40 days in the case of very dry atmosphere (Humidity < 40%). If the exposure period exceeds the above limits, additional temporary corrosion protection must be carried out such as application of inhibitors.

The inhibitors can be in the form of crystalline powder that sublimates and acts in the presence of moisture and oxygen to mitigate corrosion. The use of some vapor phase inhibiting powders was abandoned around 1997 due to health concerns^{29,31}. Nontoxic and biodegradable powders are now available commercially³². Results may vary; however, a recent FDOT investigation found that vapor phase corrosion inhibitors did not have a well-defined role in mitigation corrosion in simulated PTT components exposed over an 8-week period under moist conditions²⁹.

Alternatively, strands during the pre-grouting period can be coated with emulsifiable oil. The oil can be flushed with water before grouting, and the tendon subsequently treated with compressed air to remove water³⁰. However, it has been reported that insufficient water removal could lead to grouted tendons having voids and corrosion damage, so it may be preferably to

leave the oil on the strands³³. In the report “Conclusions, Recommendations and Design Guidelines for Corrosion Protection of Post-Tensioned Bridges”⁹ it was reported that if grouting is delayed more than 4 weeks, a protective solution (Rust-Ban 310) was applied and showed good temporary protection. Marti et al.³⁴ conducted laboratory and field tests to evaluate the temporary corrosion protection performance of different oil-based inhibitors (Rust-Ban 310, Shellcool M3, and Aseol Milem 23-31) in different concentrations. Visual examination indicated that Rust-Ban 310 with concentration of at least 25 % aqueous emulsion provided the best protection performance. Isecke et al.³⁵⁻³⁶ reported, based on potentiostatic polarization tests, mass loss, and visual examination, the successful corrosion protection of pre-stressing steels against hydrogen induced stress corrosion by film forming agents such as Rust-Ban 310 and Rust-Ban 393.

While efficient corrosion protection is the objective of an inhibitor application, concern exists as to the possible undesirable effect of reducing bond strength between the strand and grout, especially if the inhibitor is of the oil variety. This issue is considered next.

Loss of bond due to the lubricating action of oil-based inhibitors is known from pre-stressing construction experience. There friction force losses (30-40%) can reduce significantly the ultimate tensile strength of a pre-stressed component³⁷. Kittleman et al.²⁸ performed corrosion, friction and adhesion tests on pre-stressing strands coated with emulsifiable oils, sodium silicate solution, stearate soap and powdered graphite. Visual examination and open circuit potential monitoring indicated that, the un-treated samples were found to corrode just after 4 days of exposure to 3.5% NaCl solution, while the application of coatings provided protection up to 39 days. However, in all unflushed samples, except that of graphite, adhesion between the strand and the hardened grout was severely degraded. The sodium silicate solution and water-soluble oils reduced adhesion by 50% and 75 %, respectively. However, stearate soap was not found to influence the adhesion properties. Laco and Borzovic³⁸ reported more than 60% reduction in bond stress loss of pre-stressing strands by the application of emulsifiable oil coatings.

In PTT investigations, the loss of bond has been reported as well. In the work by Marti et al. mentioned earlier³⁴, the treated samples showed ~ 60% reduction in bond shear stress when compared to the untreated samples. Borzovič and Laco³⁷ performed pull out tests on grouted PTT samples and reported that the bond stress of samples coated with emulsifiable oil and thixotropic compounds reached only 33% and 82% of that of uncoated samples, respectively. It was assumed that the difference in bond stress is related to the decrease in friction between the pre-stressing unit and grout. In another study³³, the effects of two emulsifiable oils (Citgo Trukut NC205 and Daubert VCI NoxRust 703D) on bond and friction losses of grouted PTT was investigated. Bond tests (ASTM A981-97) results indicated that the ultimate strengths of oiled and un-oiled samples were similar, although the slip was greater in the case of oiled samples. Friction tests results indicated ~15% reduction in the friction coefficient of oiled samples.

The above observations highlight the need for evaluating the extent to which the impregnation system investigated may affect the bond of the strand to the surrounding grout. That study is scheduled as part of Task 2 of the project and should examine the immediate effect of impregnation on bond as well as any possible indicators of long-term changes in that effect.

While no direct antecedents to the method subject of this investigation appear to be present, some procedure sharing features of interest have been used before. In U.S. Patent No.

5,460,033³⁹, the corrosion condition of un-bonded pre-stressed elements in post-tension concrete structures are evaluated by a method whereby a minimum of two openings (inlet and outlet ports) are created along the length of the structure. The humidity of a gaseous sample extracted from the outlet port is measured providing an evaluation of corrosion conditions of pre-stressed elements located between the inlet and outlet ports. This method is limited to un-bonded pre-stressed elements in post-tension concrete structures. The cycled gaseous environment can also contain dry gas for the protection of the pre-stressed elements by maintaining a desirable humidity level.

Another method, WO 87/06958⁴⁰, involves the migration of a vapor phase corrosion inhibitor through the porous matrix of a reinforced structure of masonry or cementitious material, to inhibit the corrosion of the reinforcement. The inhibitor can also migrate along the interface between the structure material and the reinforcement. This method is limited by the need for a channel or path around the reinforcement.

A corrosion mitigation method for pre-stressed concrete structures that was developed by PMD-ATEAV⁴¹ consists of drilling a hole through the concrete cover, the duct and the grout down to the tendons, followed by the injection of corrosion inhibitor solution using an ultrasonic pump, and finally the introduction of additional grout in the duct in order to fill any initial injection defects that might have been formed during the prior grouting step. The subject tendon impregnation method and the corrosion control evaluation are discussed next.

Tendon impregnation uses the naturally occurring tiny spaces between the center “king” wire and the surrounding six wires in a seven-wire steel strand (Figure 2-1) to inject, starting at one of the tendon ends or even from the middle, a pressurized low viscosity fluid (viscosity estimated to be in the order of 100 centipoise⁴²), that travels along the tendon. Some fluid leakage can take place laterally as well as at any minor breaks between the non-king wires, so at local areas of grout deficiencies the fluid may fill voids and part of the unsaturated grout pores. The fluid may contain a corrosion inhibitor, and is expected to act as water repellent, as well as to cover the surface of the steel with a protective film to prevent and/or arrest corrosion⁴³⁻⁴⁴. It is found that a relatively low pressure (50 – 100 psi) is sufficient for the impregnation liquid to flow through the length of a typical tendon, coat the strand, impregnate the grout and drive off moisture⁴⁵.

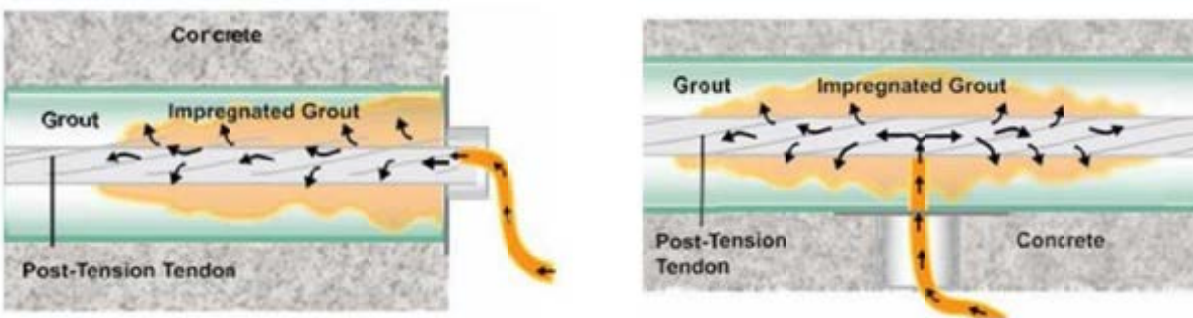


Figure 2-1: Schematic of application of impregnation fluid⁴⁶

The operating concept is described in detail in the cited patent⁴⁵ so it will not be repeated in detail here. A summary of laboratory evaluations is provided instead. The information on the laboratory tests including protection capability and flow ability as well as field injection practices

of the impregnation material has been adapted from available documents from Vector, FDOT, and Virginia Department of Transportation (VDOT).

It was reported that steel plates and PTT treated with the impregnation liquid did not show visual evidence of corrosion (Figure 2-2) when exposed to periodic salt, seawater and sulfate spray tests for up to 30 days^{43,46-47}. Potentiostatic polarization tests^{26,44,46,48} showed that chloride free impregnated samples containing 4.5% grout voids exhibited ~ 95% reduction in the corrosion current as indication of corrosion rate reduction. Void-free samples containing 2% chloride showed ~93% reduction in corrosion current, whereas void- and chloride-free samples showed ~ 81% reduction in corrosion current after treatment (It should be mentioned here that these tests were conducted over test periods of only up to one hour, and data reproducibility was not indicated).



Figure 2-2: Corrosion protection effect of impregnation fluid applied on a steel plate exposed to salt spray test. Compare with untreated upper left portion.⁴⁷

Following laboratory validation, field impregnation verification for tendons that contain soft and water-unsaturated grout was conducted on three bridges in Florida (Ringling Bridge in Sarasota, the I-95/I-295 Interchange in Jacksonville, and the I-4 Connector in Tampa) and Varina-Enon bridge in Virginia^{43,46,48-49}.

In tests performed on a Florida bridge⁴⁷ drying of the strand and surrounding grout was reported not to be required prior to impregnation and the free water/moisture was reported to be pushed out of the tendons during the pressurized impregnation process. Moreover, the fluid was found to successfully flow through the interstitial spaces for up to about 250 and 100 ft when injected from end and intermediate locations, respectively (Figure 2-3). After impregnation was terminated, tendon autopsy was carried out at different locations along the entire length of the tendon which confirmed the successful performance of the impregnation system (Figure 2-4).



Figure 2-3: Impregnation fluid reported to successfully displace moisture from a tendon end opposite to the injection end.⁴⁷

The laboratory work reviewed above involved relatively short-term tests. A longer duration test was conducted recently by the FDOT corrosion research laboratory⁵⁰. Samples with and without treatments were placed inside a salt fog chamber (3% and 5% NaCl solution). Linear Polarization Resistance (LPR) and corrosion potential were recorded for up to 3700 and 5000 hours of exposure, respectively. The corrosion potential measurements indicated that the treated samples showed shift of the potential towards more positive values (indicative of improvement) compared to that of the control samples. LPR tests showed lower corrosion rates in two of three impregnated samples compared with those of the untreated controls. Autopsies showed also only minor corrosion in the treated samples as opposed to extended corrosion in the controls. These results are encouraging but not entirely conclusive, highlighting the need for extended evaluation under this project. The following discussion examines some basic aspects of fluid transport as they pertain to the feasibility and practical aspects of fluid impregnation of tendons.



Figure 2-4: Impregnation material seep out of the far end of a >250-ft-long tendon.⁴⁷

The porosity of typical cementitious materials is in the range of 8-15 % by volume. The pores have wide size range from the nano to micro range (2 nm-100 μm)⁵¹. The compaction pores have sizes in the mm scale⁵². The transport of liquids in porous media can take place via diffusion, suction, and capillary absorption. Liquids including water and its ions transport through the pores primarily by capillary action⁵³. The penetration of water, sulfate ions and chloride ions into the pore spaces are key factors in determining the service life and durability of concrete structures. The penetration of aggressive media (capillary absorption and diffusion) can be hindered by surface treatment practices such as surface coatings, the use of sealants such as sodium silicates, and the use of water repellent materials such as silanes and siloxane⁵⁴⁻⁵⁵. When applied to concrete, the water repellent agent transports inside the concrete by capillary action, polymerizes and forms a fine network of silicon resin on the walls of the pores⁵⁶. The surface properties of concrete treated with a water repellent agent will change from hydrophilic to hydrophobic, where the pores are now only open for gaseous diffusion.

Linseed oil is used as a water repellent additive for the production of integral water repellent concrete and reduced chloride penetration was indeed observed for treated samples^{54,57}. That and other surface protection methods for concrete structures and subsequent chloride penetration decrease have been extensively reported^{54,58-66}. Johansson⁵⁶ reported the reduction in moisture fixation and transport through a layer of concrete treated with water repellent. The effective penetration depth as an indication of the performance of the treatment was found to depend on different factors including duration of contact, degree of saturation and porosity. Zhu et al.⁵⁸ tested the performance of saline based integral water repellent and surface treatment methods on recycled aggregate concrete. They reported that the latter was more effective in reducing water absorption, carbonation and chloride penetration. Medeiros and

Helene⁶⁶ studied the efficiency of different surface treatment materials such as hydrophobic agents, acrylic coating and polyurethane coating. The capillary water absorption was reduced by up to 98% and chloride diffusion coefficient by 86%. These results⁶⁶ indicated that the surface life of a reinforced structure can be extended up to 7.8 times. In conclusion, sorptivity reduction is the main protection mechanism for these agents.

The above discussion highlights beneficial corrosion control effects of cementitious medium impregnation with an organic substance. That information is encouraging to the expectation that comparable benefits may be derived from the tendon impregnation method. Nevertheless, it will be necessary to assess the grout sealing and water repellent characteristics of the impregnation material investigated here regarding the ability to retard the transport of corrosive species within the grout. The following discussion addresses the separate issue of the feasibility of achieving sufficient impregnating material delivery to regions of grout deficiency in a practical time frame. Next, the combined review of basic literature evidence with exploratory calculations of impregnating agent feasibility issues will be discussed next.

The pressurized flow of the impregnation liquid through the interstitial spaces of the wires was modeled here according to Poiseuille flow⁶⁷. For fully developed flow, where the liquid reaches the entire length (LO) of a channel, the potential and kinetic energies are under equilibrium and can be expressed using Bernoulli's equation⁶⁸:

Equation 2-1:
$$\frac{P}{\rho g} = f \frac{L}{D} \frac{V^2}{2\rho}$$

where P is the static pressure applied at one end of the channel while the other end is at zero pressure, ρ is the density of the fluid, g is the gravitational acceleration, V is the velocity of the fluid, f is the friction coefficient, L and D are the length and the diameter of a circular channel, respectively. For simplicity, the interstitial spaces between the wires will be treated as having circular cross section.

The friction coefficient of a fluid under laminar flowing conditions can be estimated for the appropriate Reynolds number condition (Re < 2300) as⁶⁹⁻⁷⁰:

Equation 2-2:
$$f = \frac{64}{Re}$$

Equation 2-3:
$$Re = \frac{\rho V D}{\mu}$$

where μ is the dynamic viscosity of the medium. From equations 1-2 and 1-3, the steady state velocity of the fluid can be calculated by:

Equation 2-4:
$$V = \frac{1}{32} \frac{P D^2}{\mu L}$$

The above equations may be adapted to a dynamic case where an initially fluid free strand (tendon) is subject to fluid injection at one end, to evaluate the time duration needed for the fluid front to reach a certain distance into the tendon. The simplifying assumptions are made that there is no acceleration effect, very small initial development zone, and small entrance loss. The answer was obtained numerically by a finite difference approach that considers the progressive penetration through increasingly long paths. Results are summarized for a variety of ranging scenarios in Figure 2-5. There the time required for the impregnation liquid to flow

through the entire length of strand (tendon) and beginning to appear at the free end is shown for various standard strand sizes (with corresponding inter-wire channel sizes). The calculations were all made for a 256 ft long tendon (replicating the length reported in field tests⁴⁸), and assuming fluid viscosity values ranging from very small (1 cp, bracketing that of a very fine penetrating oil²⁴) and quite large (1000 cp, bracketing that of some two-component liquid epoxy compounds²⁴). Applied pressures were chosen to be in the range of 50 to 150 psi, which encompasses that understood to be used in actual impregnation systems⁴⁵. The resulting travel times ranged from as little as ~ 2 minutes to as much as ~ 1 week, the later for the most viscous materials and lowest applied pressures. The results are encouraging in that over a wide range of operating conditions, the fluid impregnation front is projected to reach within a practical time window from one end to the other of a long tendon. The result agrees with the field observation of reasonably rapid fluid flow in actual conditions^{43,46,48-49}.

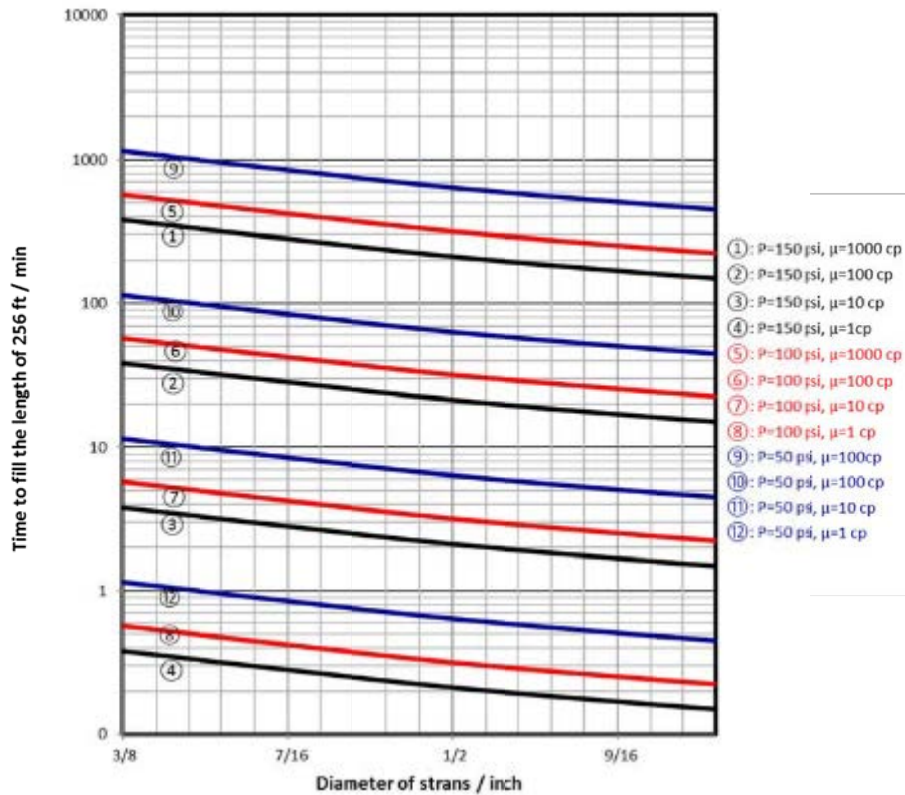


Figure 2-5: Projected time required for the impregnation fluid to seep out of the far end of 256-ft tendon.

A related question is whether the impregnating fluid flow rate is enough to fill in a deficiency, such as a grout void, within a practical amount of time. This was explored using Equation 2-4, assuming a 22-strand tendon with a 4-inch internal duct diameter and having a void with a length equal to the internal duct diameter. The calculations were made for positions of the void ranging from 10 ft to 256 ft from the fluid injection point, and assuming that all 22 strands are being used as conduits. The result is shown in Figure 2-6 for a baseline case for ½ inch strands, an applied pressure of 100 psi and $\mu=100$ cp. The projected fill durations ranged from a few minutes, for voids near the injection point, to about 1 hour at the far end of the tendon. Projected fill durations increase proportional to viscosity and inversely proportional to applied pressure and number of strands fitted for injection so estimates for other conditions are

straightforward. In general, void fill durations are of an order not much different from the time required to reach the void so, the overall time requirement for impregnation still remains within practical bounds for many anticipated conditions.

The above calculations and underlying assumptions are highly simplified. Nevertheless, the projections suggest that the time required for fluid to reach and fill defects like grout voids can be practical in many plausible scenarios. This observation is in turn indicative that the impregnation concept may be physically workable with other alternative fill materials should this investigation show others to be desirable.

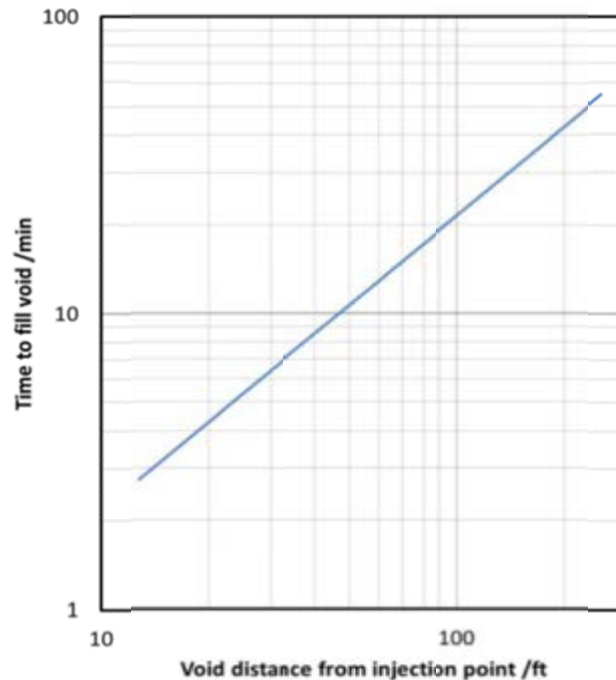


Figure 2-6: Projected time for the impregnation fluid to fill a void present at the indicated distance from the injection point.

Now, the closing comments on the findings in the literature review will be discussed. This review has not found, as anticipated, significant direct precursors to the subject tendon impregnation technique for corrosion control in PTT. Prior technology had explored injection of inhibitors through the grout matrix, but taking advantage of transport through the inter-wire interstices for transport of corrosion control substances does not appear to have been the subject of prior important work. Impregnating materials have been long used to control corrosion in reinforced concrete and some of the commercially available fluids for that purpose may merit consideration as alternative substances for tendon impregnation. Corrosion inhibitors have been used for control of corrosion of strand prior to grouting (although with mixed results), and incorporation of those inhibitors in the presently used impregnating fluid could be an option for investigation. At present the impregnating fluid composition is proprietary so it is possible that it already contains an inhibitor; this issue will become clear as subsequent tasks of the project are conducted.

The review revealed several investigations that documented substantial loss of bond of strand with the cementitious medium when inhibitors containing oil or similar lubricants were

used. Those findings emphasize the importance of characterizing the degree of bond strength change that takes place upon application of the currently used impregnation agent, and assessing any observed change in the context of the corrosion protection benefit. Task 3 of this project will address that issue in detail.

The corrosion test evidence initially obtained provided some encouraging findings on the ability of the penetration method to control corrosion of PTT. However, as stated in our research proposal, potentiostatic tests (and other electrochemical methods) are only indicative of processes that need interaction with the rest of the system to proceed, but may miss the presence of possibly strong local cell action processes in occluded regions shielded by the presence of the impregnating material. Hence, more stringent evaluation with a diversity of methods plus extended duration testing is needed to verify that a substantial and sustained protection effect is actually present.

Also as identified in our research proposal, knowledge of the mechanism of corrosion mitigation is an essential factor to guide the type and duration of testing to be used to evaluate the usefulness of impregnation for corrosion control. Central to that knowledge is the relative role of the three prevalent modalities of resistance- vs activation- vs concentration- polarization mitigation of corrosion. That knowledge would permit estimating the possibility and extent of local cell corrosion, and the development of means both electrochemical and otherwise to better monitor corrosion control performance. Experimentation for mechanistic understanding together with appropriate physical modeling of the system should be an integral part of the assessment effort and that will be addressed in the subsequent tasks of this project.

The available field evidence indicated good ability of the method to deliver impregnating material through long tendons. The exploratory calculations performed here showed projections in agreement with that evidence, and provided a favorable prognosis for successful application over a wide range of impregnating material property values. That projection is encouraging in regard to the possibility of identifying attractive alternatives to the presently used proprietary compound.

2.1 SUMMARY

While initial preliminary testing results and application of the impregnation technology have been highly encouraging concerning the practical feasibility of delivering the fluid to grout deficiency regions and preventing the development of corrosion activity, the key issues with associated critical questions have not been or only partially addressed to date, and will be addressed in the remainder of this investigation. The technical questions under investigation are:

- (1) Does impregnation actually (sufficiently) mitigate corrosion, and by which mechanism(s) and for how long?
- (2) When can impregnation be effectively implemented and are there better alternative impregnating materials?
- (3) How does impregnation affect mechanical tendon performance i.e. the bond of the strand to surrounding protective grout?

The outcome in producing answers to these questions were the subject of subsequent tasks, which are described next.

CHAPTER 3 EXPOSURE AND ELECTROCHEMICAL TESTING

The literature review confirmed that tendon impregnation with a corrosion control substance delivered via the inter-wire channels has strong potential for successful treatment of PTT with grout deficiencies⁷³. Tendon impregnation could be performed in long tendons up to ~ 250 and 100 ft when injected from end and intermediate locations, respectively⁷⁴. This was supported by the simplified fluid flow analysis reported in chapter 1 which confirmed the practicality of fluid injection and suggested good prognosis over a wide range of impregnating material properties. The method was successfully used in several field projects. The corrosion test evidence initially obtained provided some encouraging findings on the ability of the penetration method to control corrosion of post tensioned tendons. With this being said, the objective of this task is to characterize the ability of tendon impregnation material(s) to prevent or delay corrosion in new and in-service tendons, and to arrest the continuation of corrosion.

The present chapter comprises three sections. In the first two sections, experimental results are presented to assess the corrosion prevention and arresting ability of two different impregnation fluids; (1) a commercially available organic mixture rich in aliphatic hydrocarbons that is commonly used for lubrication, penetrating action and water displacement toward corrosion control which will be referred to as the alternative fluid, and (2) the impregnation medium used by Vector Corrosion Technologies, Inc. (Vector) for the process named Post-Tech® PTI Impregnation System which will be referred to as the VPF. In the third section, modeling was conducted to obtain further insight on which of the candidate mechanisms for corrosion mitigation was dominant. Modeling was also used to further examine a possible detrimental aspect of impregnation application on corrosion control (insufficient inhibitor coverage) and the extent of corrosion and need for its control that could result from oxygen availability alternatives.

3.1 ALTERNATIVE FLUID TESTING

To simulate a PTT segment with an artificial deficiency for electrochemical tests, samples having a void were prepared per the following steps (Figure 3-1): 3" internal diameter HDPE ducts with 0.2" wall thickness were cut into 8" long segments. A 9" long seven-wire 0.5" diameter steel strand segment was placed in the center of the HDPE duct. A 3" long Styrofoam piece (in the shape of extruded circle segment) was placed at the middle of the inner wall of the duct. A Mixed metal oxide coated titanium mesh (Ti-mesh), and a mixed metal oxide coated titanium rods (Ti-rod) were placed inside the duct. The Ti-mesh was positioned inside the duct surrounding the steel strand. The distance between the strand and the Ti-rod was approximately 1 cm. During grout placement, care was used to ensure that all metal components were not short circuited. The Grout (EUCO Cable Grout PTX) with water to cement ratio of 0.25, according to the manufacturer recommendation, were mixed using an agitator rotated by a drill at ~2700 rpm, and cast inside the HDPE duct. After curing, a cut out was performed on an exterior location on the duct where the Styrofoam piece was internally placed. The duct's cut out was lifted and the Styrofoam piece was carved out and discarded. The duct cut out was reattached with a silicon caulk. When needed for simulating an ongoing corrosion condition, 3%-NaCl was poured into the void through a small hole that was already made on the cut out. During exposure to the corrosive medium, salt efflorescence was visually detected on both ends of the tendon samples indicating that the entire length of the steel strand was exposed to the corrosive medium. The total outer surface area of the steel strand in contact with grout was approximately 50 cm². A representative photograph of a sample for the electrochemical tests is shown in Figure 3-2.

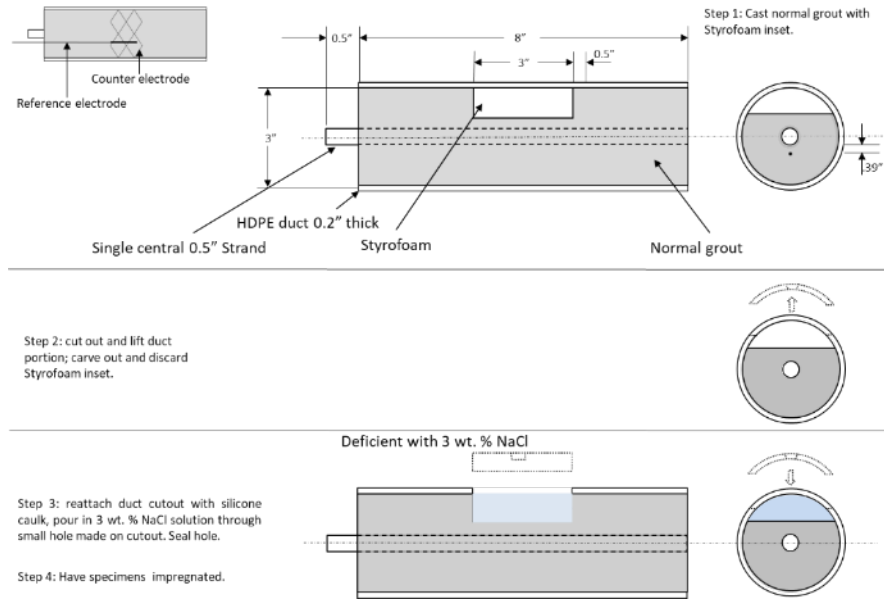


Figure 3-1: Sample preparation schematic

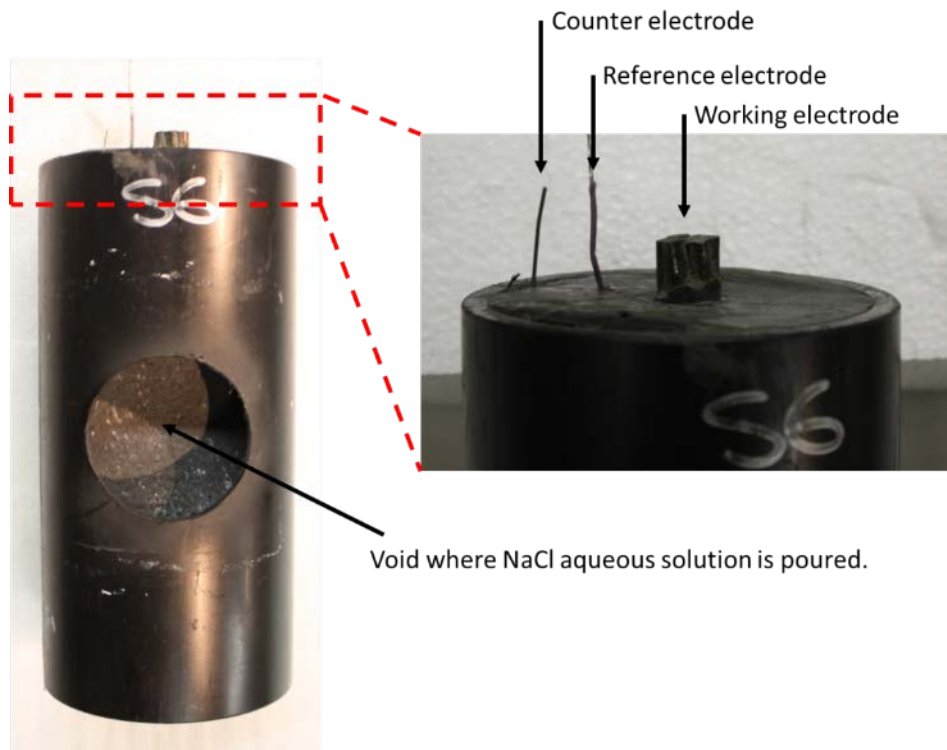


Figure 3-2: Sample of electrochemical testing

Resistivity measurements were conducted using four-point Wenner array probe (FWAP). Grout was cast into 2" diameter- 4" long cylindrical molds pre-fitted with metallic probes placed in an array with spacing $a=2.5$ cm. The openings of the cylindrical mold were sealed with epoxy

resin to minimize evaporation loss. The resistance (R , Ω) was obtained periodically with a Miller Model 400D digital resistance meter and converted to resistivity (ρ , $\Omega\cdot\text{cm}$) by⁷⁶.

Equation 3-1:
$$\rho_{app} = 2\pi aR$$

Equation 3-2:
$$\rho = K\rho_{app}$$

where K is a cell constant correction that depends on the length and diameter of the specimen as well as the array spacing. Resistivity measurements were corrected for temperature to an equivalent value at 24 °C by assuming a reduction of 3% per °C increase⁷⁷.

Semi quantitative evaluation of the viscosity of the impregnating medium was conducted with a fluid-draining experiment. A vertical clear plastic tube with an internal diameter of ~6 mm and a ~2 mm diameter, 18 mm long bottom exit channel stopcock was filled with 19 ml of liquid. The stopcock was opened and the time to emptying was measured. The result was compared with that obtained when using water instead.

Dynamic polarization methods including cathodic cyclic Potentiodynamic (PD) polarization, Electrochemical Impedance Spectroscopy (EIS) and Open Circuit Potential (E_{OC}) evolution analysis were conducted to assess the apparent corrosion rate of the steel strand in as-cast, corroding and impregnated stages. Electrochemical monitoring of all samples was conducted before and after exposure to the corrosive media as well as before and after impregnation. Samples were placed vertically and the impregnation liquid was allowed to penetrate through the interstitial sites of the strands by means of gravity and capillary forces. All electrochemical measurements were conducted using a Gamry Reference 600® potentiostat with a conventional three electrode configuration. The sample, Ti-mesh, and Ti-rod were used as the working, counter, and reference electrode, respectively. The reference electrodes were frequently calibrated against a Saturated Calomel Electrode (SCE) in contact with the grout in which the reference electrodes were embedded. 3%-NaCl was poured into the voids after 17 days from sample preparation and was removed at day 24. Samples were then allowed to drain and TIM was introduced starting from day 27.

E_{OC} was monitored periodically using SCE reference electrode. EIS tests were conducted at E_{OC} in the frequency range of 100 kHz to 10 mHz, 5 points per decade, and 10 mV rms sinusoidal potential excitation. The obtained data were then fitted using Gamry E-chem software. PD measurements were conducted in downward and upward scan at a constant scan rate of 0.05 mV/s, starting from the E_{OC} , return cathodic potential (300 mV below E_{OC}) and ended when the upward potential returned back to the E_{OC} .

All experiments including resistivity, semi quantitative viscosity evaluation, and electrochemical measurements were conducted at room temperature (24 ± 1.5 °C) and relative humidity (68 ± 3 %) until a steady state regime was approached.

3.1.1 RESULTS AND DISCUSSION

Figure 3-3 shows the change of grout resistivity with time. In this log-log diagram and based on the slope of data points, four regions were identified. During the first 10 hours (stage I), grout is characterized by relatively low resistivity ~ 100 $\Omega\cdot\text{cm}$. In the next 20 hours (stage II), the resistivity showed high increase up to ~ 1000 $\Omega\cdot\text{cm}$. In stage III (30 to 300 hr) all samples encountered further increase in resistivity due to the continuous hydration and self-desiccation and reduced connectivity of pore network⁷⁸. Finally, beyond 300 hours, resistivity curves

showed lower slope indicating an approach towards final values of $\sim 1000 \Omega \cdot \text{cm}$. This behavior is similar to that reported for other types of commercial grouts⁷⁸. This terminal value of grout resistivity (conductivity) was used as an input parameter in the modeling calculations presented later.

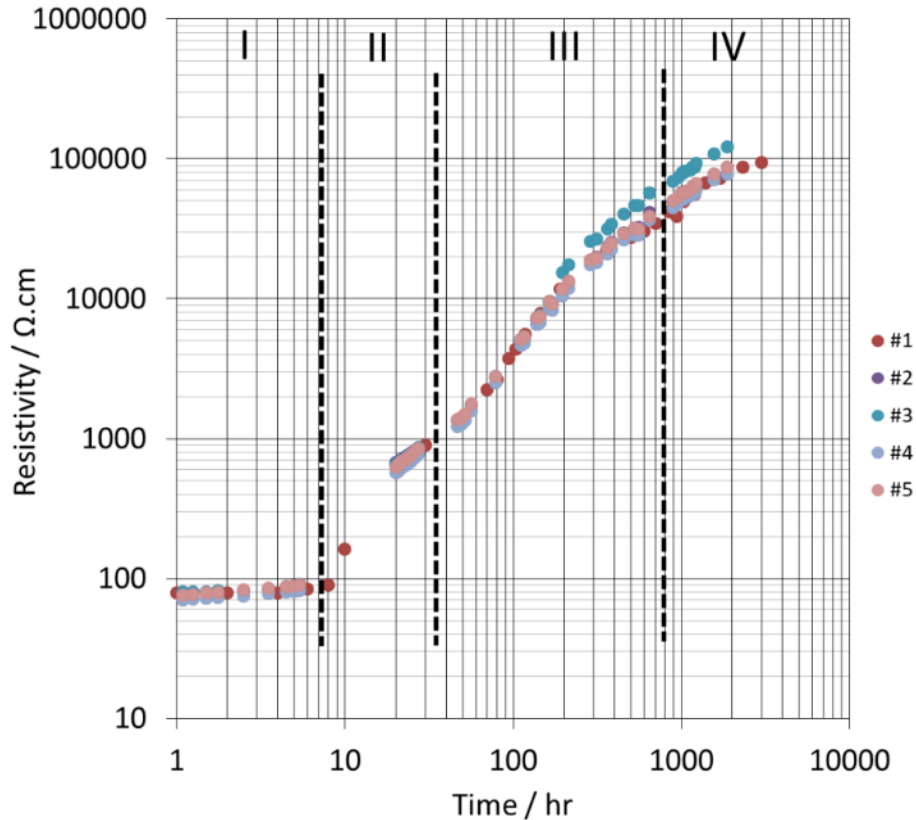


Figure 3-3: Evolution of grout resistivity. Stages designated by Roman numerals. Results from five replicate specimens.

The semi quantitative viscosity evaluation (3 tests for each fluid) yielded 5.7 (range 5:6) sec for water and 8.7 (8:9) for TIM, indicating a greater viscosity for the latter. A material data sheet reported values of 2.79-2.96 cSt for the TIM at 37 °C, compared with 0.65 cSt for water at 37 °C⁷⁵, in agreement with the semi quantitative test results.

The time evolution of E_{OC} of three replicate samples is shown in Figure 3-4. In the as-cast period, the E_{OC} stayed more positive than $\sim -180 \text{ mV vs. SCE}$. After exposure to the 3%-NaCl, there was a sudden drop in E_{OC} that might be caused by the active corrosion behavior of the strands when exposed to the corrosive medium. When the latter was removed (here grout is still contaminated with Cl⁻) the E_{OC} showed a slight increase, which was followed by another drop as TIM (WD-40) was introduced. Beyond day 36, values of E_{OC} showed another increase and then reached steady state values.

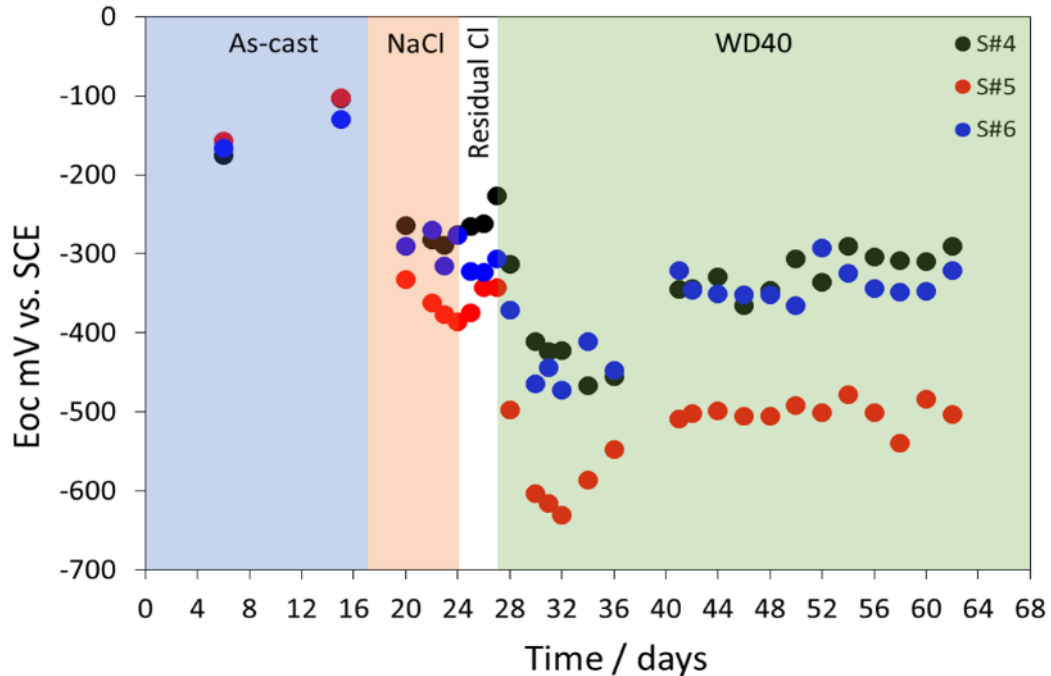


Figure 3-4: Evolution of EOC. Results from three replicate specimens.

Figure 3-5 shows the evolution of EIS behavior of one sample. Comparable results were obtained for the other two samples. For clarity, the Nyquist representation of the EIS measurement was split into three figures. The evolution of EIS was recorded before (Figure 3-5.a) and after (Figure 3-5.b) contaminating the sample with Cl^- , and after impregnation with TIM (Figure 3-5.c). The EIS data were analyzed to obtain an estimate of corrosion rate and its changes due to sample impregnation. The equivalent circuit used to determine the electrochemical parameters for corrosion rate evaluation is shown as an inset in (Figure 3-5.a). The constant phase element (CPE, with impedance represented by $Z_{\text{CPE}} = Y_0^{-1} (j\omega)^{-n}$ where Y_0 is a constant, $j = (-1)^{1/2}$, ω is the angular frequency and n is a real number between 0 and 1) is in parallel with a polarization resistant (R_p). From that last parameter the corrosion rate is calculated; the greater R_p the smaller the corrosion rate and vice versa. Both elements are in series with a solution resistance representing the resistance of the grout (R_s). Due to the presence of a constant imaginary impedance zone at intermediate frequencies, the value of R_s was obtained by fitting data limited to the 10 mHz to 1 Hz range.

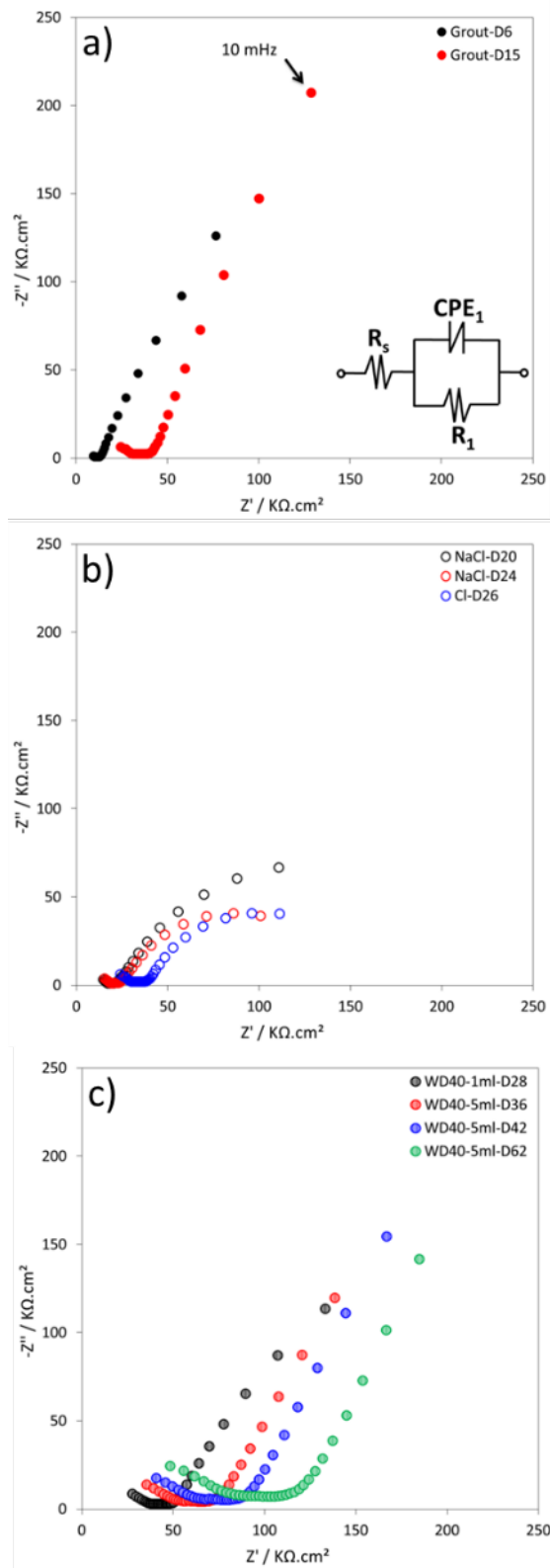


Figure 3-5: Typical evolution of EIS behavior for (a) as-cast, (b) during corrosion, and (c) following impregnation. The last figures in the legends indicate days since casting.

The evolution of the magnitudes derived from EIS tests are shown in Figure 3-6. In general R_s and R_p were found to increase as time proceeds except when the steel strand was exposed to the 3%-NaCl. Alternatively, Y_0 and n decreased as time proceeded except when the steel strand was exposed 3%-NaCl. Y_0 may be considered as a rough estimate of the value of the interfacial capacitance $C_{CPE} \sim Y_0 \cdot \text{sec}^{1-n}$ that would be measured in an EIS test at a frequency $f = 1/2\pi \text{ Hz} \sim 0.16 \text{ Hz}$. As shown in Figure 3-6.c the C_{CPE} values thus obtained were in the range ~ 30 and $70 \mu\text{F}/\text{cm}^2$ and were in the order of similarly obtained interfacial capacitance values for steel in concrete⁷⁹. It is recognized that this estimation of interfacial capacitance becomes increasingly unrepresentative as n decreases from unity.

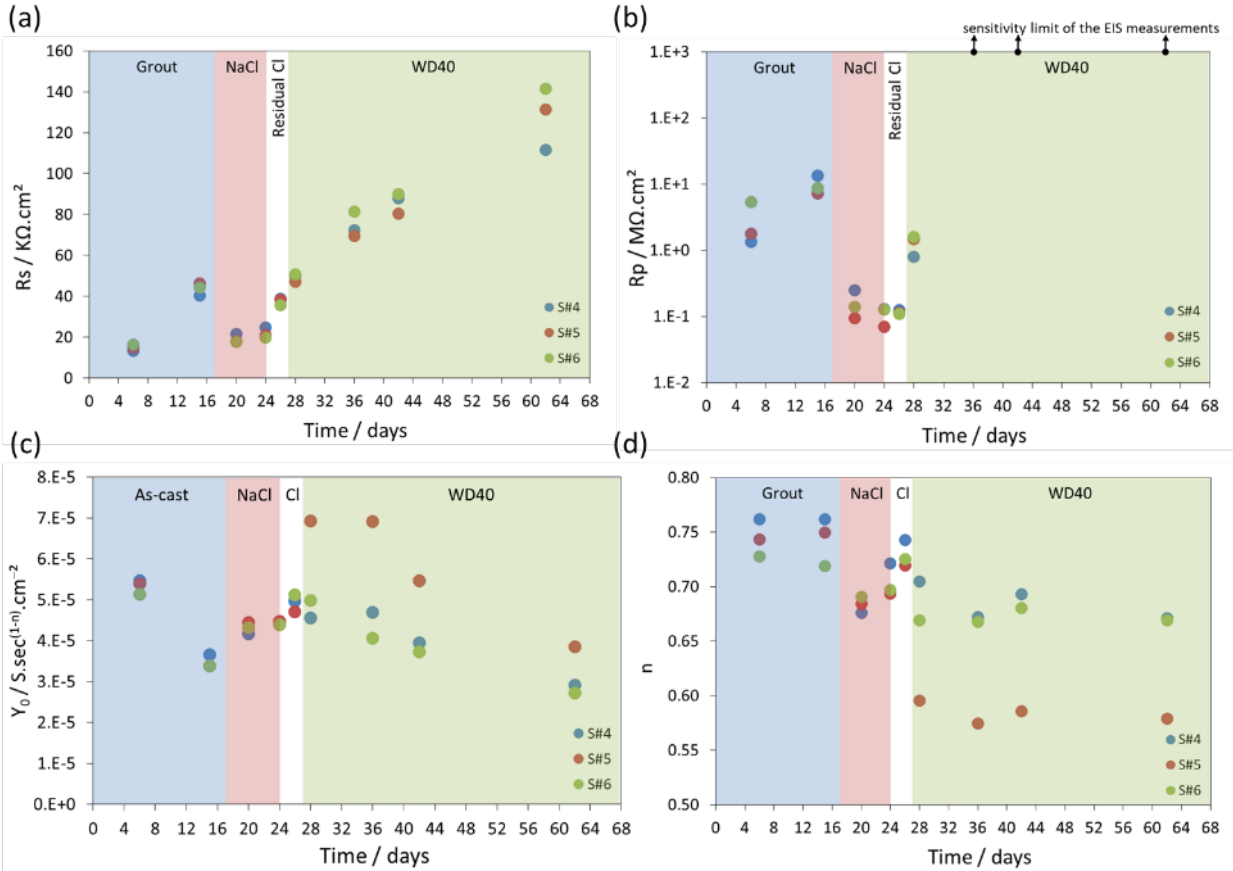


Figure 3-6: The evolution of magnitudes derived from EIS tests: (a) R_s (b) R_p (c) Y_0 and (d) n as a function of time. The legends indicate replicate specimen designations.

The results of the corrosion current density (i_{corr}) are shown in Figure 3-7.a. The corrosion rate, expressed in terms of a corrosion current density⁷³, i_{corr} was estimated from the value of R_p by the Stern-Geary relationship⁸⁰, with a selected conversion constant value $B=26 \text{ mV}$ (assuming simple activation polarization).

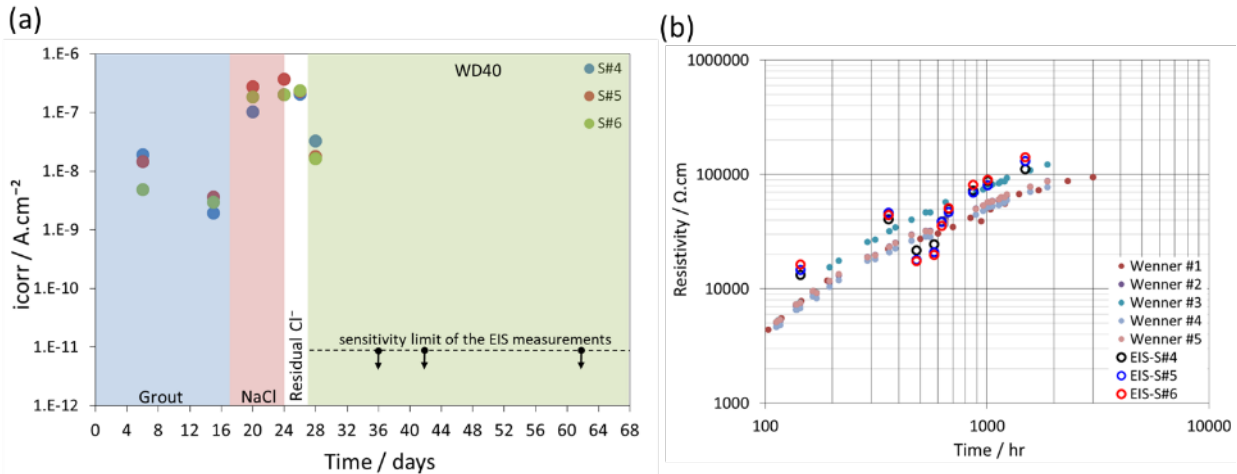


Figure 3-7: Evolution of (a) i_{corr} from EIS and (b) grout resistivity measured by EIS and FWAP

The results showed that the corrosion rate was initially very small (i_{corr} typ. $\sim 3 \times 10^{-9}$ A/cm^2), as expected for strand in non-contaminated cementitious grout. Upon introduction of 3% NaCl, the corrosion rates showed a strong and sustained increase, by almost two orders of magnitude, a behavior expected for highly chloride contaminated grout. Even after removal of the 3% NaCl, the corrosion rate remained high in the residually chloride-contaminated grout. When measured one day after impregnation, the corrosion rate had decreased by \sim one order of magnitude. Afterwards, the corrosion rate stabilized at even lower values ($\sim 1 \times 10^{-11}$ A/cm^2 , in the order of the sensitivity limit of the EIS measurements).

The EIS analysis also provided, through the value of R_s , an indication of the resistivity of the grout, at least for the region between the reference electrode and the surface of the strand. Given the system dimensions, a value of ρ can be estimated (ρ_e) to be in the order of R_s multiplied by the electrode-strand distance. The results (Figure 3-7.b) showed that after impregnation, there was a remarkable increase in ρ_e . Because there was a concurrent strong drop in i_{corr} , the results could be interpreted as an indication that the corrosion decrease was predominantly the result of electrolyte resistance polarization enabled by the increase in resistivity created by the injected fluid. However, it is noted that the grout resistivity was already increasing with time due to the natural aging of the grout, as shown in Figure 3-3. That behavior is illustrated again in Figure 3-7.b, where both ρ from FWAP measurements and ρ_e from EIS are shown together. Consequently, the increase in ρ_e after impregnation may not necessarily be related (or perhaps only partially – subject to continuing work) to impregnation. Thus, factors other than resistivity increase may be playing an important role in the mechanism by which fluid impregnation reduced i_{corr} . For example, the marked drop in E_{OC} and decrease in corrosion rate after impregnation are consistent with a mechanism that involves a decrease of the cathodic reaction. The subsequent increase in E_{OC} (i_{corr} remains low) suggested the decrease in the anodic reaction as well. That decrease could be associated with an oxygen transport limitation or a decrease in the exchange current density of the oxygen reduction reaction. The PD experiments provided additional insight into this issue as discussed next.

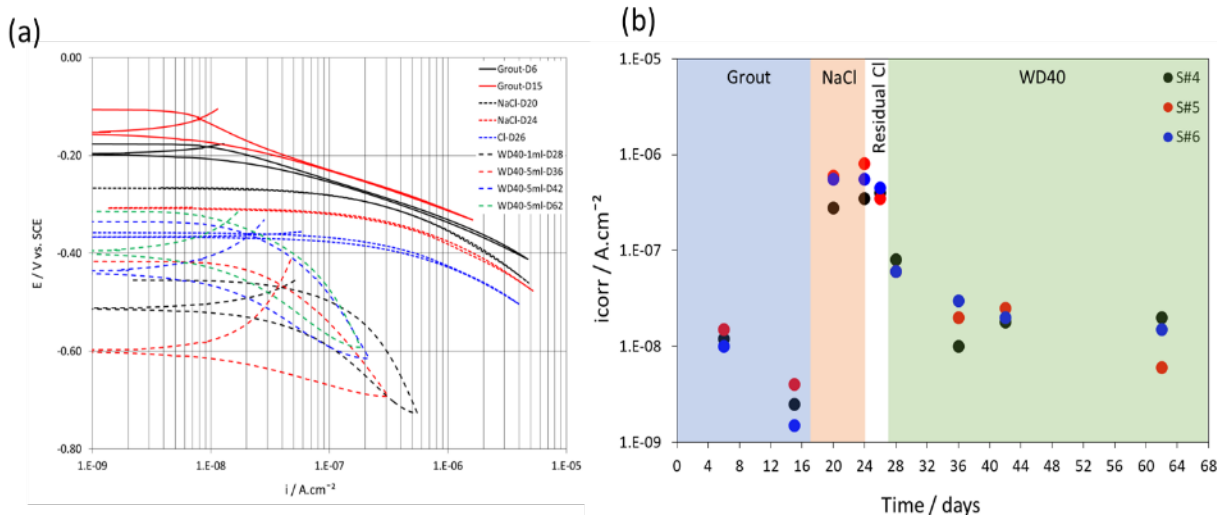


Figure 3-8: Evolution of (a) PD curves – typical. Solid lines: as-cast; Dotted lines: after chloride exposure and before impregnation; Dashed lines: after impregnation and (b) i_{corr} – all results.

Figure 3-8.a shows typical IR-drop corrected time evolution PD diagrams. Similar curves were obtained for the other two samples. Corrosion rates were estimated by the Tafel Extrapolation method⁸² and reported in Figure 3-8.b. The corrosion rate in the as-cast condition initially decreased as time proceeded and reached a minimum value of $\sim 3 \times 10^{-9}$ A/cm², in agreement with the EIS results. Upon introduction of 3%-NaCl the corrosion rate determined by this method increased by \sim two orders of magnitude and remained high in the residually chloride-contaminated grout. Upon removal of the corrosive solution and injection of TIM, E_{OC} showed further decrease which was followed by a gradual increase. When measured one day after impregnation, the corrosion rate decreased by \sim one order of magnitude. Afterwards, the corrosion rate stabilized at even lower values $\sim 1 \times 10^{-8}$ A/cm². These trends confirm the behavior previously indicated by the EIS measurements.

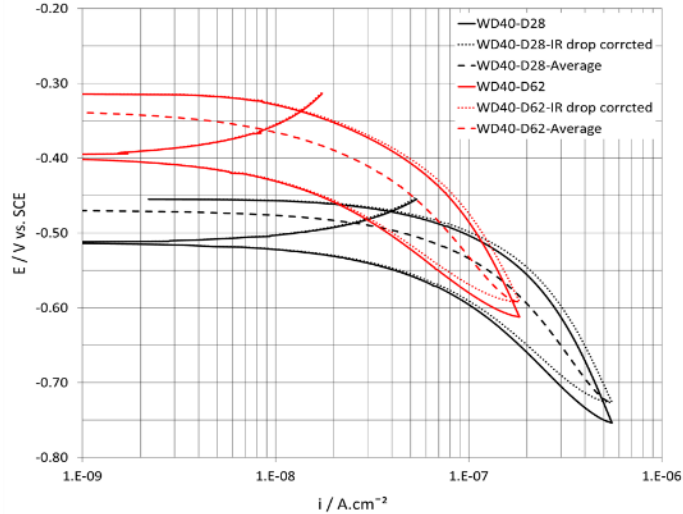


Figure 3-9: PD curves before and after IR-drop correction

After impregnation, the PD curves showed appreciable hysteresis, shown in detail in Figure 3-9. The hysteresis might be considered to result from a combination of both Faradaic and interfacial charge storage currents⁸⁰. The actual Faradaic current, of importance to elucidate corrosion processes, was estimated by averaging the downward and upward currents at the same potential value (dashed lines in Figure 3-9).

The potential as a function of the current in logarithmic scale diagrams were used also to indicate whether these curves obey Tafel behavior. During exposure to the 3%-NaCl (day 20 to day 26), the polarization curves seemed to follow Tafel behavior with $\beta_C = 160 \pm 19$ mV which is comparable to that reported for oxygen reduction in concrete⁸⁰. After impregnation, β_C showed larger apparent Tafel slopes ($\beta_C = 270 \pm 55$ mV) but with no indication of obvious oxygen diffusion limitation.

An apparent interfacial capacitance (C_{PD}) may be estimated from PD scans assuming for simplicity that the interfacial charge storage currents behave as for an ideal capacitor by⁸⁰.

Equation 3-3:
$$C_{PD} = \frac{\Delta I}{2 \frac{dE}{dt}}$$

where (ΔI) is the difference in current density of the forward and reverse scans at a specific applied potential and (dE/dt) is the scan rate. The data for conditions before impregnation did not provide enough hysteresis to reliably apply Equation 3-3. However, the larger hysteresis observed after impregnation permitted such evaluation. The evaluation of C_{PD} was usually performed at only one potential (typically ~ -550 mV below E_{OC}); confirmation tests showed that estimates of C_{PD} for one sample at various applied potential levels yielded consistent values. The values of C_{PD} were generally much higher than those obtained for C_{CPE} but that is as expected since given the slow scan rate used the impedance of the CPE at the correspondingly lower effective frequency (in the order of 10^{-4} Hz). Nevertheless, the relative time evolution of those values was in good agreement with the behavior of the interfacial capacitance discussed earlier for EIS results shown in Figure 3-6.c. Thus, the average C_{PD} of the three samples in the post-impregnation period was found to decrease from $\sim 1600 \pm 120$

$\mu\text{F}/\text{cm}^2$ at day 28 to $\sim 600 \mu\text{F}/\text{cm}^2$ at day 62. Possible artifacts in the estimates due to the increase in solution resistance noted earlier for that period are likely not important, since the IR-correction was small (Figure 3-9).

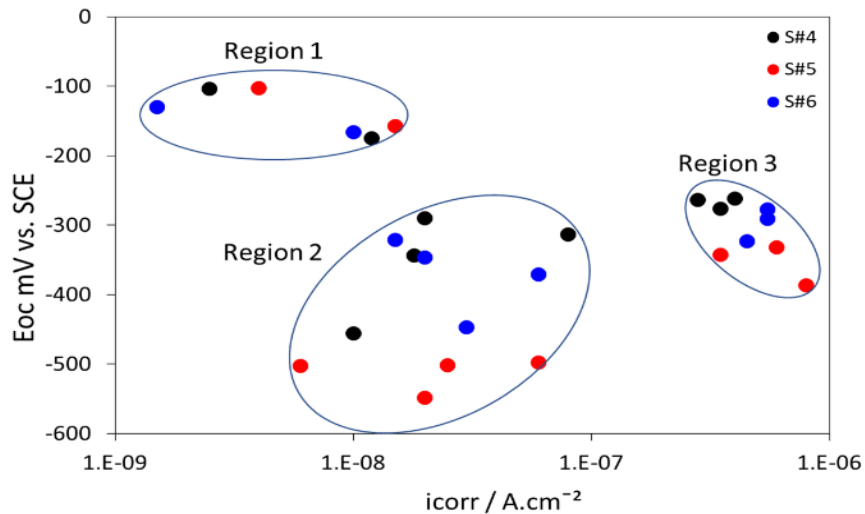


Figure 3-10: Relationship between E_{oc} and i_{corr}

Further insight may be obtained by examination of Figure 3-10 that shows the E_{OC} as a function of i_{corr} for three replicate samples. Data were found to cluster around three different regions showing clear differentiation between the passive and active behavior of steel. In region 1 (passive steel in the as-cast condition), the steel had low i_{corr} (between 1×10^{-8} and 1×10^{-9} $\text{A}\cdot\text{cm}^{-2}$) and E_{OC} was nobler than ~ -200 mV vs. SCE. In region 3 (active state during exposure to the corrosive medium) there was noticeable increase in i_{corr} to (between 5×10^{-7} and 1×10^{-6} $\text{A}\cdot\text{cm}^{-2}$) and E_{OC} decrease to ~ -400 mV vs. SCE. The behavior after impregnation centered on region 2. Here, the smallest values of E_{OC} up to ~ -600 mV vs. SCE were observed, while values of i_{corr} were \sim one order of magnitude less than that in region 2.

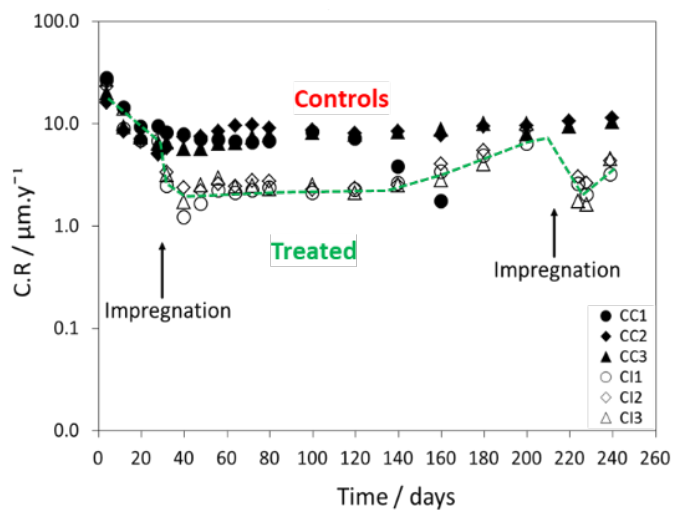


Figure 3-11: Long-term evolution of corrosion rate in control and impregnated tendons.

The previous findings illustrated corrosion abatement by the alternative impregnation fluid over a period of about two months. Importantly, additional experiments were performed over an eight-month period on mock tendons made with grout containing admixed chlorides to determine the effective service period of the alternative fluid. The corrosion rates obtained from EIS measurements of tendons that were not impregnated (control) and impregnated tendons (treated) over time is presented in Figure 3-11. Following impregnation, the corrosion rates of the treated tendons decreased by almost an order of magnitude and remained steady for approximately three months. After three months, the corrosion rates increased until they reached values not much less than those of the control tendons. Re-impregnation was at least initially effective in lowering the corrosion rates by a similar amount as the initial impregnation.

3.1.2 FINDINGS AND IMPLICATIONS

Corrosion rates estimated from electrochemical measurements indicated a favorable prognosis that impregnating PTT with TIM would be successful in substantially mitigating ongoing corrosion of steel strands – e.g. reductions in corrosion rate by an order of magnitude or more. Insight on the candidate mechanism(s) responsible for corrosion mitigation upon impregnation was obtained from the FWAP, EIS, and PD tests as discussed next.

EIS and PD tests were in good agreement and showed upon impregnation about one or more orders of magnitude reduction in corrosion rate. The marked initial drop in E_{OC} concurrent with the lowered corrosion rate is consistent with a mechanism that involves a decrease of the cathodic reaction rate. That decrease could be associated with either activation polarization or concentration polarization. However, the latter does not appear to be dominant since PD data did not show evidence of the onset of a diffusion limitation in the cathodic reaction. Therefore, the impregnating agent appears to have initially acted more by lowering the kinetics of oxygen reduction at the metal-grout interface rather than by restricting access of oxygen to the interface. Later on, there was a gradual increase in E_{OC} , while i_{corr} remained low, suggesting the subsequent onset of a decrease in the rate of anodic reaction as well. That later potential increase together with the decrease in both C_{CPE} and C_{PD} with post-impregnation time may be indicative of the progressive formation or deposition of a protective film on the steel surface. This film would be capable of variously decreasing the activation kinetics of either cathodic or anodic reactions. Grout resistivity increased after impregnation, but a rate that appeared to be more related to grout aging than to the introduction of the impregnating agent. Therefore, the decrease in estimated corrosion rates upon impregnation does not seem to be a major consequence of any increases in grout resistivity induced by the impregnating agent.

Notably, long-term experiments showed the effective service period of the impregnation fluid's corrosion arresting abilities to be several months. After this period, re-impregnation would be required. One possible reason for the limited service life is that the fluid could be absorbed into the grout spore space and therefore minimize its presence at the steel strand surface. The absorption of the fluid into the pore space of the grout. Re-impregnation was effective in reducing the corrosion rates to similar values observed following the initial impregnation.

3.2 VECTOR PROPRIETARY FLUID

The following experiments were designed to assess the corrosion performance of the VPF and method of impregnation. Tendon sections were fabricated with and without grout deficiencies to determine the material's ability to arrest corrosion. The specimens were taken to the Vector Corrosion Tampa Office to perform the impregnation between August 26 – 30, 2019. The details of the procedure are provided in Appendix 1. During that time Vector Corrosion Technologies also provided USF with samples of the impregnation fluid for further testing. Analysis of the impregnation fluid by electrochemical testing was performed to gain insight on the mechanism of inhibition and to identify any degradation modes that may limit its service period requiring re-impregnation. The experimental design and evaluation methods are presented in the following sections.

Tendon segments that were 1ft and 3ft long were cast with and without grout deficiencies to promote various levels of corrosion. A schematic of each design is shown in Figure 3-12. While the 1ft tendons with a single steel strand were convenient for laboratory research, their reflection of in-service tendons that are much longer and contain multiple steel strands is questionable. Therefore, 3ft tendons with a bundle of 3 strands were used to more closely reflect actual conditions that may facilitate tendon impregnation due to the additional inter-wire space.

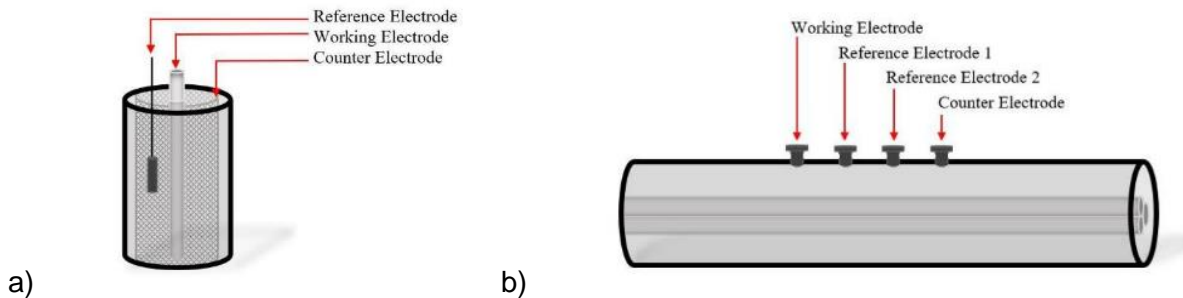


Figure 3-12: The construct of a 3-ft tendon after the curing process

The 1 ft tendons were cast with an activated titanium mesh against the internal walls of the duct and a reference electrode to facilitate corrosion rate measurements prior to and following impregnation. This was not feasible with the 3ft tendons and instead an indirect approach was implemented in which an array of 4 electrodes were inserted into the duct and in contact with the grout to allow the application of the indirect impedance method described previously in FDOT Project BDV31-977-35.

Polymer ducts similar to that of tendons in post-tensioned structures were segmented into 1ft and 3ft sections. Approximately, 18 polymer ducts each 3ft in length and 16 polymer ducts 1ft in length were cut. Cardboard circles the size of the diameter of the polymer duct were used to support a polymer nipple which supported the steel strands in the center of the duct, equally spaced from the interior duct sides. ASTM A416 steel strands were used as reinforcement; the 1ft tendons were reinforced with a single steel strand and the 3ft tendons were reinforced with a 3-strand bundle.

The tendons were grouted with two types of cementitious grout, EUCO Cable grout and Master Flow grout. As grout was being pumped into the polymer ducts, a rubber mallet was used to minimize bubbles by lightly tapping the sides of the polymer duct. The tendons were positioned upright without being disturbed until the grout was solidified.

The grouts were mixed in water to grout powder ratios of 0.25 and 0.375 and, in some instances, the grout was contaminated with chlorides. In particular, the tendons were grouted with 2% chloride ion by weight of grout, introduced by admixing the corresponding amount of NaCl which is representative of possible severe contamination in marine environments. Table 3-1 provides a detailed list of the grout types, water to grout ratios and chloride content associated with each group of tendons.

Table 3-1: Grouting conditions for all of the laboratory specimens

Tendon Length/Name/Cast Date	Grout Types	Number of Sample Tendons
1ft NaCl 05/21/2019	EUCO Cable Grout Water to Grout Ratio (W/G) = 0.25 Chloride Contaminated: 2 wt% Cl ⁻	6
1ft Normal 05/17/2019	EUCO Cable Grout W/G = 0.25 Chloride Free	6
1ft Master Flow	Master Flow Grout Chloride Free	2
1ft Master Flow NaCl	Master Flow Grout Chloride Contaminated: 2 wt% Cl ⁻	2
3ft NaCl 05/21/2019	EUCO Cable Grout W/G=0.25 Chloride Contaminated: 2 wt% Cl ⁻	6
3ft Good 05/23/19	EUCO Cable Grout W/G=0.25 Chloride Free	6
3ft Soft 05/22/2019	EUCO Cable Grout W/G=.375 Chloride Free	6

After the tendon specimens were cured for ~28 days, electrochemical impedance measurements were obtained weekly for each tendon. After 3 months, half of the tendons were impregnated with the VPF. When testing was not taking place, the 1ft test specimens were placed in a humidity chamber where the humidity was maintained at 85% relative humidity to reduce moisture loss. The 3ft tendons were sealed with caps on each end and tape was used to cover minor incisions on the polymer duct.

In the case of the 1 ft tendons, electrochemical impedance spectra were obtained by application of a perturbation of either current or potential between the metal of interest and a counter electrode. The response to the perturbation is measured with the use of a reference electrode and a transfer function is obtained for a range of perturbation frequencies that relates the perturbation to the response signal. The result is a series representation of the resistance of the grout and the impedance of the steel and grout interface. A model is described below that

may be used to obtain the steel polarization resistance from the impedance data and estimate the corrosion rate.

Additionally, an indirect impedance method was used in the case of the 3ft tendons in which the steel is indirectly perturbed by applying the perturbation signal between the outer 2 electrodes of a 4-electrode array placed on the grout surface. The response is then measured between the two inner electrodes. In this case, the transfer function comprises a parallel contribution of the grout impedance as well as a contribution of the steel and grout interface. While this technique requires advanced analysis methods, a correlation curve may be obtained to relate the measured impedance to the impedance of the steel and grout interface and obtain estimates of the corrosion rate. A detailed description of the analysis method will be presented.

The polarization resistance of the steel and grout interface is often related to the corrosion rate via the Stern-Geary relationship assuming Tafel kinetics with a single step corrosion reaction. In both the direct and indirect polarization approach, a measurement model in which a series of Voight elements, Figure 3-13, is used to fit the impedance data and obtain an estimate of the polarization resistance. Included in the model is an ohmic resistance (R_e) term that represent the electrical resistance of the grout.

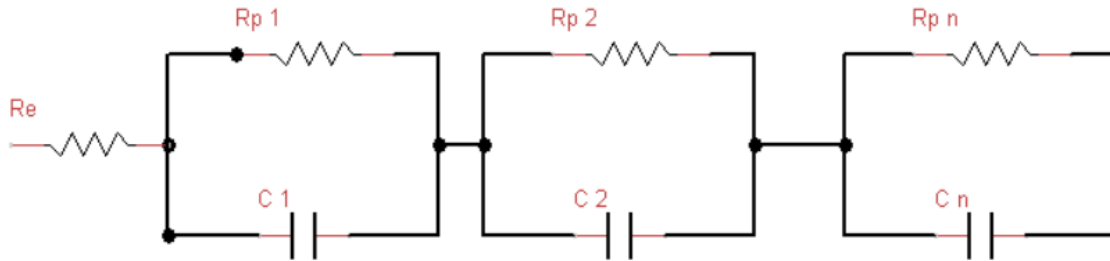


Figure 3-13: The Voigt electrical equivalent circuit model used in the regression software.

The impedance of the Voigt model may be expressed mathematically as

Equation 3-4
$$Z(\omega) = R_e + \sum_1^n \frac{R_{pn}}{1+j\omega C_n}$$

where a summation term describes the series contribution of the individual Voigt elements. A regression tool is used to fit the mathematical expression to the impedance data in a sequential fashion ending with the most elements possible while maintaining the appropriate confidence intervals for each parameter. Once the equation has been regressed to the data, the parameters are used to extrapolate the fit to frequencies of 0 and infinity. The real impedance value at infinite frequency represents the ohmic resistance while the difference in the real impedance between the frequency limits represents an estimate the polarization resistance. The result is a conservative estimate of polarization resistance that provides the greatest likely corrosion rate based on the impedance results.

The calculated polarization resistances were used to determine corrosion current using the Stern-Geary expression (Equation 3-5).

Equation 3-5
$$I_{corr} = \frac{\beta}{R_{pCalc}}$$

The variable β is recognized as the Stern-Geary constant and was assumed to be 26 mV which is the value commonly associated with iron (Fe) corrosion. The corrosion current may be converted to corrosion rate according to Faraday's law as long as the corroding surface area is known.

For the 1ft tendons, the surface area is simply based on the length of the strand in contact with the grout. Since the indirect impedance method used for the 3ft tendons does not directly polarize the steel, a finite element model was used to relate the measured polarization resistance to the surface-averaged value. This was done by calculating the oscillating potential distribution throughout the model geometry representing the grout for a range of frequencies to obtain simulated impedance values provided the measurement geometry and grout resistivity. The indirect impedance depends on the thickness of the grout cover, the grout conductivity, the size and location of the electrodes, and the steel polarization resistance. The geometry of the tendon representation was constructed to simulate the 3ft test specimens. Details of the governing equations and boundary conditions used in the impedance simulation may be found in the final report of FDOT project BDV31-977-35.

The result of the model simulations is a calibration curve, Figure 3-14, that may be used to relate the measured polarization resistance in Ω to the true polarization resistance of the steel and grout interface in $\Omega\text{-cm}^2$ provided the grout resistivity is known. Calibration curves are provided for 3 different grout resistivities. By scaling each axis by the resistivity of the grout, the curves superpose facilitating the use of a single expression that relates the measured polarization resistance to the true value of the steel and grout interface. With this approach, it is not necessary to estimate the polarized area of the steel. The equation of the overlapping constant sloped portion of this plot may be expressed as

Equation 3-6
$$\frac{R_{p,true}}{\rho} = 0.0178 \left(\frac{R_{p,meas}}{\rho} \right)^{0.99}$$

where the coefficient of 0.0178 may have units of cm^2 if the exponential term is equal to one.

All of the measured values of polarization resistance scaled by the grout resistivity corresponded to values within the constant sloped portion of this plot. The resistivity of the grout was measured using test cylinders according to the procedure described in Section A and Equation 3-1 Equation 3-2 to convert the measured resistance to resistivity. Due to the near unity value of the power in Equation 3-6, any error in the measurement of resistivity has little influence on the calculation of the true polarization resistance.

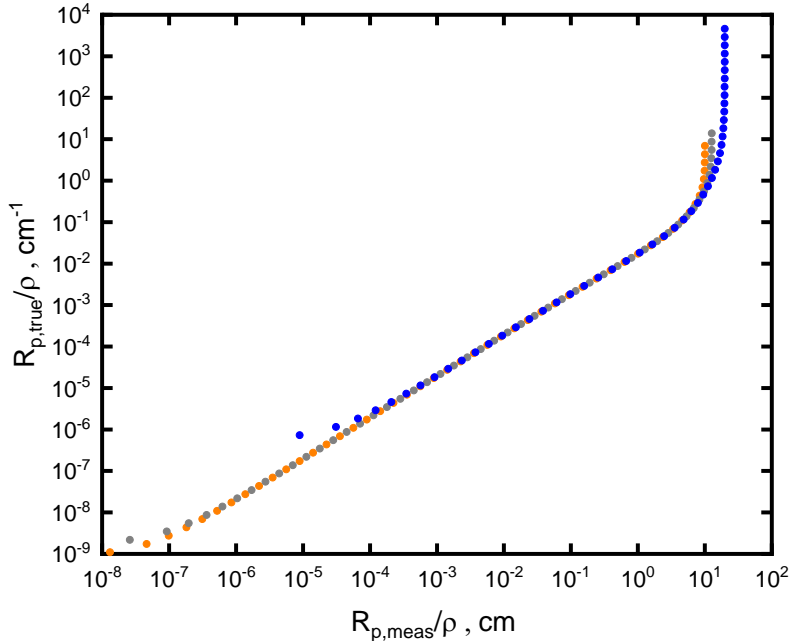


Figure 3-14: The calibration curve of polarization resistances multiplied by the relative grout conductivities

3.2.1 RESULTS AND DISCUSSION

Results are presented for the 1ft and 3ft tendons with and without impregnation fluid over a period of ~250 days (>8 months). The corrosion rates obtained as a function of time provide an indication of the impregnation fluid's ability to arrest corrosion that has initiated or prevent corrosion from occurring while the ohmic resistance provides indication of the ability of the impregnation fluid to penetrate the grout pores which will likely reduce the need for re-impregnation.

3.2.1.1 1-FT TENDONS

The corrosion rates of the 1ft tendons without chloride contamination is shown in Figure 3-15 a. Prior to impregnation, the corrosion rate decreased with time as the grout continued to cure and the passive film developed on the steel surface. After 50 days, a relatively steady value is reached of ~ 0.04 $\mu\text{m}/\text{yr}$ which would indicate passive behavior. Upon impregnation, the rates increased slightly but then trailed off and returned to the previous value prior to impregnation. The increase in corrosion rate following impregnation may be a result of the inhibition mechanism. Despite the slight increase, the corrosion rate values were indicative of passive behavior.

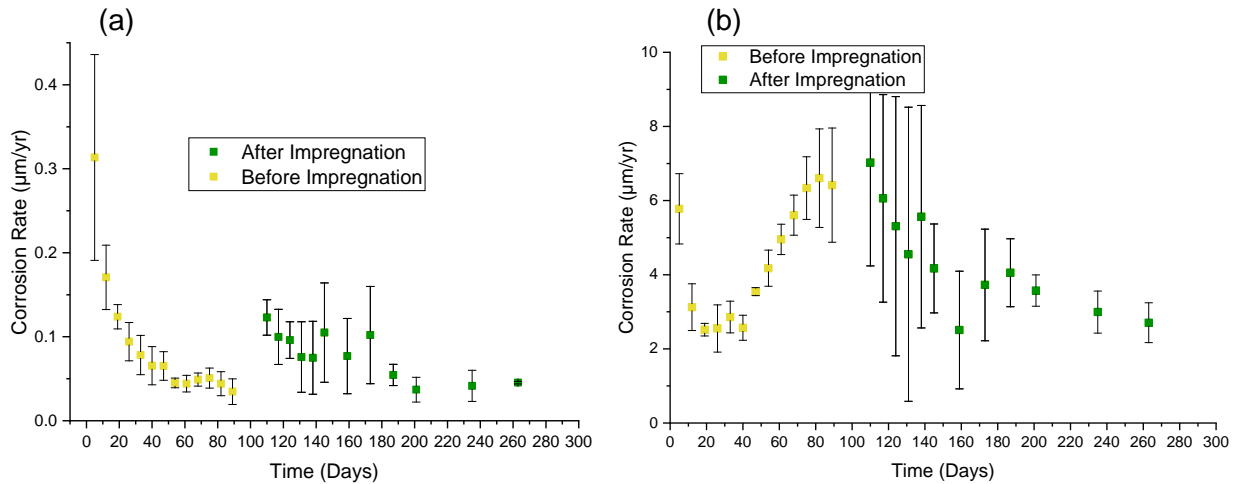


Figure 3-15: Corrosion rate as a function of time prior to and following impregnation of 1-ft tendons: (a) Chloride-free; (b) Chloride-contaminated

The corrosion rates as a function of time prior to and following impregnation for the chloride containing 1-ft tendons is shown in Figure 3-15 (b). The corrosion rates obtained before impregnation ranged between 2 and 8 µm/yr, which is an order of magnitude greater than those of the chloride free tendons. The rates increased with time reaching an averaged maximum value of ~6.5 µm/yr after which impregnation caused a gradual decrease over 60 days before reaching a somewhat steady value of 3 µm/yr, and therefore reducing the corrosion rate by half of the maximum value prior to impregnation. While the impregnation value reduced the corrosion rates, the final values were still much greater than those of the chloride free tendons possibly indicating that some corrosion was still occurring. Since corrosion rates reported are surface averaged values, it will be important to ensure that the impregnation fluid was effective in arresting corrosion across the entire surface.

Another function of the impregnation fluid is to penetrate the pores of the grout and increase its resistivity and therefore limit macrocell corrosion. The increase in the ohmic resistance of the grout obtained from impedance measurements is presented in Figure 3-16 (a) for the normally grouted 1-ft tendons. Prior to impregnation, the grout resistance increased due to continued curing. Following impregnation, there was a slight increase in the grout resistance of ~ 300 Ohms, effectively causing an increase of 25-30%. While an increase in grout resistivity should reduce macrocell corrosion rates, model simulations presented in Chapter 3 Section C showed that the affect on the macrocell current would be minimal.

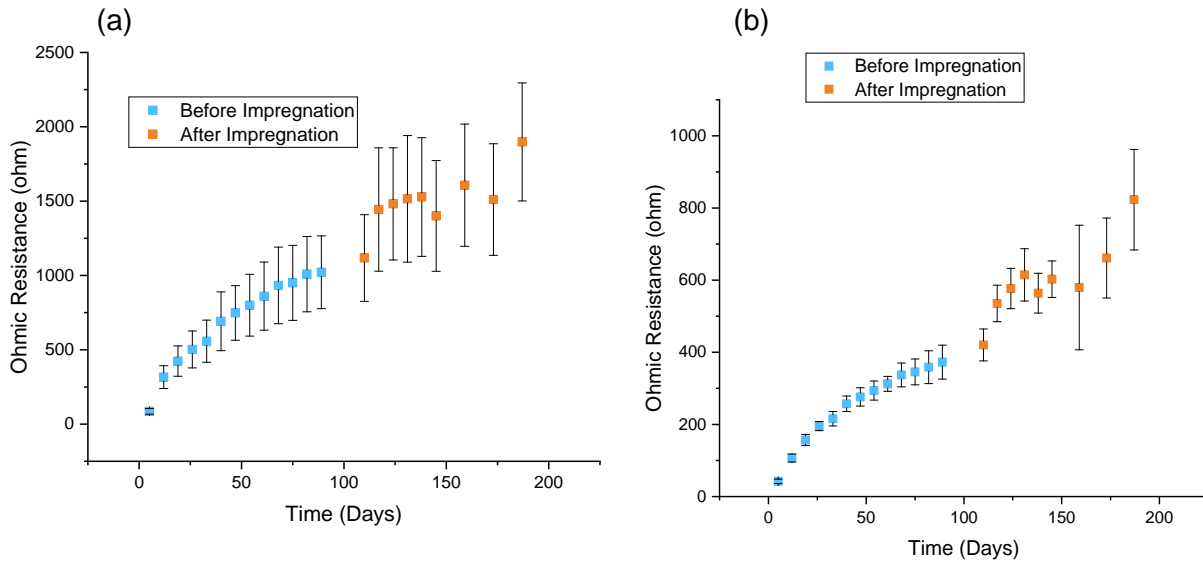


Figure 3-16: The ohmic resistance of the grout contained within the 1-ft tendons before and after impregnation: (a) Chloride-free; (b) Chloride-contaminated

As was the case with the chloride-free tendons, the impregnation fluid caused an increase in the grout resistance as shown in Figure 3-16b. In this case, the grout resistance continued to increase more so over time than in the chloride free grout which may indicate subsequent fluid penetration into the grout as well as some degree of continual grout aging. Nevertheless, the ohmic resistance of the impregnated chloride contaminated grout was still half of that of the chloride free grout.

3.2.1.2 3-FT TENDONS

An indirect impedance spectroscopy method was used to obtain the corrosion rate plots described in this section. The first calculation for estimating corrosion rate after impregnation indicated an increase in corrosion rate after impregnation which was not an expected result. The increase in corrosion rate was attributed to the increase in ohmic resistance due to the impregnation fluid within the pores and interstitial spaces in the grout. The finite element model used to calculate polarization resistances in the indirect approach required an input parameter for the conductivity of the grout. However, the conductivity of the grout changes upon impregnation thus producing inflated estimates for corrosion rate. To correct for the inflation, a correction factor was obtained based on the ratio between the ohmic resistance of the 1 ft tendons before and after impregnation. Upon developing this correction factor, the indirect measurements were corrected by computing the product of the correction factor and the polarization resistances from impedance data after impregnation. The following figures provide corrosion rate information after applying the correction factor.

The indirect impedance measurement only senses the location of the strands directly beneath the location of the electrode array. Therefore, the corrosion rates presented are only indicative of the central portion of the 3ft tendons. The corrosion rates as a function of time are presented in Figure 3-17a for the chloride-free tendons. The impregnation caused an abrupt and substantial decrease in the corrosion rates of almost an order of magnitude, greatly exceeding the reduction in corrosion rates measured on the 1ft tendons. It is odd that this behavior was not

observed for the 1ft chloride-free tendons but there may be more variation in the application of the impregnation material in the longer tendons possibly resulting in locations of excess fluid. Another possible explanation is that the longer tendons contained 3 bundled strands that may have provided easier flow of impregnation fluid.

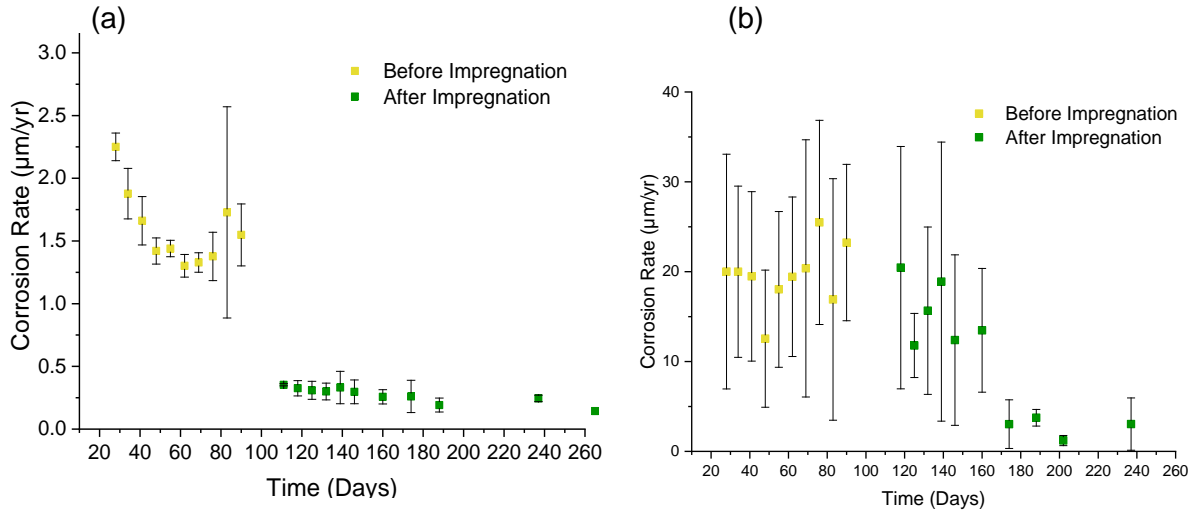


Figure 3-17: Corrosion rate as a function of time prior to and following impregnation of 3-ft tendons: (a) Chloride-free; (b) Chloride-contaminated

A more gradual decrease in the corrosion rates were observed following impregnation of the chloride contaminated 3ft tendons. Immediately after impregnation, it seems as though the fluid has little to no influence on the corrosion rates. However, after a period of ~60 days the rates decrease to 2-3 $\mu\text{m/yr}$, a reduction greater than an order of magnitude which greatly exceeds the reduction in corrosion rate measured on the 1ft chloride-contaminated tendons. As stated in Appendix 1 which details the impregnation procedure, impregnation of the 3ft tendons was adequate as indicated by complete fluid flow through the entire length of the tendon, which was not achieved for the 1ft chloride-contaminated tendons. The incubation time required for the impregnation fluid to cause a decrease in the corrosion rates could be due to the necessity of the fluid to penetrate into the already formed corrosion product layers.

The ohmic resistance as a function of time is shown in Figure 3-18a for the chloride-free 3ft tendons. In this case, impregnation resulted in an increase of the grout resistance by a factor of 10. Again, one possible reason for this is that the greater interstitial space available could have facilitated the flow of the impregnation fluid and perhaps allowed for a greater amount of the fluid to penetrate into the grout pore space. Interestingly, a similar increase in the ohmic resistance was not observed for the chloride-contaminated 3ft tendons, shown in Figure 3-18b. Nevertheless, the ohmic resistance was increased by a factor of 2 following impregnation.

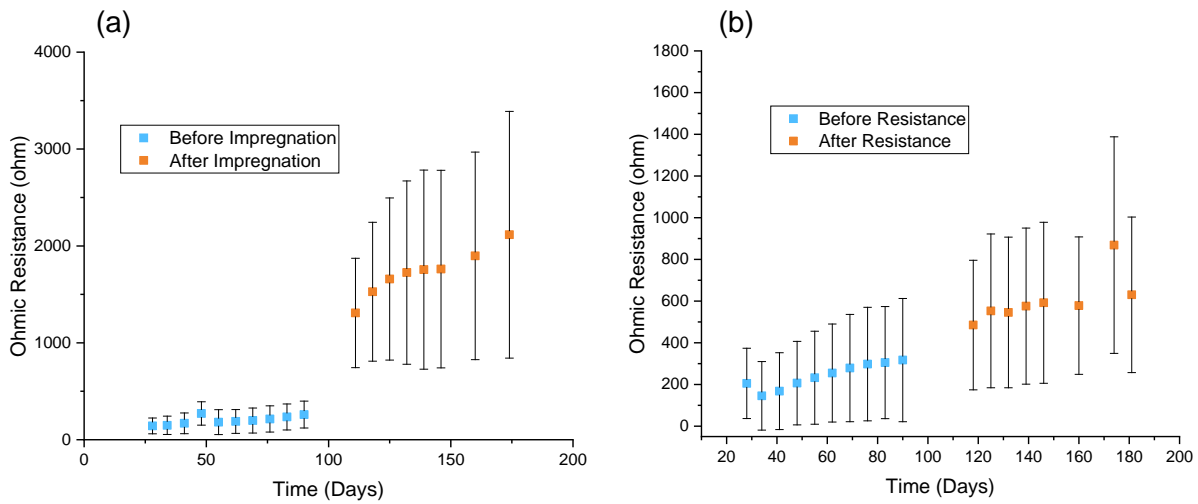


Figure 3-18: The ohmic resistance of the grout contained within the 3-ft tendons before and after impregnation: (a) Chloride-free; (b) Chloride-contaminated

An additional set of 3ft tendons were made comprising grout with a greater water to cement ratio in the hopes that a soft grout would be formed and therefore provide a scenario that may make the flow of impregnation fluid difficult. At the very least, the grout is expected to have a larger porosity than the chloride free grout mixed to the manufacturer's specifications. The corrosion rate and ohmic resistance is expressed as a function of time in Figure 3-19. Unexpectedly, prior to impregnation the corrosion rates were slightly less than the chloride free tendons indicating that the added water during mixing may not have had a significant impact on the grout quality. Following impregnation, however, the corrosion rates did not drop immediately as in the chloride free tendons but instead stayed relatively the same for ~ 80 days before decreasing by a factor ~60%.

The ohmic resistance prior to impregnation was similar to the values measured on the chloride free and contaminated tendons. Following impregnation, the ohmic resistance increased by a factor of 3 similar to the results of the chloride contaminated tendons. In this case the increase could be due to a slightly higher porosity as a result of the additional water added during the mixing process.

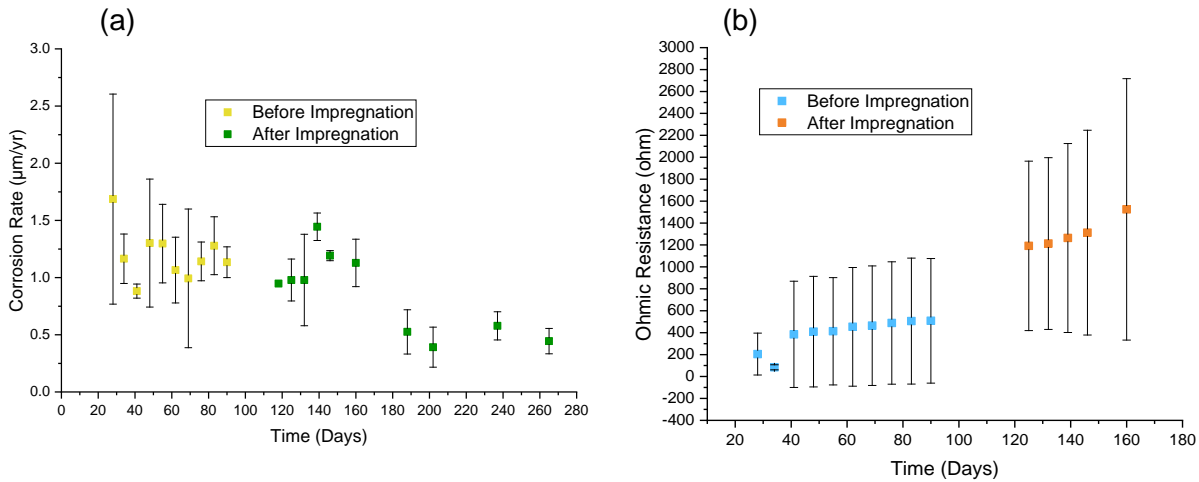


Figure 3-19: Results over time for a 3-ft tendon made with a high water to cement ratio: (a) Corrosion rate; (b) Ohmic resistance

3.2.2 FINDINGS AND IMPLICATIONS

For 3ft chloride contaminated tendons, the impregnation fluid was effective in arresting corrosion noted by the gradual decrease in corrosion rate upon impregnation of at least 1 order of magnitude. Conversely, difficulties in adequately injecting the VPF into the chloride-contaminated tendons, as detailed in Appendix 1, likely compromised its corrosion mitigating abilities as there was only ~ 50% decrease in corrosion rate (from 6.5 µm/yr to 3 µm/yr). The difficulty of impregnating the 1ft specimens was likely due to pre-existing corrosion products that may have blocked the flow of the fluid. Following impregnation, the resistance of the grout increased by a substantial enough amount to indicate that the increase could not be due to continued curing alone. Therefore, it is likely that the fluid was at least partially able to fill the grout pores and prevent adsorption of the corrosion protecting film present on the steel surface into the grout, which was likely the reason for the short service period of the alternative fluid. The corrosion rates have remained low up to 5 months following impregnation which is almost twice as long as the service period of the alternative fluid. Selected autopsies of control and treated tendons were performed to confirm the electrochemical testing results presented in this section. The autopsy results are presented in Chapter 5 along with tendon failure forecasts based on the corrosion damage results.

3.3 PREDICTIVE CORROSION MODELING

Predictive corrosion modeling of the impregnated tendon system was conducted to provide quantitative estimates of the effect of application of the impregnation treatment on a tendon that had already experienced chloride induced corrosion, under key representative scenarios. The experimental results discussed previously were used to choose corrosion kinetic parameters and grout properties to be used as input to the model. The model was built on a Comsol Multiphysics finite element platform. The model explored possible ways in which impregnation can mitigate corrosion by examining the effects on corrosion rate of increasing grout resistivity, decreasing oxygen transport (lowering oxygen diffusivity), or decreasing corrosion kinetics (lowering exchange current density as in cathodic, anodic or combined inhibition). The model assumed that active corrosion was taking place on only a part of the strand surface, and also examined the possible effect of enhanced localized corrosion if the active portion of the surface became even smaller.

3.3.1 DATA AQUISITION

The system simulated was a simple grouted PTT segment with a single axially placed 7-wire strand and a grout deficiency at the middle as shown in Figure 3-20. For simplicity, the strand geometry was considered as a uniform cylinder with effective circular diameter of 0.5". A centrally located 2" long segment of the strand (thus 20% of its surface) was designed as an actively corroding portion where anodic and cathodic reactions take place. The rest of the surface area of the strand was considered as a passive region where only cathodic reaction takes place. The grout was treated for simplicity as a homogeneous medium with uniform electrical and mass transport parameters.

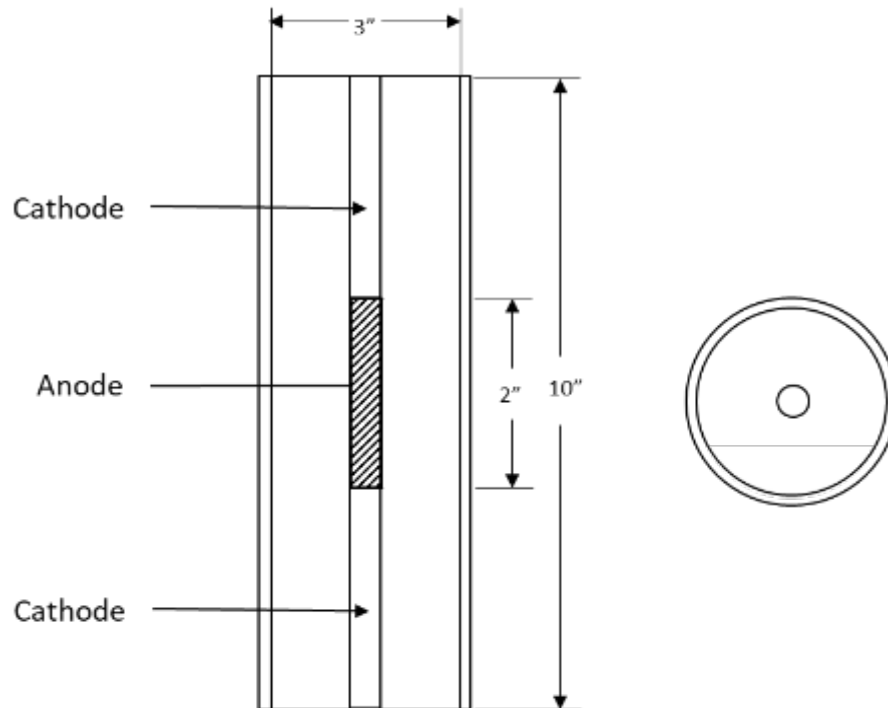


Figure 3-20: Concrete column schematic diagram

The predominant cathodic and anodic reactions on the steel surface were assumed to be respectively oxygen reduction (Equation 3-7, consistent with the usual alkaline conditions in cementitious systems) and iron dissolution (Equation 3-8)



For the main series of calculations, the PTT segment was regarded as having an electrically insulating external surface, and oxygen flow through the HDPE duct or through the end surfaces was not allowed. This assumption simulated an ideal condition where no cracks were present on the HDPE ducts and the ends were completely sealed. However, this assumption is not limiting and alternative cases where oxygen can penetrate through duct cracks such as those found in the Mid-Bay and Skyway bridges in Florida or even lengthwise via inter-strand interstices will be considered on discussion of the results. In this model, corrosion inside the tendon was addressed by the Time Dependent Study feature of the Comsol Multiphysics model.

The total initial oxygen concentration in the grout (moles per m³ of grout) was assigned a value $C_{eo} = 0.772 \text{ mol/m}^3$. The pores were assumed to be partially filled with pore solution, with a parameter $0 \leq Q \leq 1$ describing the degree of saturation, with $Q=1$ indicating pores filled with solution. Q was assumed to be = 0.5. The above value of C_{eo} was estimated from the oxygen concentration in the grout pore solution (assuming $C'_{eo} = 0.3 \text{ mol/m}^3$, corresponding approximately to water having been ideally in equilibrium with atmospheric oxygen), and the amount of oxygen present in gas (assumed to be air) in the remaining pore space⁸³, by;

Equation 3-9:
$$C_o = C'_o * \varepsilon * S$$

Equation 3-10:
$$S = Q + R(1 - Q)$$

where ε is the volumetric porosity of the grout (assumed to be 0.15), R is the equilibrium ratio of oxygen concentration in pure water to that in air, both in mass per unit volume, resulting in $R = 33.33$ for assumed normal atmospheric conditions (oxygen concentration in water value at 760 mmHg and 24 °C⁸⁴) and adopted for this model. The diffusion coefficient of oxygen in grout (D_o) was assumed to be of value consistent with that used by Kranc⁸³ in other models for concrete of intermediate moisture conditions. The value D'_o used in that work corresponds to the proportionality between gradient of concentration of oxygen in pore water and oxygen flux in the bulk of the concrete. Since here the oxygen concentrations are given per unit volume of grout, the corresponding value D_o used for this model is obtained by

Equation 3-11:
$$D_o = \frac{D'_o}{\varepsilon * S}$$

The polarization behavior for active dissolution and oxygen reduction was determined following Butler-Volmer kinetics⁸⁵, where the anodic reaction taking place on the anodic region is given by;

Equation 3-12:
$$ia = ioa * 10^{\frac{E - E_{oa}}{\beta a}}$$

with E being the potential of the steel minus that of the grout as measured by a reference electrode ideally placed in the grout at a point immediately next to the steel surface, the various parameters described and assigned values in Table 3-2, and the c and a subscripts denoting cathodic and anodic reaction, respectively.

Table 3-2: Parameters and variables with descriptions and values

Parameters / variables	Description	Value
ε	Porosity	0.15
Q	Degree of saturation	0.5
R	Ration of oxygen concentration in water to that in air	33.33
β_a	Tafel slope for the anodic reaction	102 mV
β_c	Tafel slope for the cathodic reaction	140 mV
C_{eo}	Effective oxygen concentration estimated by Equation 3-9 and 11.	0.772 mol/m ³
D_o	Effective oxygen diffusivity, estimated by Equation 3-11.	Range
E_{oa}	Nominal redox potential for the Fe/Fe ²⁺ + 2e system	-600 mV
E_{oc}	Nominal redox potential for the OH ⁻ /O ₂ + 2H ₂ O + 4e system	80 mV
i_{oa}	Nominal exchange current density for the Fe/Fe ²⁺ + 2e system	Range
i_{oc}	Nominal exchange current density for the OH ⁻ /O ₂ + 2H ₂ O + 4e system	Range
ρ	Grout resistivity	Range
c_o	Oxygen concentration at a point in the bulk of the grout	Model output

The concentration dependent cathodic reaction was chosen to take place on the active and passive region on the steel strand according to the following;

Equation 3-13:
$$i_c = -i_{oc} * \frac{c_o}{C_{eo}} * 10^{\frac{E_{oc}-E}{\beta_c}}$$

The mass flux (N) of oxygen associated with its reduction at the entire surface of the steel strand is given by;

Equation 3-14:
$$N = \frac{i_c}{n * F}$$

In a time dependent coordinate system, the current density distribution in the grout domain is given by a general form of ohm's law (ignoring displacement currents in this slowly evolving system);

Equation 3-15:
$$J = \sigma * E_f$$

where J is the current density (A/m²), σ is the electrical conductivity of the grout (S/m) and E_f is the electric field (V/m).

The transport of oxygen was modeled using a transport of diluted species interface. Only a diffusional transport mechanism was selected. The mass balance is given in the bulk of the grout;

Equation 3-16:
$$\frac{\partial c_o}{\partial t} + \nabla \cdot (-D_o \nabla c_o) = 0$$

where c_o is the concentration (mol/m³) and D_o is the diffusion coefficient (m²/s) of oxygen, respectively.

The cathodic and anodic parameters in table 1 (i_{oc} , i_{oa} , β_c , and β_a) were assigned values that approximated results from PD tests such as those shown in Figure 3-8.a, choosing the data for day 26 (chloride-induced corrosion already in progress) as a representative example. The parameter values chosen are intended for exploratory purposes and subject to more refined evaluation in follow up investigation. Resistivity values were chosen for a base condition (PTT without impregnation) representative of mature grout (1000 Ω .m, corresponding to the FWAP-measured values shown in Figure 3-3 for age ~ 80 days), with variations above and below the base condition values. Variations for oxygen diffusivity and exchange current densities were considered only for values smaller than the base condition, to serve as a test of alternative hypotheses of corrosion mitigation by the decrease of either of those parameters. The portion of the strand surface that was designated as anodic was kept at 20% for base condition calculations.

Equations (9) through (13) were solved simultaneously to yield the electrical potential and oxygen concentration in the grout domain, from which the corresponding current densities at the strand surface are derived. The various simulation scenarios were modeled by varying one parameter while fixing the others as listed in

Table 3-3.

Table 3-3: List of scenarios modeled and parameters used

Parameters	Base conditions	Variations	
P (Ω .m)	1000	500	5000
D_o (m ² /s)	1×10^{-8}	1×10^{-9}	1×10^{-10}
i_{oc} (A/m ²)	3×10^{-5}	3×10^{-6}	3×10^{-7}
i_{oa} (A/m ²)	1×10^{-4}	1×10^{-5}	1×10^{-6}
Fraction of strand surface that is anodic (%)	20	0.2, 2, 6, 10	

Simulations were normally performed using the finest predefined element size setting in the model platform, labeled as “Extremely Fine”. Results sensitivity to mesh refinement and coarsening was examined by choosing one case ($\rho = 1000 \Omega$.m, $D_o = 1 \times 10^{-8} \text{ m}^2/\text{s}$, $i_{oa} = 1 \times 10^{-4} \text{ A/m}^2$, and $i_{oc} = 3 \times 10^{-5} \text{ A/m}^2$) and using as a metric the percent change in anodic current density

after 40 days for different mesh sizes. The calculations for that case were repeated using the predefined coarser mesh size setting labeled as “Extra Fine” and a custom finer mesh size with a maximum element size half as large as that used for the “Extremely Fine” setting. It was found that the measured value for either of the variations did not change by more than 1% from the normally evaluated value. That level of stability was deemed to be adequate for the comparative evaluations reported here.

3.3.2 RESULTS AND DISCUSSION

Because oxygen reduction was assumed to be the only cathodic reaction to take place, maps showing remaining oxygen concentration after a given age (chosen to be 100 days for the first set of examples) were selected as useful indicators of corrosion conditions. As simulation time increases, oxygen starts to deplete due to its consumption by the cathodic reaction. The minimum oxygen concentration values are found near the anodic region of the steel strand where corrosion potentials are expected to be lowest.

The possible effects of tendon impregnation (e.g., lowered oxygen diffusivity and the other variations contemplated in Table 3-3) are shown in Figure 3-21 through Figure 3-24 as projected maps of oxygen concentration in mol/m³ at 100 days age. Each figure reproduces at the left (a) the final oxygen map for the base conditions in Table 3-3. The other maps to the right (b,c) show the effect of the particular parameter variation addressed in each figure. The minimum and maximum values of the color legends of these maps serve to compare final oxygen concentration for the various cases. The color-coded trends were found to match expected results, i.e., for a given age, the amount of consumed oxygen decreased with increase in grout resistivity and with decreases in oxygen diffusivity as did the kinetic constants for the interfacial reactions (exchange current densities i_{oc} and i_{oa}). A decrease in the amount of oxygen consumption is an indicator of the decrease in corrosion activity. The color gradient maps also indicated that, consistent with the model premises, oxygen was consumed by the cathodic reaction (Equation 3-8) over the entire length of the steel strand.

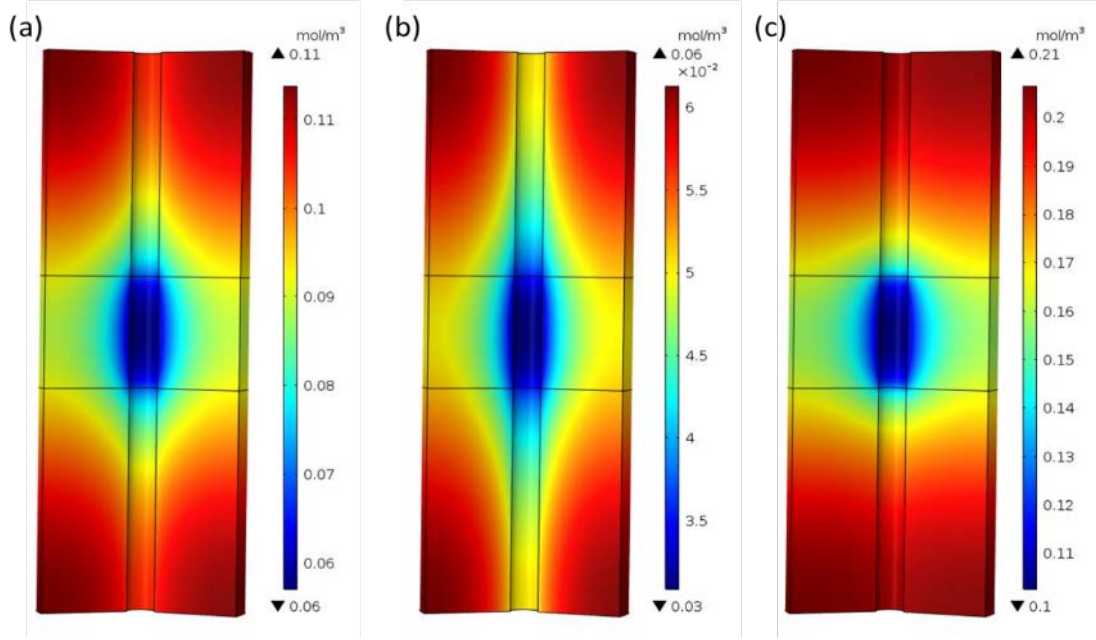


Figure 3-21: Grout resistivity effect on oxygen concentration maps after 100 days for (a) $\rho = 1,000 \Omega m$, (b) $\rho = 500 \Omega m$, and (c) $\rho = 5,000 \Omega m$

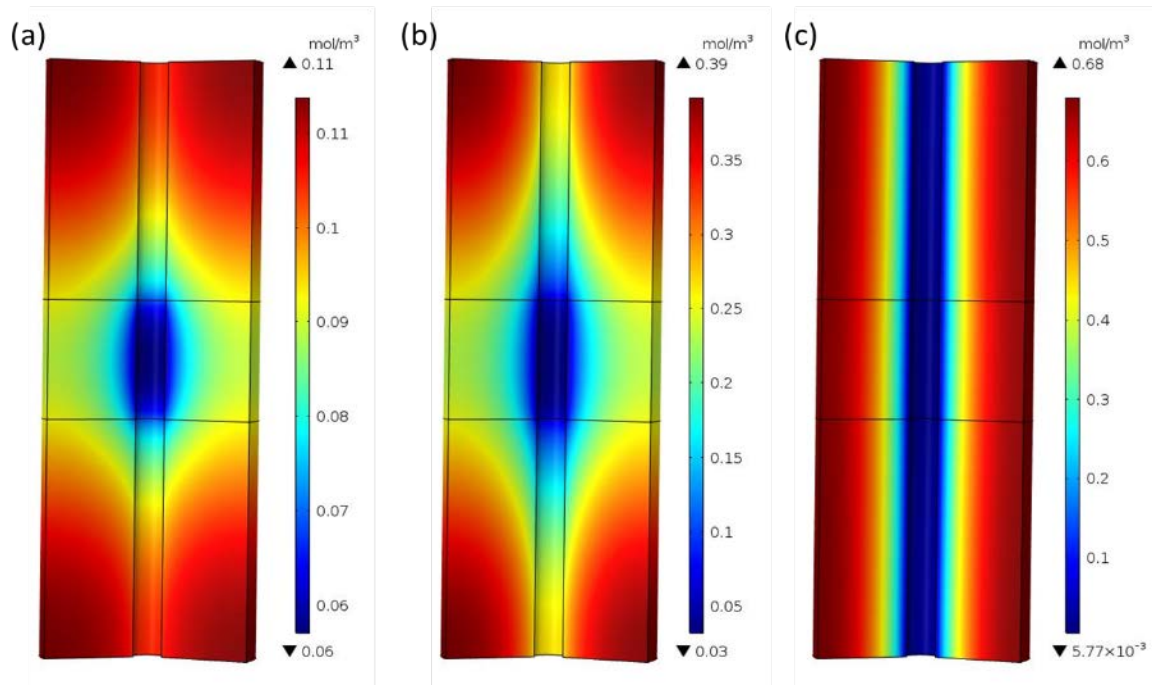


Figure 3-22: Oxygen diffusivity effect on oxygen concentration maps after 100 days for (a) $D_0 = 1 \times 10^{-8} m^2/s$, (b) $D_0 = 1 \times 10^{-9} m^2/s$, and (c) $D_0 = 1 \times 10^{-10} m^2/s$

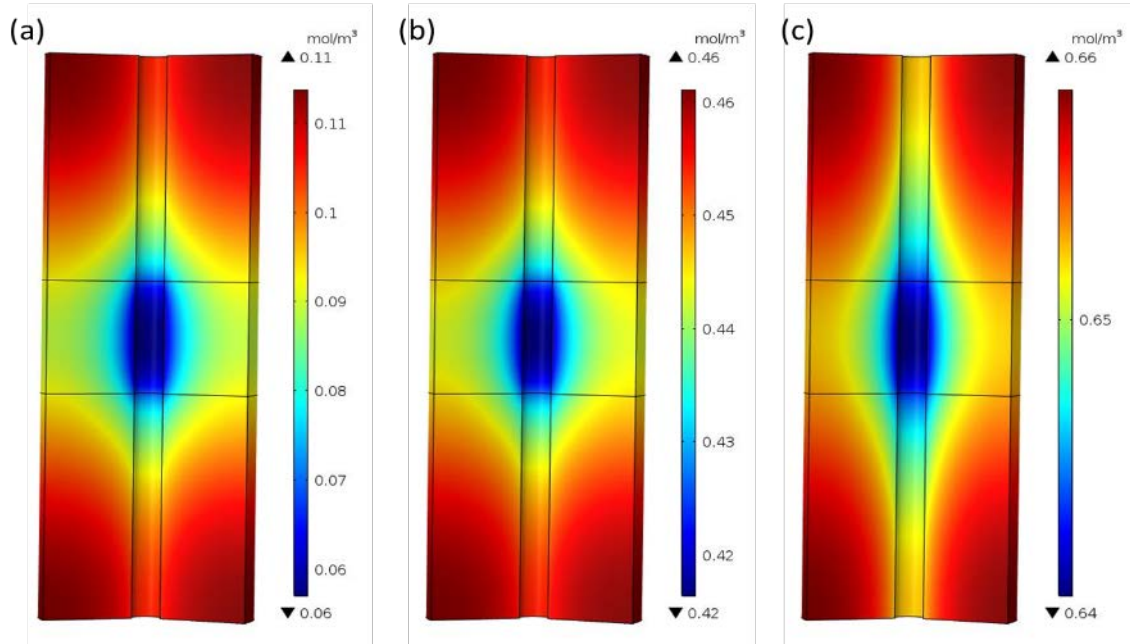


Figure 3-23: Cathodic exchange current density effect on oxygen concentration maps after 100 days for (a) $i_{oc}=3 \times 10^{-4} \text{ A/m}^2$, (b) $i_{oc}=3 \times 10^{-5} \text{ A/m}^2$, and (c) $i_{oc}= \times 10^{-6} \text{ A/m}^2$

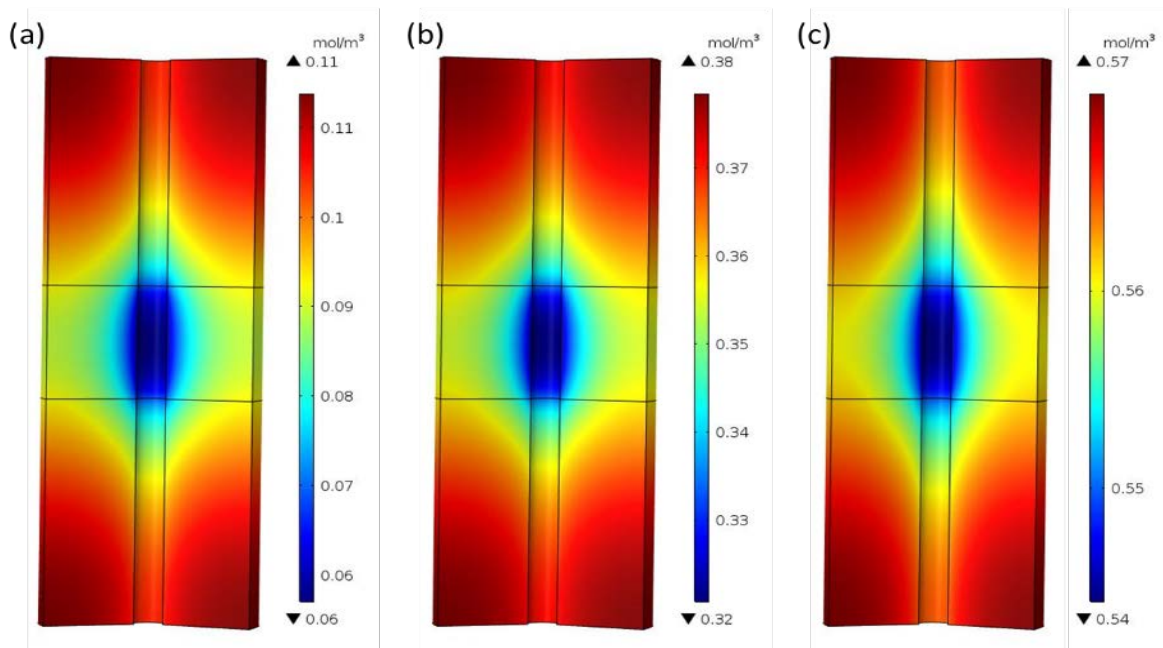


Figure 3-24: Anodic exchange current density effect on oxygen concentration maps after 100 days for (a-base) $i_{oc}=3 \times 10^{-4} \text{ A/m}^2$, (b) $i_{oc}= \times 10^{-5} \text{ A/m}^2$, (c) $i_{oa}=3 \times 10^{-6} \text{ A/m}^2$

The above results indicated reasonable model operation and, projected that for many of the conditions explored, much of the native oxygen had been consumed by age 100 days. To better establish differentiation between the corrosion rates prevalent in the various cases,

corrosion extent was further examined by evaluation at a shorter system age, i.e. 40 days, leaving discussion of longer-term regimes to the end of this section.

The time-integrated corrosion rate was expressed as local steel strand radius loss in μm at age 40 days. This was done under the idealized geometric assumption of a solid cylindrical strand with a diameter of 0.5 in. It is understood that in the actual system, corrosion geometry will involve more complicated cases with localization in individual strand wires. As it will be shown next, however, that simplification provides ample insight on the questions at hand. The radius loss was calculated by Faradaic conversion after integrating the anodic current densities in A/m^2 (after 40 days, $1 \text{ A}/\text{m}^2$ corresponds to $\sim 130 \mu\text{m}$ radius loss). The results were in good agreement with the consumption of oxygen noted earlier, and are plotted in Figure 3-25 as a function of the position in the PTT segment length, all cases with the base anode size of 20% of the strand length. The projected radius loss of the steel strand was found to decrease from $\sim 3 \mu\text{m}$ to $\sim 1.3 \mu\text{m}$ and to $\sim 0.5 \mu\text{m}$ by decreasing the cathodic exchange current density by one and two orders of magnitudes, respectively. Likewise, the projected radius loss of the steel strand was found to decrease from $\sim 3 \mu\text{m}$ to $\sim 1.7 \mu\text{m}$ and to $\sim 0.8 \mu\text{m}$ by decreasing the anodic exchange current density by one and two orders of magnitudes, respectively. These relatively modest amounts of reduction of projected radius loss did not correspond well with the strong decrease (by an order of magnitude or more) in corrosion rate upon impregnation that was estimated from the experimental results in Sections A and B of this chapter. However, when simultaneously decreasing both anodic and cathodic exchange current densities by the same amounts indicated above (Figure 3-25.c), the projected radius loss of the steel strand was found to decrease from $\sim 3 \mu\text{m}$ to $\sim 0.5 \mu\text{m}$ and to $\sim 0.08 \mu\text{m}$ respectively. This much stronger decrease is in closer agreement with the results from the mechanistic experiments in section A, supporting corrosion mitigation via a decrease in surface kinetics as long as both the anodic and cathodic reactions are being hindered.

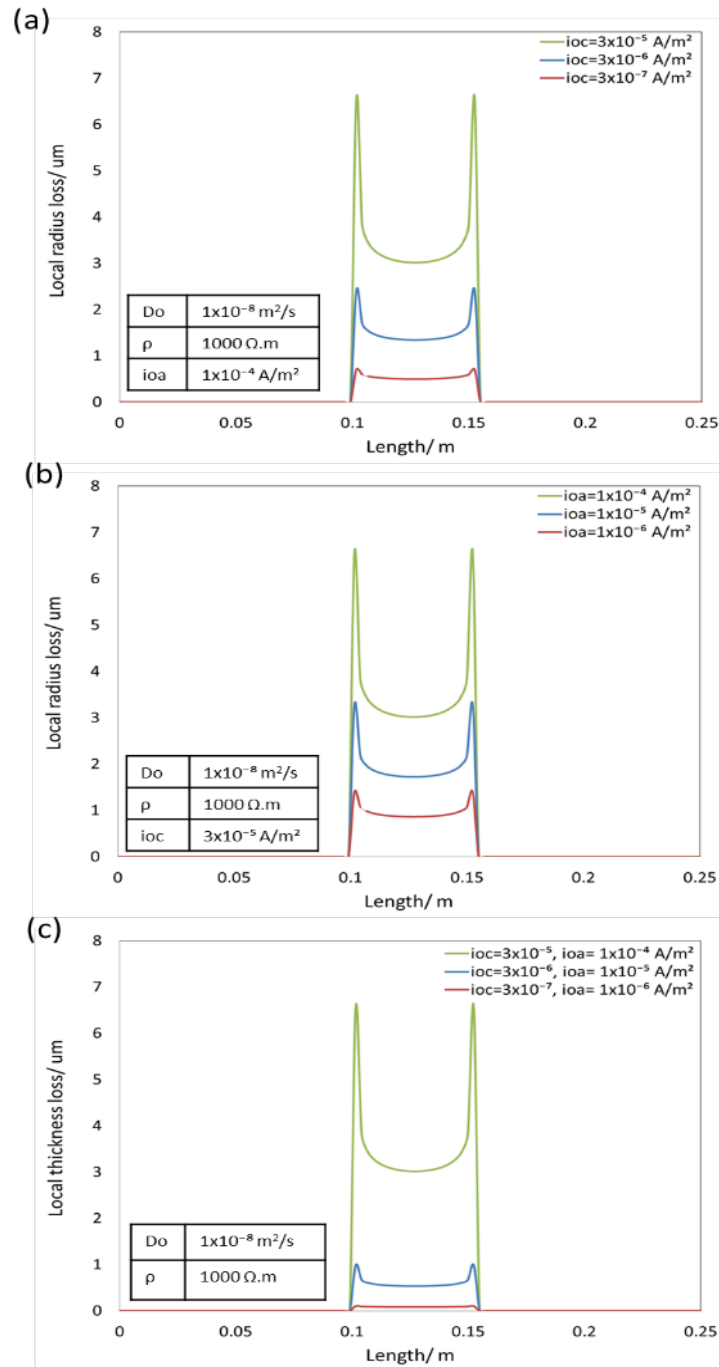


Figure 3-25: Local radius loss at day 40 for varying (a) ioc, (b) ioa, and (c) both ioc and ioa. The green profile corresponds to baseline conditions. All variations are for an active zone of 20% of the strand length.

Increasing grout resistivity (Figure 3-26.a) was found to have only a minor effect in the projected amount of corrosion, also consistent with the interpretation of the experimental findings. The model projections also indicated some degree of corrosion mitigation by decreasing oxygen diffusivity (Figure 3-26.b). The projected mitigation was however relatively

modest (by about a factor of three when the oxygen diffusivity was lowered even by a factor of 100). This result seems to be consistent with the lack of experimental signs of significant oxygen transport corrosion limitation, noted in section 4.2.

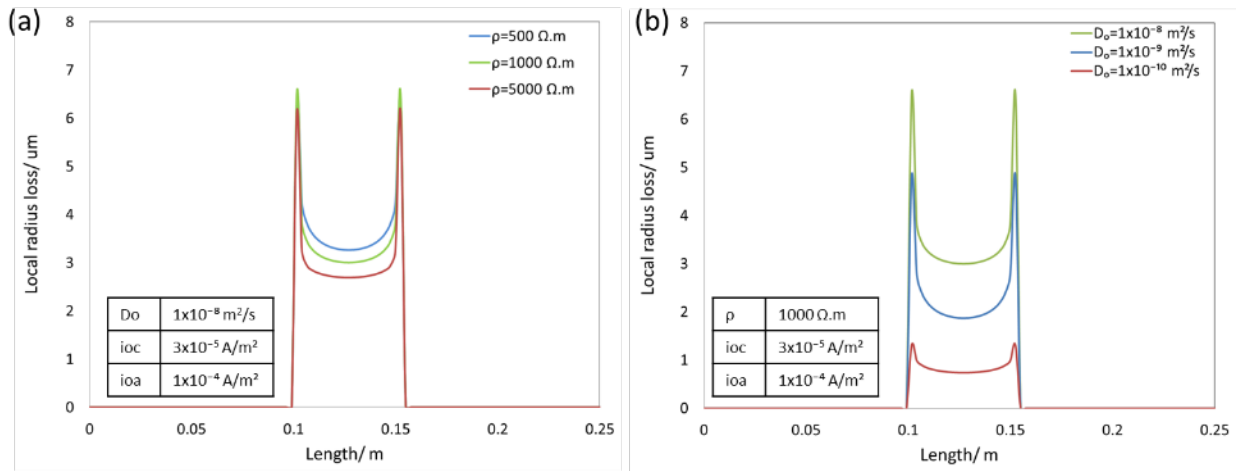


Figure 3-26: Local radius loss at day 40 for varying (a) grout resistivity, (b) oxygen diffusivity. The green profile corresponds to baseline conditions. All variations are for an active zone of 20% of the strand length

Concerning possible detrimental electrochemical effects of impregnation, as reported elsewhere⁸⁷, it is noted that if an anodic inhibitor was added in insufficient quantity, corrosion rate could be locally enhanced by coupling between small anodes and relatively large cathodes. This may lead to much higher local corrosion rates⁸⁸. This situation was simulated by considering the effect of decreasing the percent of the central region that was actually anodic (Figure 3-27) to values less than the 20% base value. The corrosion extent in the restricted anodic regions increased, as expected. Restricting the anodic zone to just 0.02% (100 hundred times less than the 20% base condition) of the central region resulted in an amount of local radius loss (96 μm after 40 days) which is much higher than the loss when 20% of the strand is anodic (3 μm after 40 days). This issue should be revisited in later stages of this project, for example by autopsy of specimens after exposure testing.

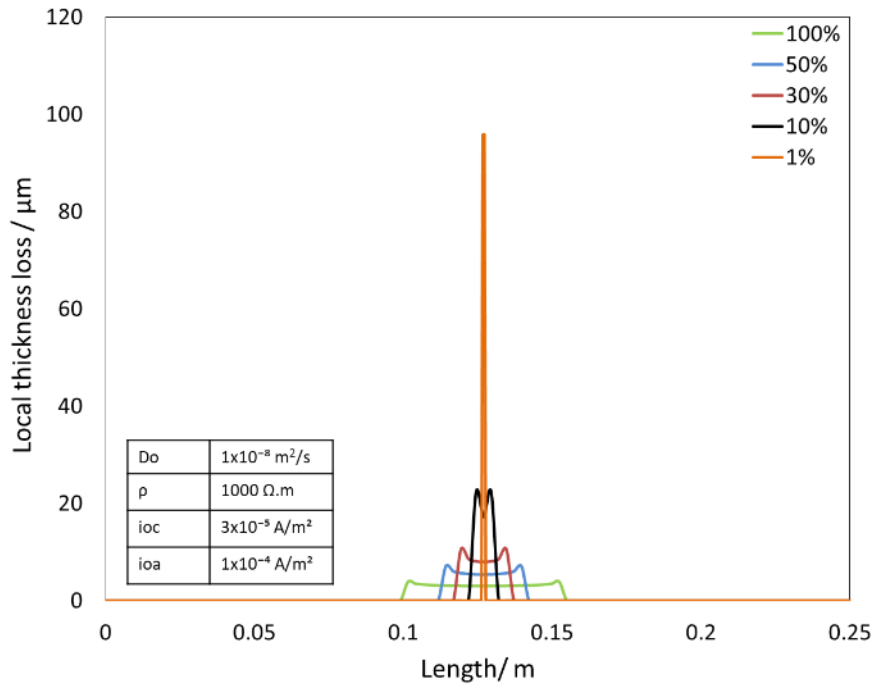


Figure 3-27: Local radius loss at day 40 for varying active anodic size. Baseline conditions. 100% corresponds to the entire central 5-cm-long region being active.

It is also of interest to consider how much corrosion deterioration could take place in the absence of protective action. The simulations assumed an ideal condition where no cracks are present on the HDPE ducts and the ends were completely sealed, so oxygen was not allowed to replenish to support the cathodic reaction. Figure 3-28.a showed the time evolution of average oxygen concentration of the entire grout domain and radius loss averaged by the length of the anode. The model projected that for the base condition the native oxygen was nearly completely consumed by age ~ 140 days. In such case, the maximum projected radius loss with 20% anode localization was $< 8 \mu\text{m}$. An idealized steel strand under these conditions would retain more than 99.7% of its cross-sectional area as shown as a solid line in Figure 3-28.b. Such small loss under ideal conditions would seemingly have little effect on mechanical performance, and supplemental protective measures such as impregnation would be of limited need barring some form of extreme localization of corrosion as noted above. However, the assumption of no oxygen replenishment is not limiting. An alternative case where oxygen is allowed to replenish inside the duct by penetrating through duct cracks, or even lengthwise via inter-strand interstices, was simulated for the otherwise base condition as well. As shown by the dashed line in Figure 3-28.b, the corrosion continues at an even rate. Under that simplified nominal scenario the steel strand in that case would be projected to lose 30% of its cross-sectional area in ~ 20 years, a severe durability reduction. Moreover, even shorter time to damage events would be projected if all the corrosion were concentrated on only one or two wires. Consequently, corrosion protective and prevention practices including impregnation would be much needed in those cases.

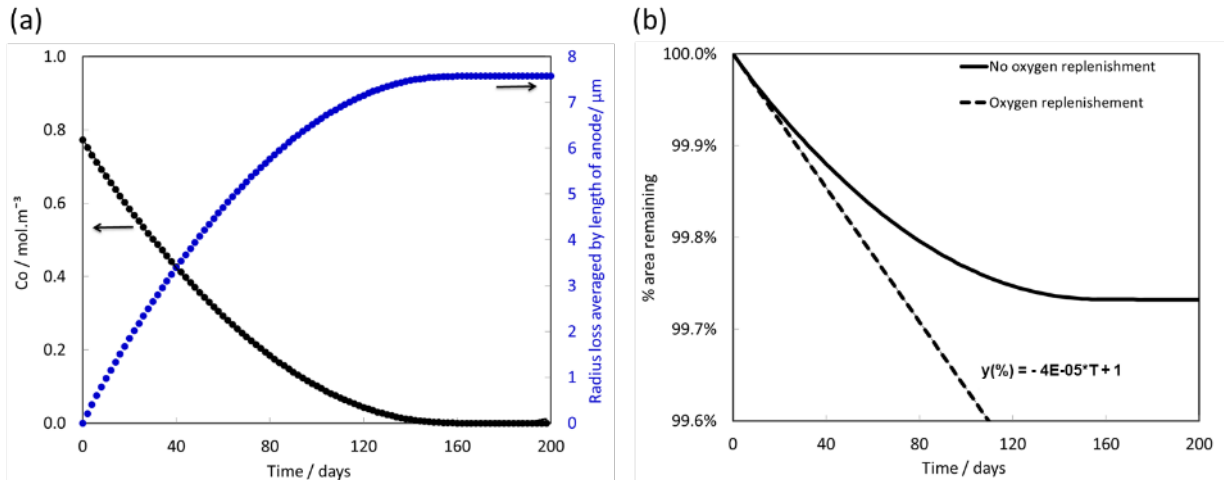


Figure 3-28: (a) Evolution with time of oxygen concentration and nominal radius loss averaged over the anode. (b) Decay of percentage of remaining nominal strand cross sectional area with and without, oxygen replenishment. Calculations for base condition anode on 20% of the strand length.

3.3.3 FINDINGS AND IMPLICATIONS

The calculations explored the relative corrosion mitigation extent that could result from various anticipated impregnation consequences (decreases in exchange current density and in oxygen diffusivity and increases in grout resistivity). In general, the projected metal loss was found to be mitigated by decreases in the cathodic and anodic exchange current densities separately and to a higher extent by decreasing both of them simultaneously. The model projections also indicated some mitigation by a decrease in oxygen diffusivity. In contrast, even when assigned an initial value less than that of the base condition, increasing grout resistivity was found to have only a minor effect in the projected amount of corrosion. These outcomes therefore suggested a corrosion mitigation process associated with increases in both activation and concentration polarization, and less importantly by ohmic resistance polarization. With some qualification, the modeling results were consistent with the conclusions from the experiments. As a note of caution, the model identified a potentially adverse effect, consisting of enhancing the corrosion rates of remaining anodes, if the impregnation caused mainly an activation polarization increase on the anodic reaction but not covering the entire metal surface. The model calculations also indicated that for an ideal condition where oxygen was not allowed to replenish inside the HDPE duct, supplemental protective measures such as impregnation would be of limited need. However, for more realistic conditions of no-airtight ducts, or when oxygen might flow through strand's interstitial sites, the model projections supported the need for implementation of protection and or prevention practices.

CHAPTER 4 BOND STRENGTH TESTING

While the results of Chapter 3 indicate that the alternative fluid and the VPF is capable of at least temporarily arresting corrosion, there remains concern of the possible adverse affect on the bond strength within PTT. The objective of the work presented in this chapter was to recreate the defects that occur in grouted post-tensioned tendons, determine the bond effects of defective grout, evaluate the injection capabilities of various penetrants, and determine whether the penetrant adversely affects bond after impregnation. Two alternative fluids (WD-40 an PB Blaster) as well as the VPF were tested and the results are presenting in two separate sections.

4.1 ALTERNATIVE FLUIDS

The procedure for creating voids in small scale, single strand tendons/ducts was a trial and error process because at present, there are no suitable methods for creating grouting deficiencies. The process results for each trial and error will not be discussed in detail, however, the best suited procedure for creating defective grouted ducts will be discussed.

4.1.1 CONCRETE SPECIMEN TESTING

To prepare mono-strand tendons for testing bond strength capacities, 24 samples were cut from a 24-ft long, 14-in square prestressed pile each at 1-ft lengths as shown in Figure 4-1. Using prestressed concrete pile specimens provided a convenient means to load the specimens without splitting bond failures due to the standard spiral steel confinement. After cutting the pile into 1-ft long segments, four individual 1-in diameter holes were cored into the end / cut faces of the segments positioned on the inside of the confinement steel shown in Figure 4-1.

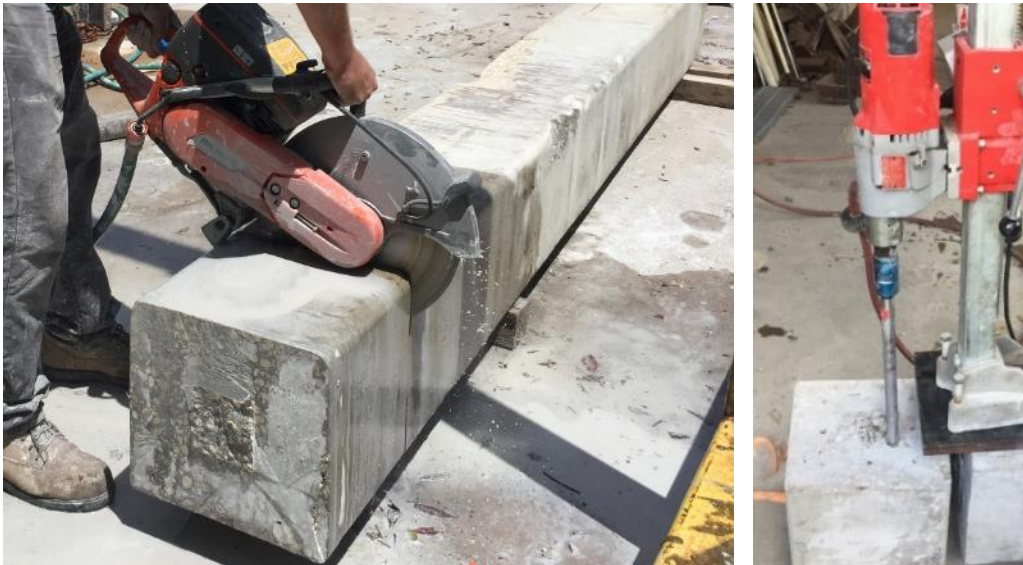


Figure 4-1: Cutting 14-inch square pile for concrete specimens and coring simulate duct corridors into 1ft concrete segments

4.1.1.1 CONSTRUCTION OF CONCRETE SPECIMEN 1

The duct grouting procedure that will be described is this procedure was adopted from the trial and error process previously discussed. After four ducts were cored out of the concrete,

four 48-in long ½-in prestressing strands were cut and set aside. ¾-in I.D. SCH 40 PVC (1-in O.D.) pipe was cut into eight 3-in long length sections as extension to snugly fit into the 1-in core holes. PVC elbows and end caps were drilled with a 9/16-in diameter hole in the center for strand installation. The elbows and end caps were slid onto each of the 3-in-long PVC pipe sections, and the completed half sections were wrapped in duct tape 1 in of the free end creating a de-bonded surface. The taped ends were placed into the concrete and the strands were fed through the 9/16-in holes in the PVC sections. Silicon was used around the 9/16-in holes and strands as well as the concrete faces and PVC duct extensions, which sealed any grout from leaking out. Before grout was installed, the front face of the concrete specimen was raised on a 2-in thick steel brick as shown in Figure 4-2. The syringe with flexible hose was filled with water and the hose was installed through the opening of the elbow until it reached near the back of the specimen. Table 4-1 shows the amount of grout, water, and water injected into each tendon for concrete specimen 1. Once tendons 1 and 2 were grouted and cured for one day, the specimen was flipped upside down for tendons 3 and 4 to be grouted. Figure 4-3 shows the entire grouting and water injection process.



Figure 4-2: Concrete specimen 1 completely set up before grout installation

Table 4-1: Concrete specimen 1 material weights and water injections with ½-in strands.

Tendon Number	Water (grams)	Grout (grams)	W/C	Water Injection (cc)
1	172.7	687.7	0.25	0
2	172.7	688	0.25	10
3	171.8	687.4	0.25	25
4	172.1	688.3	0.25	50

Once the grout cured for 7-days the back of the tendons were cut off with an angle grinder as well as the 90° portion of the elbow to allow the 60-ton hydraulic jack to slide over the tendon as show in Figure 4-4. Figure 4-5 shows tendons 2, 3, and 4 were not fully grouted. The grout filled the tendons partially due to the air not being able to escape causing a sloped geometry. With discovery of the tendons not being fully grouted a new method of preparation and grouting needed to be accomplished.



Figure 4-3: Feeding flexible hose into tendon for water injection (top left); Mixing grout in 4x8 concrete cylinder (top right); Pouring grout into funnel to prevent grout spillage (middle left); Removing steel brick to place concrete specimen horizontal and injecting water into tendon (middle right); Extracting flexible hose from tendon (bottom left); Water wicking out of the strand from water injection (bottom right).



Figure 4-4: Cutting of the back of the duct extensions (left); cutting off part of the elbow for clearance (right).



Figure 4-5: Tendon 1 with no water injection (top left); Tendon 2 with 10-cc water injection (top right); Tendon 3 with 25-cc water injection (bottom left); Tendon 4 with 50-cc water injection (bottom right).

4.1.1.2 CONSTRUCTION OF CONCRETE SPECIMEN 2

Concrete specimen 2 was modified to facilitate normal pumping type flow conditions from the field. This meant all duct extension connections to the cored concrete ducts would now be required to withstand pumping pressures estimated to be 10 psi for the given system. On each end of the concrete specimen, $\frac{3}{4}$ -in metal threaded pipe flanges were installed by predrilling into the concrete for tap-con concrete anchor screws. The bottoms of the flanges were coated with silicon to provide a suitable seal. Figure 4-6 shows the flange installation process using Tap-Con concrete screws.



Figure 4-6: Predrilling holes into the concrete face (top left); Silicon applied to the bottom of the metal flanges (top right); Anchoring the metal flanges to the concrete face (bottom left); All flanges anchored and silicon placed around the flanges (right).

Once the metal flanges were installed $\frac{3}{4}$ -in closed thread metal nipples were screwed into the metal flanges, and then $\frac{3}{4}$ -in 90° threaded elbows were screwed onto the open ends of the $\frac{3}{4}$ -in metal nipples as shown in Figure 4-7. The strands were then placed through the front duct extensions drilled $\frac{9}{16}$ -in hole in the elbow until the end of the strand touched the back of the elbow. Silicon was placed around the gaps between the strand-to-PVC and PVC-to-concrete.



Figure 4-7: Concrete specimen 2 back (left) and front (right).

Before installing grout PVC standpipes were installed to all the elbows since the specimen was placed at an angle amount of grout in the tendon would spill out leaving unintentional air voids after the specimen was repositioned horizontally for water injection. 3/4-in threaded adapters were placed to the back extensions for a grout pump attachment. Water filled syringes and flexible hoses were then installed inside the ducts for water injection. The concrete specimen was raised in the front approximately 3-in to allow air to escape while grout was pumped in from the back using air over grout pressure pot. Figure 4-8 shows both the front (strand end) and back (pumping end) of the second concrete specimen.

The grout was measured using the equations mentioned previously and mixed in a 5-gal pressure pot container. Once the grout was uniformly mixed and no dry grout was visible the lid was sealed on the container and pressurized to 10-psi. The grout pump hose was attached to the 3/4-in PVC adapters at the back of the concrete specimen. Each tendon was filled one at a time until the grout was visible in the standpipe in the front duct extension. The specimen was repositioned horizontally and water was injected into the ducts.



Figure 4-8: Water-filled syringe with flexible hose in the tendon (left); Back of the specimen with the standpipes and adapters (right).

Table 4-2: Concrete specimen 2 material weights and water injections with 1/2-in strands.

Tendon Number	Water (lbs.)	Grout (lbs.)	W/C	Water Injection (cc)
1	6.37	25.47	0.25	20
2	6.37	25.47	0.25	30
3	6.37	25.47	0.25	60
4	6.37	25.47	0.25	100

After the grout cured for 7-days the back PVC pipe extensions and elbows were removed for inspection and the concrete specimen was repositioned vertically on the concrete blocks for pullout tests. The front duct standpipes were removed and the 90° elbows were cut for clearance for the hydraulic 60-ton jack.



Figure 4-9: Removal of PVC fittings leaving grouted strands exposed.

4.1.1.3 CONSTRUCTION OF CONCRETE SPECIMENS 3-8

Concrete specimens 3 through 8 were prepared using the same procedure as concrete specimen 2. After specimen 5 was cast a smaller 2.5-gal pressure pot was used for the remainder of the specimens in this section, since the larger pressure pot wasted grout after casting. Specimens 6 through 8 were mixed in a 5-gal bucket and then transferred to the 2.5-gal pressure pot. This would reduce the volume of grout needed to pressurize the concrete tendons.

Table 4-3: Concrete specimen 3 material weights and water injections with ½-in strands.

Tendon Number	Water (lbs.)	Grout (lbs.)	W/C	Water Injection (cc)
1	7.97	31.83	0.25	0
2	7.97	31.83	0.25	50
3	7.97	31.83	0.25	80
4	7.97	31.83	0.25	100

Table 4-4: Concrete specimen 4 material weights and water injections with ½-in strands.

Tendon Number	Water (lbs.)	Grout (lbs.)	W/C	Water Injection (cc)
1	7.97	31.83	0.25	0
2	7.97	31.83	0.25	10
3	7.97	31.83	0.25	25
4	7.97	31.83	0.25	50

Table 4-5: Concrete specimen 5 material weights and water injections with ½-in strands.

Tendon Number	Water (lbs.)	Grout (lbs.)	W/C	Water Injection (cc)
1	7.89	31.5	0.25	20
2	7.89	31.5	0.25	30
3	7.89	31.5	0.25	60

Tendon Number	Water (lbs.)	Grout (lbs.)	W/C	Water Injection (cc)
4	7.89	31.5	0.25	100

Table 4-6: Concrete specimens 6–8 material weights and water injections with ½-in strands.

Tendon Number	Water (lbs.)	Grout (lbs.)	W/C	Water Injection (cc)
1	2.15	8.59	0.25	0
2	2.15	8.59	0.25	0
3	2.15	8.59	0.25	0
4	2.15	8.59	0.25	0

4.1.1.4 ALTERNATIVE FLUID INJECTION FOR CONCRETE SPECIMENS 4-8

After the third specimen was cast, corrosion inhibiting oil was introduced. A low viscosity oil was pressurized at anchorage and midpoints along a bridge tendon through the prestressing strands⁸⁹. Concrete specimens 4, 5, 7, and 8 were altered to fit the pressure pot hose adapter for oil injection. The strands extended too far for the hose adapter to fit around the threaded nipples, so the strands were reduced almost flush with the ends. The 2.5-gal pressure pot was filled with WD-40 and was connected to each tendon one at a time at a range of 10 to 20-psi. The strands were pressurized until the oil was visible at the other end as shown in Figure 4-10.



Figure 4-10: Specimen pressurized with WD-40 (left); WD-40 traveling along strand (right).

4.1.1.5 CONSTRUCTION OF CONCRETE SPECIMEN 9

Further investigation from the literature⁹⁰, the corrosion inhibiting oil needed to be pressurized for 24-hrs so the oil would travel around the strand and into the grout. Concrete specimen 9 was installed with ¾-in PVC tees instead of the 90° elbows. 3-in long PVC pipe were installed on both sides of the tee and duct taped one end to create a de-bonded surface like all specimens previously casted. ¾-in end caps were drilled with 9/16-in holes and installed to free end of the tee as shown in Figure 4-11. The strands were fed through the openings of the end caps and silicon was placed around the strand-to-PVC and PVC-to-concrete interface.

The back of the specimen was prepared using the same procedure as Concrete Specimen 3-8. Grout was measured and mixed using the same procedure as concrete specimens 6 through 8.

Table 4-7: Concrete specimen 9 material weights and water injections with ½-in strands.

Tendon Number	Water (lbs.)	Grout (lbs.)	W/C	Water Injection (cc)
1	2.87	11.46	0.25	0
2	2.87	11.46	0.25	0
3	2.87	11.46	0.25	0
4	2.87	11.46	0.25	0



Figure 4-11: Concrete specimen 9 before grout installation.

4.1.1.6 ALTERNATIVE FLUID INJECTION FOR CONCRETE SPECIMEN 9

After concrete specimen 9 cured for 7-days the ends caps were removed and ¾-in to ½-in reducers were installed with ½-in PVC pipe which covered the exposed free end of the strands. The free ends of the PVC pipe were sealed with ½-in PVC and brass adapters which led to brass valves where the flow of oil could be stopped and monitored with a removable pressure gauge. In order to pressurize all the tendons at once a PVC manifold was made to split the oil to each tendon. Table 4-11 shows the finished prepared concrete specimen for 24-hr pressurized oil.

The manifold was created out of ¾-in PVC pipe, tees, elbows, and couplers. The couplers were attached to the ¾-in metal nipples first, since the entire manifold would be glued together and once installed could not be removed until oil had been pressurized for 24-hrs. Once the manifold was prepared and attached to the back of the tendons, the pressure pot filled with WD-40 and was pressurized to 10-psi as shown in Figure 4-12. Expecting oil to travel through the strands and fill the ½-in PVC pipes quickly the specimen was monitored for 4-hrs. Oil never came out of the ends of the PVC pipes while being monitored. After 24-hrs the PVC pipes and adapters were removed for inspection of oil. As shown in Figure 4-13 oil traveled through all of the strands and began to collect near the adapter where the grouted section ended and exposed strand began.



Figure 4-12: Concrete specimen 9 prepared for WD-40 injection for 24-hrs. Concrete specimen 9 with PVC manifold (lower left); specimen 9 WD-40 injection (lower right).



Figure 4-13: Strand coated in WD-40 (left) and extracted strand after WD-40 injection (right).

4.1.1.7 CONSTRUCTION OF CONCRETE SPECIMENS 10-24

Based on the strands extracted from concrete specimen 9, specimens 10 through 24 were grouted without water voids to compare plain grout to pressurized oil grout. Figure 4-14 shows 11 of the 15 new specimens prepared for grout installation.



Figure 4-14: Concrete specimens 10–24.

Specimens 10 through 15 had workability issue during the grouting process. Once the grout was uniformly mixed the lid was sealed to the container and pressurized to 10-psi, but the grout became too thick to pump even though this did not occur during the previous specimens. The first tendon was able to be grouted but did not flow as fast as the previous specimens. Specimen 10 was believed to have not enough grout in the pot, so a new batch of grout was mixed for tendons 2 through 4.

Specimens 11 through 15 were grouted using the 5-gal pressure pot, but now there was enough grout to prevent air from being entrapped and explode out the front of the tendon. Within 1 minute the grout started to behave the same way as specimen 10. The container was examined and the grout was observed to be cured. An electric paddle wheel was used to remix the grout, the gel-like grout became liquid, and the grout was pump-able for about 1 minute until it became gel-like again.

Thixotropic grout becomes gel-like when still, but becomes liquid when agitated. When grouting concrete specimens 1 through 9 this property never was an issue, but in order to fix this problem more grout was mixed to ensure the level of grout was not low enough for air to be entrapped in the grout. The level of grout in the 2.5-gal pressure pot container was high enough for the paddle wheel from the lid to keep the grout agitated during the grout installation process. Figure 4-15 shows the effect of the thixotropic property of the grout, where the grout was liquid from the paddle wheel agitating the grout, and the surrounding area of grout was gel-like. Figure 4-15 also shows where the inlet pipe was for the grout to travel from the container to the pressure pot hose. The grout was mixed in a 5-gal bucket and then transferred to the 2.5-gal pressure pot container which was placed inside the 5-gal container. Specimens 16 through 24 were cast one day at a time using this new method.



Figure 4-15: The property of thixotropic grout.

Table 4-8: Concrete specimens 10–24 material weights and water injections with ½-in strands.

Specimen Number	Tendon Number	Water (lbs.)	Grout (lbs.)	W/C	Water Injection (cc)
10	1	1.77	7.07	0.25	0
10	2-4	2.87	11.46	0.25	0
11	1-3	5.93	23.68	0.25	0
12	1-4	5.93	23.68	0.25	0
13	1-4	5.93	23.68	0.25	0
14	1-4	5.93	23.68	0.25	0
15	1-4	5.93	23.68	0.25	0
16	1-4	1.99	7.91	0.25	0
17	1-4	2.87	11.46	0.25	0
18	1-4	2.86	11.46	0.25	0
19	1-4	2.86	11.45	0.25	0
20	1-4	2.87	11.45	0.25	0
21	1-4	2.87	11.45	0.25	0
22	1-4	2.86	11.46	0.25	0
23	1-4	2.87	11.45	0.25	0
24	1-3	2.87	11.45	0.25	0

4.1.1.8 ALTERNATIVE FLUID INJECTION FOR CONCRETE SPECIMENS 15-19

The concrete specimens cured for 7-days and were pressurized with oil for 24-hrs. To impregnate the concrete specimens with oil another intake manifold needed to be made. The new manifold was made with the same basic design but was re-usable. The manifold used the same ¾-in PVC inlet which fed into tees that splits the flow to all four tendons. After the elbows, PVC pipe was installed as extensions for ¾-in PVC threaded adapters, which thread onto PVC couplers and barbed hose adapters. This allowed flexible clear hoses to be attached and move

freely. The other end of the hose was attached with the same barbed adapter and coupler. All of the hoses were tightened with hose clamps. The free end couplers were attached to the $\frac{3}{4}$ -in metal nipples at the backs of the concrete specimens. Before the oil was injected, the end caps attached to the front duct extensions were removed, and $\frac{3}{4}$ -in to $\frac{1}{2}$ -in PVC reducers were attached. Clear tubing was cut to the exposed strand length and slid on to each strand with PVC end caps at the free ends. The tubes were moved away from the reducers to leave the strands partially exposed to observe when the oil would be visible.

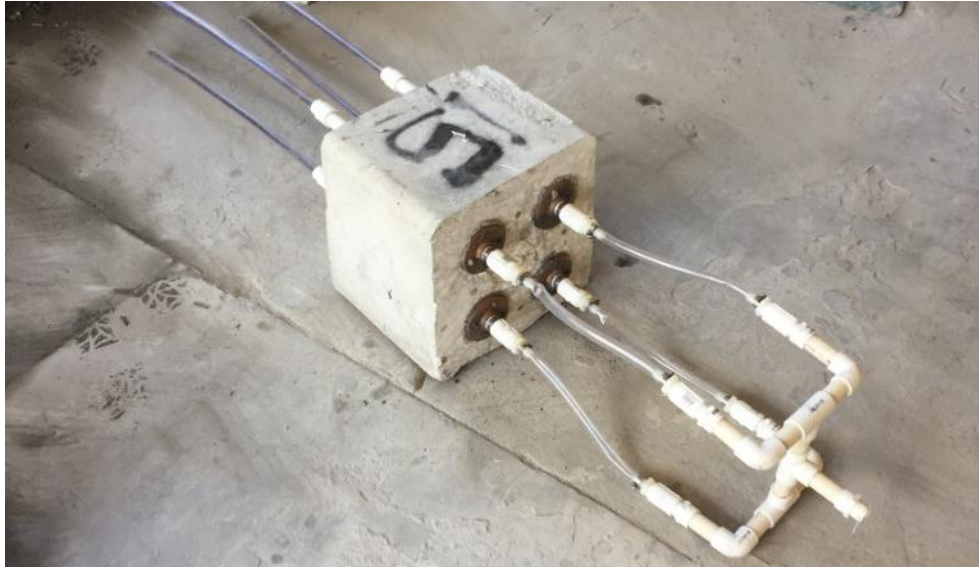


Figure 4-16: Concrete specimen 15 before WD-40 injection.

Once oil began to fill the backs of the tendons, time was taken to see how long it took the oil to travel to the exposed strand. As soon as oil was visible at the exposed side, the clear tubing was slid into the reducer to seal the strand. Once oil was noted to have passed through the grouted portion, the tendon remained pressurized with oil for 24 hrs. If the strands did not leak oil within 30 minutes, it was assumed there was some type of blockage due to corrosion within the interstitial spaces between wires. After the 24-hr period, the clear tubing was removed and inspected for visible oil on the strands, only one strand did not show any oil after 24 hrs. Figure 4-17 shows the flexible manifold attached to the back of the specimen and WD-40 filling the front end of the strands.



Figure 4-17: Manifold attached to the back of the specimen (left); Clear tubing filled with WD-40 (right).

4.1.1.9 PB BLASTER INJECTION FOR CONCRETE SPECIMENS 20-24

In this section a different type of oil penetrant was used to compare the WD-40 specimens and plain specimens. Concrete specimens 20 through 24 were prepared the same way as the WD-40 specimens. But in this case, the 2.5-gal pressure pot was filled with PB Blaster and the manifold was attached to the back of specimens 20 to 24 one day at a time. The tendons were pressurized to 10-psi and left for 24-hrs. The next day the manifold was removed as well as the clear tubing over the strands and the specimen was placed vertically for pullout tests. Figure 4-18 shows concrete specimen 24 after PB Blaster has been pressurized through the tendons.



Figure 4-18: Concrete specimen 24 after 24 hrs of PB Blaster injection.

4.1.2 RESULTS AND DISCUSSION

Twenty four concrete specimens were cast with 4 bonded strands in each. Five of the specimens were injected with water at the time of grouting and some were also injected with a corrosion inhibiting penetrant (WD-40) after the grout had cured. The remaining specimens were grouted without an attempt to create voids to fully assess the effects of just the penetrant on the strand to grout and grout to concrete bond interfaces.

The grouted specimens were left to cure for 7-days after grouting and pullout tests were conducted. Selected specimens were pressurized with two types of corrosion inhibiting oils, WD-40 or PB Blaster, for 24-hrs. For oil-injected specimens, pullout tests were conducted on the eighth day.

Once the grout had cured, the general procedure was to remove the PVC fittings on the back metal flanges and the PVC elbows on the front duct extensions were cut to fit the 60-ton hydraulic jack. Pressure was applied to the hydraulic jack by a 10,000-psi manually operated hydraulic pump. A 50-ton load cell was placed onto the hydraulic jack. Two metal plates were placed on top of the load cell, the first was a 2-in steel plate followed by a ¼-in steel plate as shown in Figure 4-19. A spring loaded ½-in strand wedge set (chuck) was installed on the strand and slid down in soft contact with the steel plates. A displacement transducer (LVDT) was secured to a magnetic stand and the stand was attached to the side of the hydraulic jack.

The initial phase of each load test was to determine the peak bond force. Once all four samples were tested an electric hydraulic pump was connected to the jack to fully extract the strands from the ducts allowing inspection of the internal bonding surface.



Figure 4-19: Pullout test setup for concrete specimen 9.

4.1.2.1 PULLOUT TEST RESULTS FOR CONCRETE SPECIMENS 1-5

The test results for concrete specimens 1 through 5 are listed in which represent those specimens with purpose built voids/flaws. Figure 4-20 through Figure 4-24 show load traces for each specimen during pullout testing, respectively. No displacement data was recorded for this series of tests. Subtle variation in the actual bond length were taken into account by normalizing the pullout capacity to that of a 12in bond length whereby a multiplier was applied to the measured pullout force values. This multiplier was determined from the ratio of 12-in to the actual bond length also in inches.

Table 4-9: Pullout loads for concrete specimens 1–5

Specimen-Strand Number	Injected Water Volume (cc)	Penetrant	Pullout Force (lbs)	Bonded Length (in)	Normalized Pullout Capacity (lbs)
1-1	0	None	15298	10.5	17484
1-2	10	None	1846	10.75	2061
1-3	25	None	8233	11.25	8782
1-4	50	None	10694	11	11666
2-1	20	None	19771	12.625	18792
2-2	30	None	23305	12.375	22599
2-3	60	None	14956	12.375	14502
2-4	100	None	16217	12.625	15414
3-1	0	None	8902	12.75	8379
3-2	50	None	10283	12.875	9584
3-3	80	None	12999	12.5	12479
3-4	100	None	11554	12.375	11204
4-1	0	WD-40*	6328	12.125	6263
4-2	10	WD-40*	4569	12	4569
4-3	25	WD-40*	9232	12.5	8863
4-4	50	WD-40*	10496	12.5	10077
5-1	20	WD-40*	12915	12.5	12399
5-2	30	WD-40*	16957	12.875	15805
5-3	60	WD-40*	7318	12.5	7025
5-4	100	WD-40*	3686	12.5	3539

Note: * were not pressurized for 24-hrs.

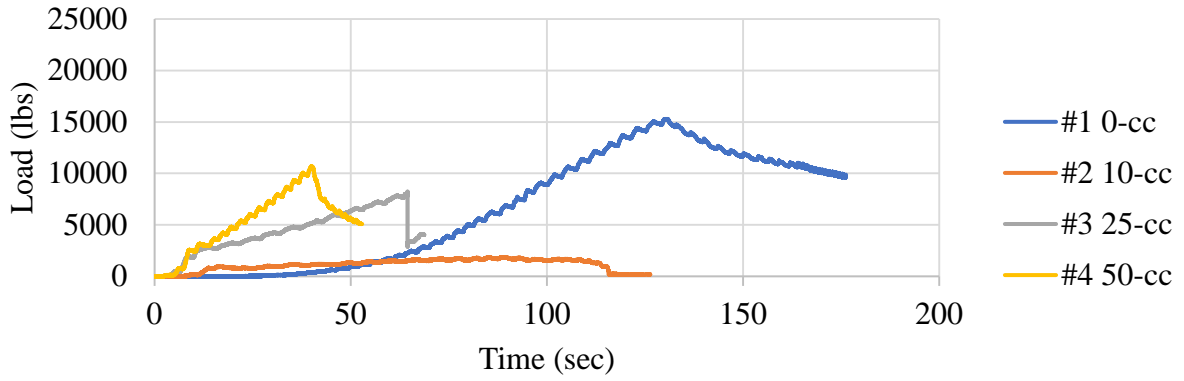


Figure 4-20: Results from specimen 1 load (lb) vs. time (sec).

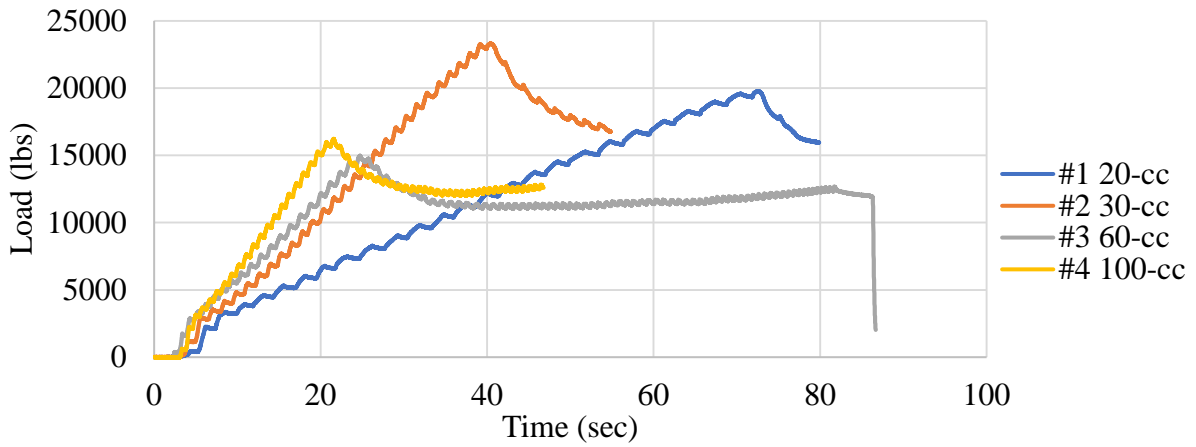


Figure 4-21: Results from specimen 2 load (lb) vs. time (sec).

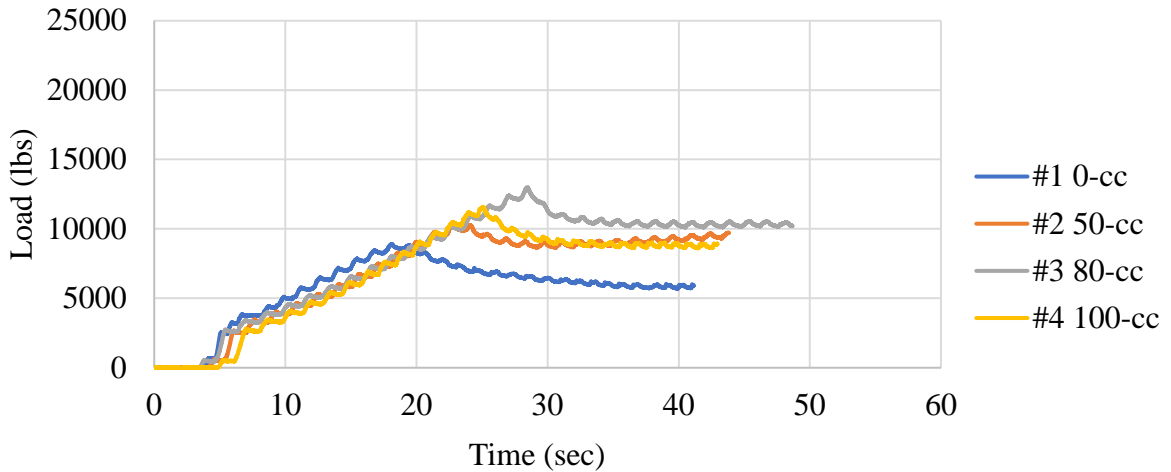


Figure 4-22: Results from specimen 3 load (lb) vs. time (sec).

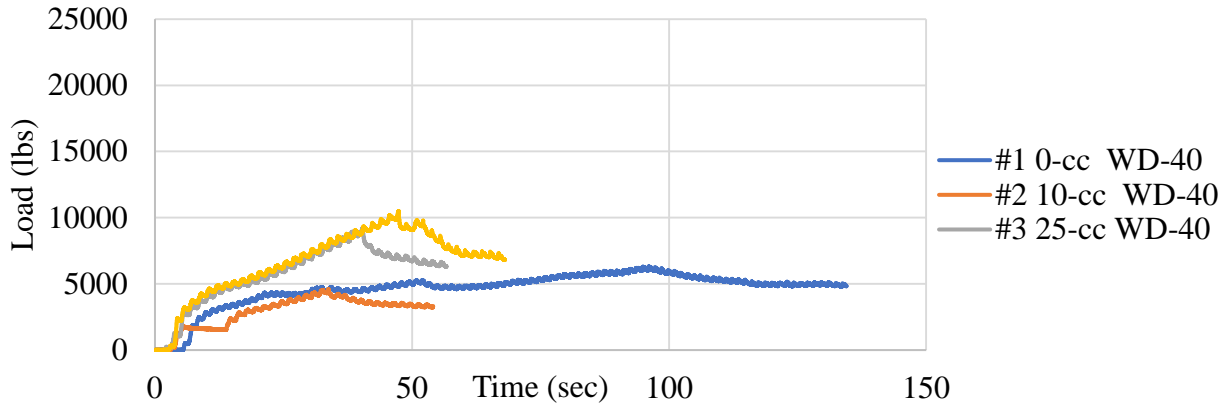


Figure 4-23: Results from specimen 4 load (lb) vs. time (sec).

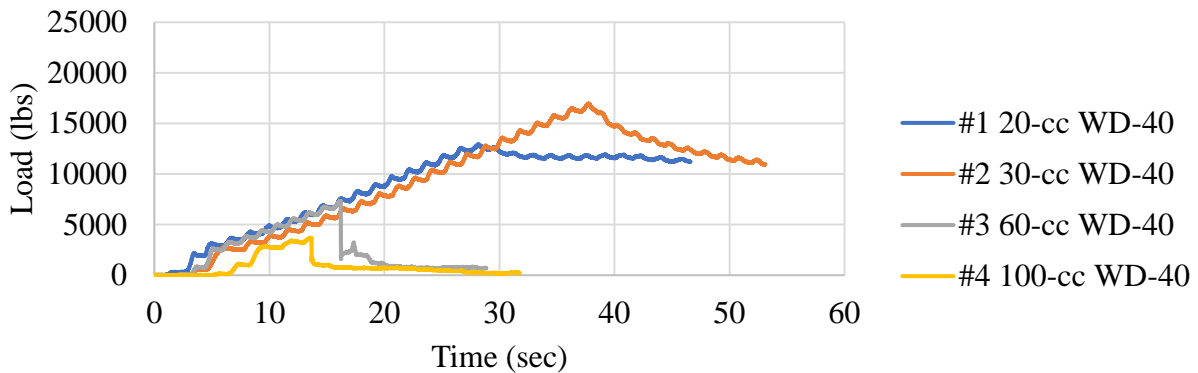


Figure 4-24: Results from specimen 5 load (lb) vs. time (sec).

4.1.2.2 PULLOUT TEST RESULTS FOR CONCRETE SPECIMENS 6-24

Pullout testing for all subsequent specimens was performed similarly but where no attempt was made to impose an artificial void in the bonded region of the strands. Specimens 20-24 were an extension of the originally slated testing where a second rust inhibiting penetrant was used called PB Blaster. Table 4-10 lists each of the strand pullout test values and the normalized forces.

Figure 4-25 – Figure 4-43 show the load traces for each strand pullout test for specimens 6 to 24. In this set of specimens, 26 pullout samples had no penetrant, 30 were exposed to WD-40 of which 6 were not pressurized for 24-hrs (24 were pressurized), and 19 were impregnated with PB Blaster with 24-hr pressurization. Penetrant pressure was consistently set at 10-psi whether with or without prolonged exposure.

Table 4-10: Pullout load for concrete specimens 6–24.

Specimen-Strand Number	Penetrant	Pullout Force (lbs)	Bonded Length (in)	Normalized Pullout Force (lbs)
6-1	None	16,960	12.5	16,282

Specimen-Strand Number	Penetrant	Pullout Force (lbs)	Bonded Length (in)	Normalized Pullout Force (lbs)
6-2	None	18,218	13.125	16,657
6-3	None	18,949	13.25	17,162
6-4	None	15,328	12.75	14,426
7-1	None	19,522	13	18,020
7-2	None	16,550	13.25	14,989
7-3	WD-40*	20,505	12.875	19,111
7-4	WD-40*	21,788	13.125	19,921
8-1	WD-40*	20,488	12.75	19,283
8-2	WD-40*	20,427	13.125	18,676
8-3	WD-40*	19,101	13.125	17,464
8-4	WD-40*	20,679	12.875	19,274
9-1	WD-40	18,270	13.25	16,547
9-2	WD-40	19,085	12.75	17,962
9-3	WD-40	18,881	12.875	17,598
9-4	WD-40	17,041	12.75	16,039
10-1	None	3,335	12.75	3,139
10-2	None	13,950	12.5	1,3392
10-3	None	8,600	12.75	8,094
10-4	None	7,888	12.75	7,424
11-1	None	20,159	12.75	1,8973
11-2	None	7,673	12.25	7,517
11-3	None	14,914	12.625	1,4175
12-1	None	12,469	12.625	11,852
12-2	None	9,306	12.75	8,759
12-3	None	16,530	12.5	15,869
12-4	None	15,751	12.5	15,121
13-1	None	16,799	12.25	16,456
13-2	None	5,374	12.625	5,108
13-3	None	10,745	12.75	10,113
13-4	None	18,914	12.875	17,628
14-1	None	8,382	13	7,737
14-2	None	7,657	13.25	6,935
14-3	None	9,921	13	9,158
14-4	None	10,526	13	9,716
15-1	WD-40	12,669	11.875	12,803
15-2	WD-40	13,361	11.5	13,942

Specimen-Strand Number	Penetrant	Pullout Force (lbs)	Bonded Length (in)	Normalized Pullout Force (lbs)
15-3	WD-40	6,335	11.5	6,610
15-4	WD-40	1,863	12.375	1,806
16-1	WD-40	7,926	12.375	7,686
16-2	WD-40	3,770	12.5	3,620
16-3	WD-40	8,340	12	8,340
16-4	WD-40	5,843	12.25	5,724
17-1	WD-40	17,323	11.75	17,691
17-2	WD-40	16,990	11.875	17,168
17-3	WD-40	18,108	12	18,108
17-4	WD-40	17,213	12.125	17,035
18-1	WD-40	12,259	12.5	11,768
18-2	WD-40	9,481	12.25	9,288
18-3	WD-40	8,265	11.75	8,441
18-4	WD-40	5,791	12.5	5,560
19-1	WD-40	16,042	11.75	16,383
19-2	WD-40	16,744	11.75	17,100
19-3	WD-40	12,766	11.625	13,178
19-4	WD-40	14,283	11.25	15,235
20-1	PB Blaster	14,079	13.25	12,751
20-2	PB Blaster	16,553	13	15,280
20-3	PB Blaster	16,317	13.25	14,778
20-4	PB Blaster	19,340	13.25	17,516
21-1	PB Blaster	15,780	12.75	14,852
21-2	PB Blaster	11,467	12.875	10,687
21-3	PB Blaster	12,010	13.25	10,877
21-4	PB Blaster	15,758	13	14,545
22-1	PB Blaster	14,380	13	13,274
22-2	PB Blaster	12,116	12.875	11,293
22-3	PB Blaster	14,652	13.125	13,396
22-4	PB Blaster	12,197	13.125	11,152
23-1	PB Blaster	12,715	13.5	11,302
23-2	PB Blaster	12,653	13.375	11,352
23-3	PB Blaster	12,207	13.25	11,055
23-4	PB Blaster	10,315	13.25	9,342
24-1	PB Blaster	15,234	12.25	14,923
24-2	PB Blaster	10,244	12.25	10,035

Specimen-Strand Number	Penetrant	Pullout Force (lbs)	Bonded Length (in)	Normalized Pullout Force (lbs)
24-3	PB Blaster	11,188	12.5	10,741

Note: * were not pressurized for 24-hrs.

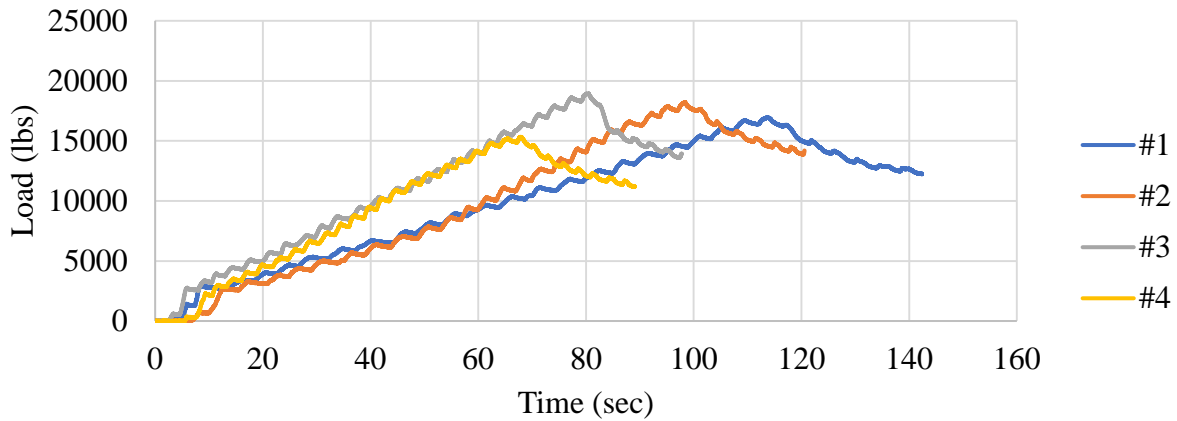


Figure 4-25: Results from specimen 6 load (lb) vs. time (sec).

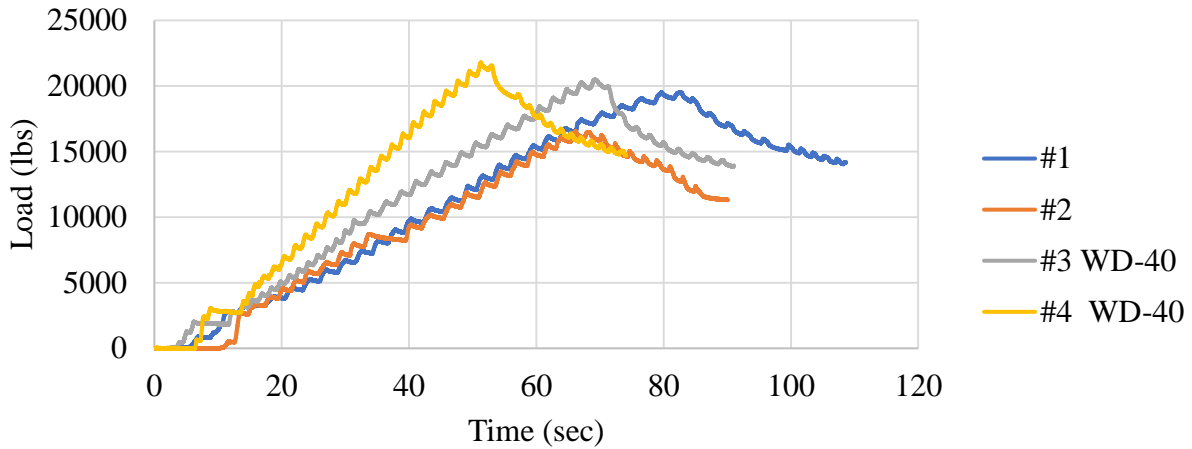


Figure 4-26: Results from specimen 7 load (lb) vs. time (sec).

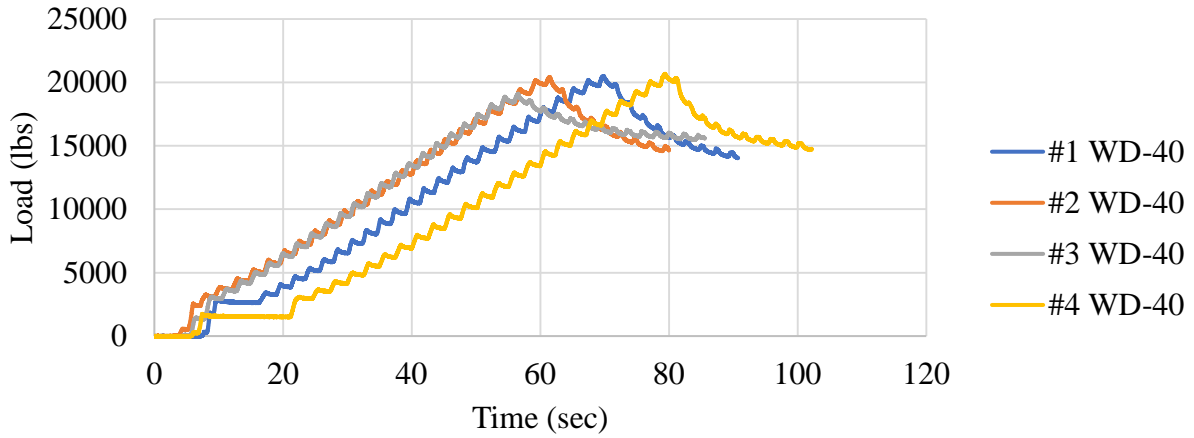


Figure 4-27: Results from specimen 8 load (lb) vs. time (sec).

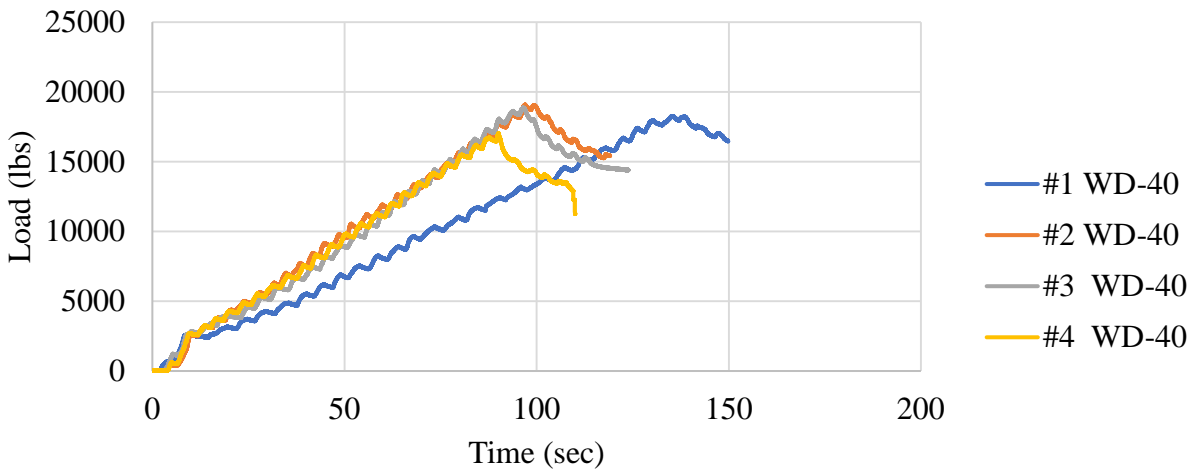


Figure 4-28: Results from specimen 9 load (lb) vs. time (sec).

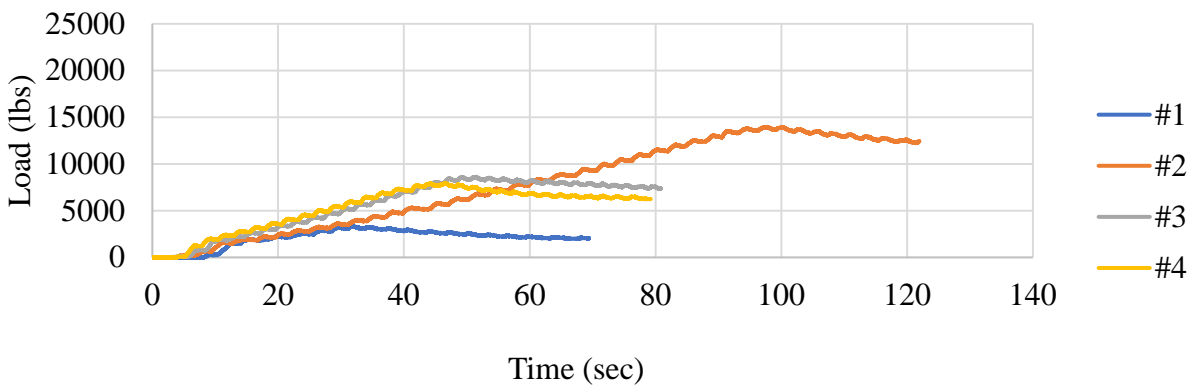


Figure 4-29: Results from specimen 10 load (lb) vs. time (sec).

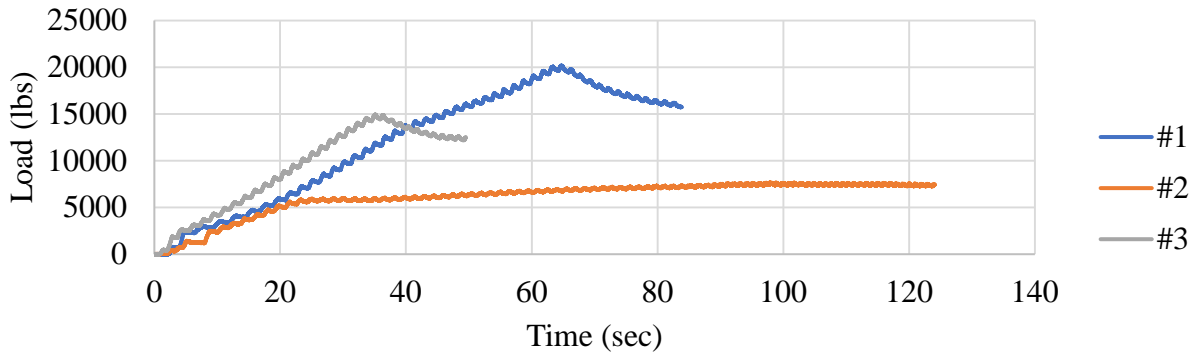


Figure 4-30: Results from specimen 11 load (lb) vs. time (sec).

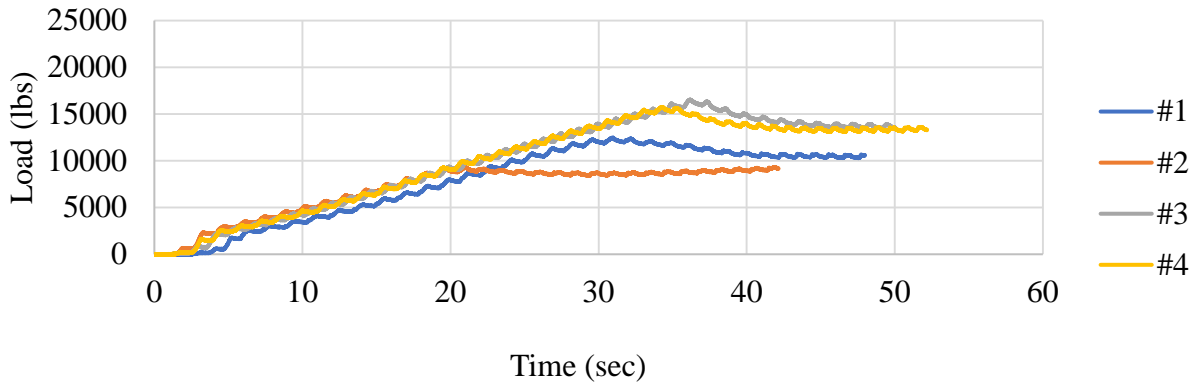


Figure 4-31: Results from specimen 12 load (lb) vs. time (sec).

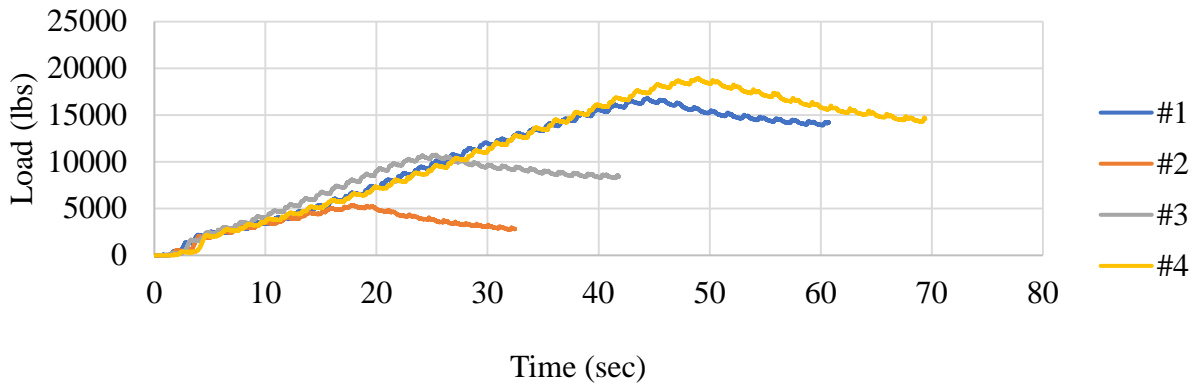


Figure 4-32: Results from specimen 13 load (lb) vs. time (sec).

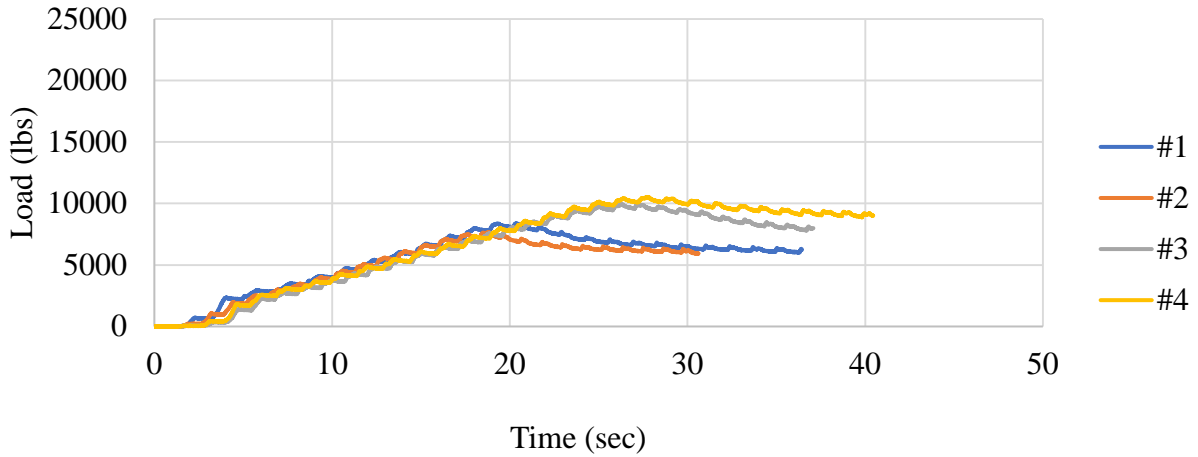


Figure 4-33: Results from specimen 14 load (lb) vs. time (sec).

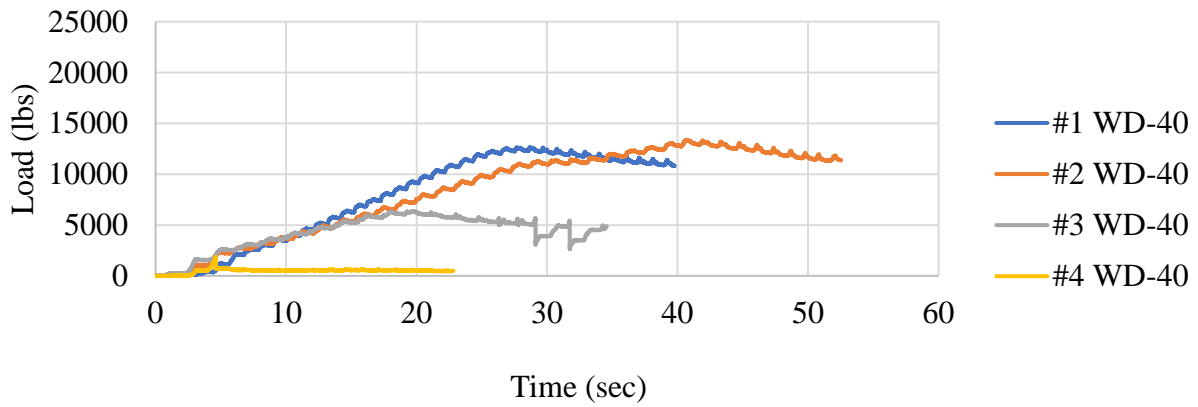


Figure 4-34: Results from specimen 15 load (lb) vs. time (sec).

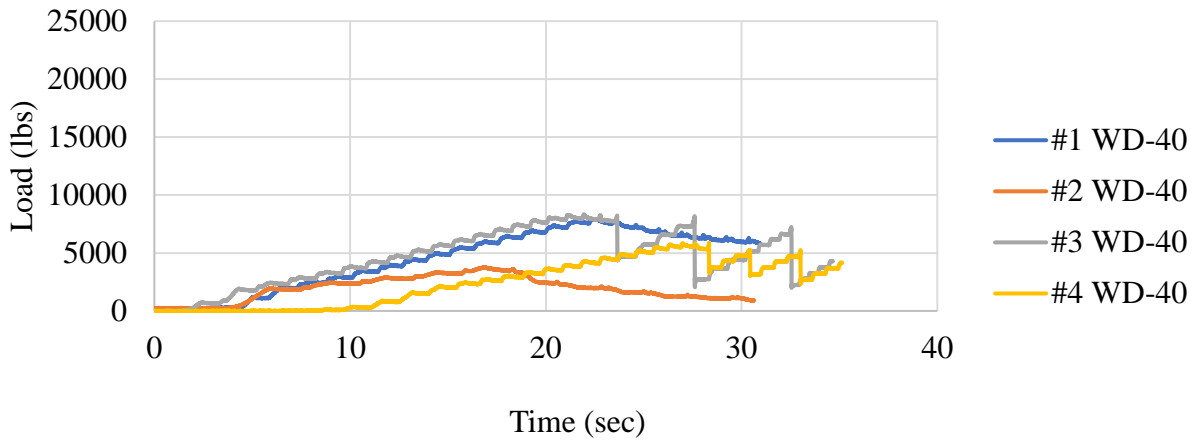


Figure 4-35: Results from specimen 16 load (lb) vs. time (sec).

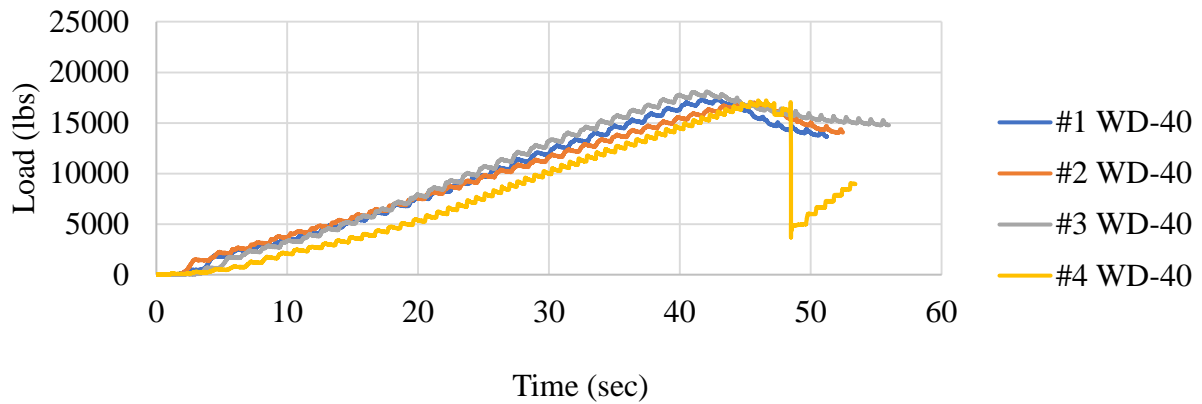


Figure 4-36: Results from specimen 17 load (lb) vs. time (sec).

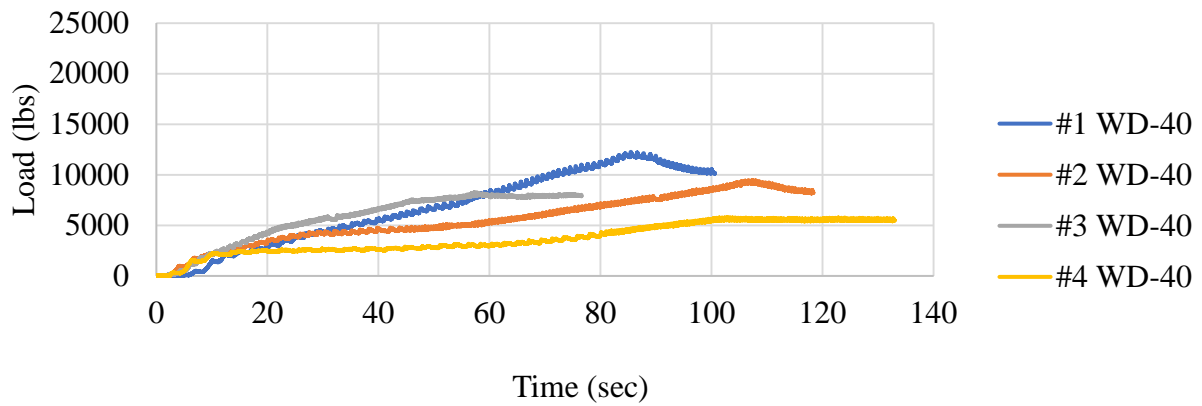


Figure 4-37: Results from specimen 18 load (lb) vs. time (sec).

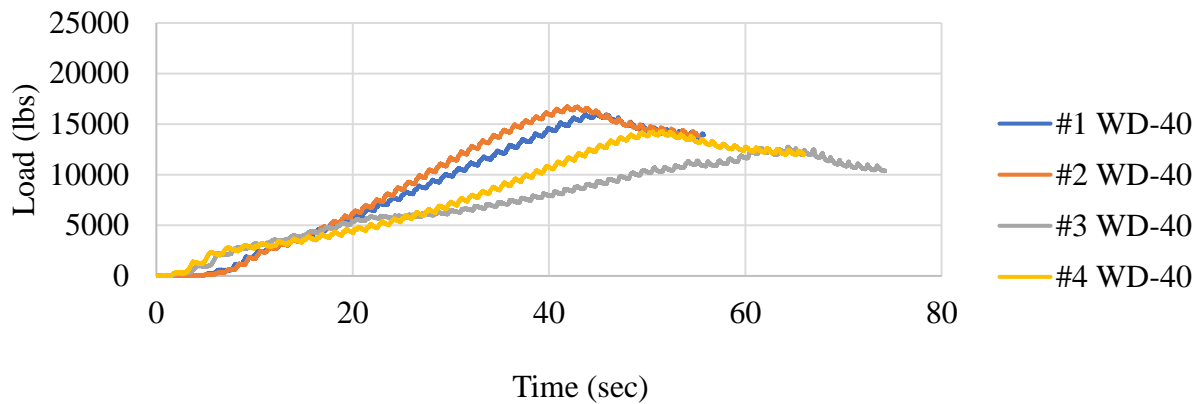


Figure 4-38: Results from specimen 19 load (lb) vs. time (sec).

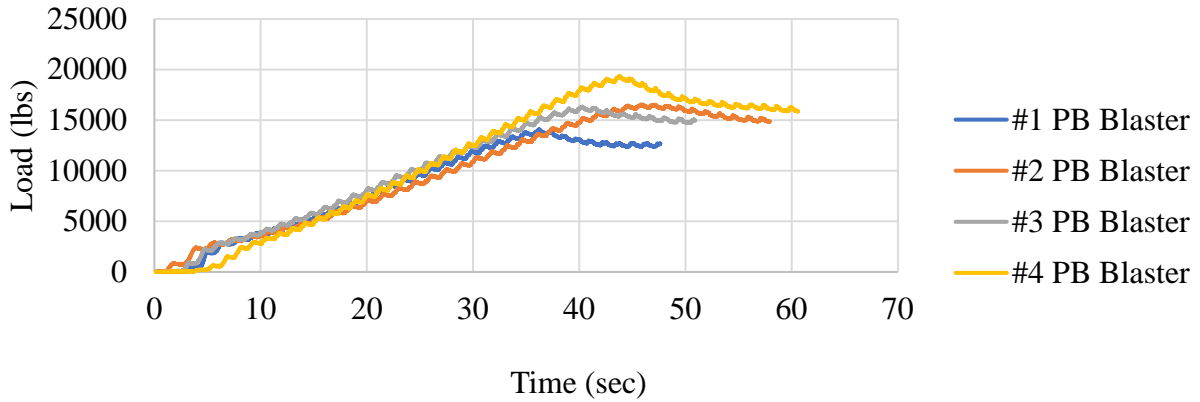


Figure 4-39: Results from specimen 20 load (lb) vs. time (sec).

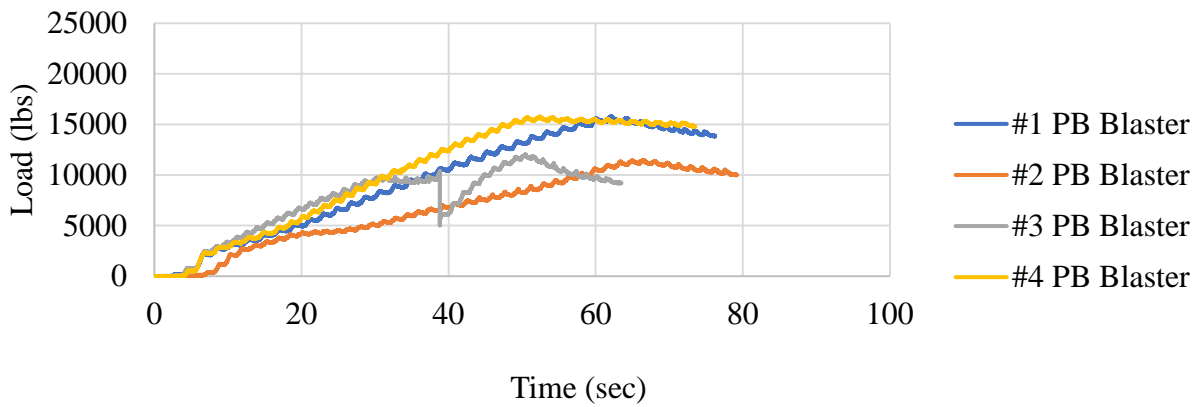


Figure 4-40: Results from specimen 21 load (lb) vs. time (sec).

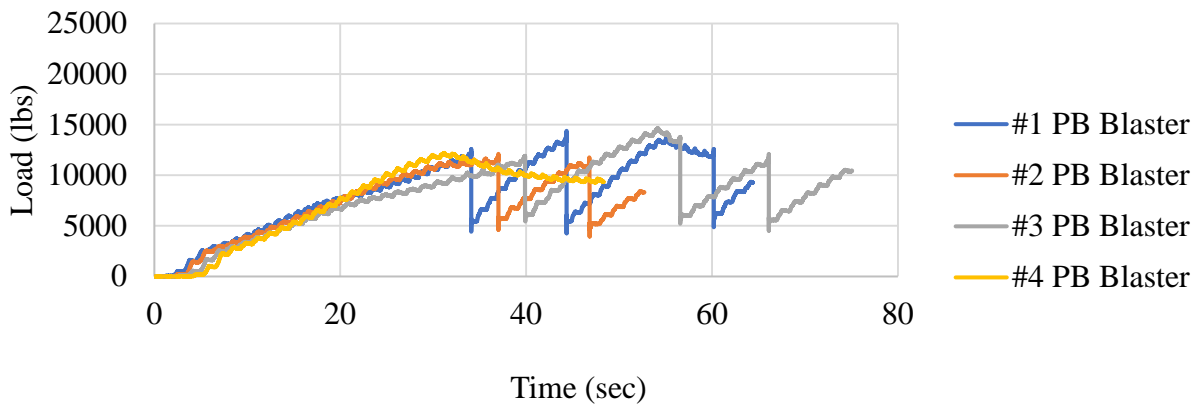


Figure 4-41: Results from specimen 22 load (lb) vs. time (sec).

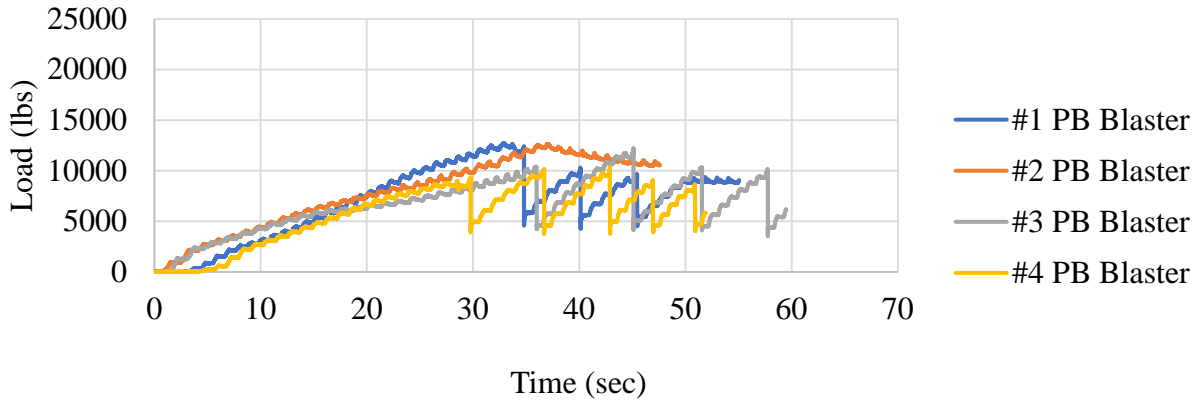


Figure 4-42: Results from specimen 23 load (lb) vs. time (sec).

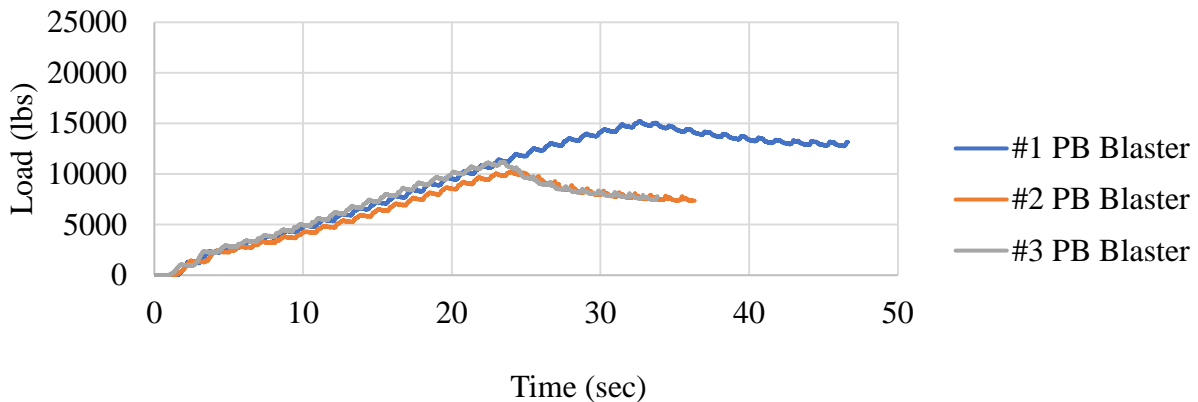


Figure 4-43: Results from specimen 24 load (lb) vs. time (sec).

The average normalized pullout capacity, standard deviation and coefficient of variation for Specimens 6 – 24 are listed in Table 4-11.

Table 4-11: Pullout capacity statistics for impregnated and un-impregnated specimens.

Impregnation Material	Average Normalized Pullout Force (lbs)	Standard Deviation	Coef. of Variation	Number of Specimens
None	12,188	4,573	0.38	26
WD-40	13,645	5,368	0.39	30
PB Blaster	12,587	2,213	0.18	19

Through the evolution of the small scale specimen a void creating process was established where water was injected in the tendon after grout had been installed. The first sets of small scale specimens were made with PVC, but were able to be cut to inspect grout quality. The last series of small scaled specimens were made with a clear duct material, so the small tendons were able to be inspected qualitatively without damaging the grout. The concrete specimens used the water injection process, but due to the surrounding concrete, ducts and

void volume were not able to be inspected for voids. Therefore a method was devised to assess the as-built void volume created from the water injection process.

After the strands were extracted from the grouted ducts, a rubber plug was squeezed into each tendon on the front face of concrete specimen 1. A 100-cc syringe was with water and weighed (filled beyond the marked scale). The water was injected into the tendon on the back face of specimen 1 until it reached the concrete surface as shown in Figure 4-19. The syringe was weighed again and the difference between the water weighed before the injection and after was used to compute the true volume of the duct which contained the bonded grout but without the volume of the strand. In all cases, the strand pulled from the grout leaving an imprint of the strand/spiraled wires.



Figure 4-44: Rubber plug installed into the front face of concrete specimen 1 (left); water injection into vacated duct (right).

Since concrete specimen 2 through 9 were prepared and grouted with metal flanges and nipples a $\frac{3}{4}$ -in PVC threaded end cap was screwed onto the exposed metal nipple after the strands were extracted and water was injected in the grouted duct and weighted in a similar fashion. In order to calculate the true void inside the tendon adjustments were made to correct for the difference between the syringe weighed before and after the test. Strand volume that occupied the space before the strand was pulled out was subtracted out of the weight difference of injected water as well as the interstitial space that occupied between the 7-wires. Due to the lack of information on the area of the interstitial spaces in strands one needed to be calculated and included as part of the strand (assuming grout would never occupy the interstitial spaces within the strand wires). The strand was drawn in AutoCAD and then trimmed to find the area of the spaces as shown in Figure 4-45. Along with the strand and interstitial space, the end cap and de-bonded areas needed to be subtracted as well. The end cap was always screwed on $\frac{1}{4}$ -in on the metal nipple and the de-bonded area was always an inch into the concrete. Table 4-11 shows all of the variables used to compute the true void in the tendon assembly except the de-bonded volume because it was the same for all of the tendons.

Table 4-12: Measured and calculated values for true void in the tendon specimens 1–24.

Specimen - Strand Number	Predicted Void (cc)	Water (g) Before	Water (g) After	End Cap Vol. (cc)	Strand Vol. (cc)	Strand Space (cc)	Measured Void (cc)
1-1	0	131.2	90.3	0.00	26.33	1.14	0.57
1-2	10	164.2	81.1	0.00	26.95	1.16	42.11
1-3	25	167	57.7	0.00	28.21	1.22	67.01
1-4	50	167	83.3	0.00	27.58	1.19	42.06
2-1	20	166.3	99.8	5.43	31.65	1.37	15.18
2-2	30	165.1	94.3	5.43	31.03	1.34	20.13
2-3	60	166.1	97.3	5.43	31.03	1.34	18.13
2-4	100	166.5	90.3	5.43	31.65	1.37	24.88
3-1	0	165.7	96	5.43	31.97	1.38	18.05
3-2	50	165.7	99.2	5.43	32.28	1.39	14.53
3-3	80	165.7	101.2	5.43	31.34	1.35	13.51
3-4	100	165.7	85.1	5.43	31.03	1.34	29.93
4-1	0	163.1	96.1	5.43	30.40	1.31	16.99
4-2	10	163.9	85.8	5.43	30.09	1.30	28.42
4-3	25	165	92.9	5.43	31.34	1.35	21.11
4-4	50	165.2	91.7	5.43	31.34	1.35	22.51
5-1	20	164.6	96.9	5.43	31.34	1.35	16.71
5-2	30	165	96.3	5.43	32.28	1.39	16.73
5-3	60	165.2	60.9	5.43	31.34	1.35	51.00
5-4	100	330.3	192.2	5.43	31.34	1.35	69.80
6-1	0	165.7	98.1	5.43	31.34	1.35	16.61
6-2	0	165.7	98.9	5.43	32.91	1.42	14.17
6-3	0	165.5	98.4	5.43	33.22	1.43	14.15
6-4	0	165.5	106.2	5.43	31.97	1.38	7.65
7-1	0	165.8	96.3	5.43	32.59	1.41	17.20
7-2	0	165.7	91.3	5.43	33.22	1.43	21.45
7-3	0	166	100.4	5.43	32.28	1.39	13.63
7-4	0	165.5	95.9	5.43	32.91	1.42	16.97
8-1	0	162.7	98.3	5.43	31.97	1.38	12.75
8-2	0	165.5	98.7	5.43	32.91	1.42	14.17
8-3	0	165.3	108.5	5.43	32.91	1.42	4.17
8-4	0	165.1	92.6	5.43	32.28	1.39	20.53
9-1	0	166.4	104.2	5.43	33.22	1.43	9.25
9-2	0	165.9	100.7	5.43	31.97	1.38	13.55
9-3	0	166	105.1	5.43	32.28	1.39	8.93

Specimen - Strand Number	Predicted Void (cc)	Water (g) Before	Water (g) After	End Cap Vol. (cc)	Strand Vol. (cc)	Strand Space (cc)	Measured Void (cc)
9-4	0	166.4	102.1	5.43	31.97	1.38	12.65
10-1	0	328	194.3	5.43	31.97	1.38	82.05
10-2	0	164.6	90.6	5.43	31.34	1.35	23.01
10-3	0	327.7	201.5	5.43	31.97	1.38	74.55
10-4	0	163.4	103.6	5.43	31.97	1.38	8.15
11-1	0	163.5	96.7	5.43	31.97	1.38	15.15
11-2	0	163.6	58.5	5.43	30.71	1.32	54.76
11-3	0	163.9	62.9	5.43	31.65	1.37	49.68
12-1	0	163.8	56.9	5.43	31.65	1.37	55.58
12-2	0	322.5	168.5	5.43	31.97	1.38	102.35
12-3	0	165.9	56.9	5.43	31.34	1.35	58.01
12-4	0	159.2	69.2	5.43	31.34	1.35	39.01
13-1	0	164.2	98.4	5.43	30.71	1.32	15.46
13-2	0	320.2	189.3	5.43	31.65	1.37	79.58
13-3	0	155.5	85.8	5.43	31.97	1.38	18.05
13-4	0	165.4	87.1	5.43	32.28	1.39	26.33
14-1	0	300.3	205.4	5.43	32.59	1.41	42.60
14-2	0	324.2	188.4	5.43	33.22	1.43	82.85
14-3	0	326.5	206.6	5.43	32.59	1.41	67.60
14-4	0	166.5	96.2	5.43	32.59	1.41	18.00
15-1	0	166.1	76.8	5.43	29.77	1.28	39.94
15-2	0	161.5	96.9	5.43	28.83	1.24	16.22
15-3	0	325.9	213.6	5.43	28.83	1.24	63.92
15-4	0	307.5	183.8	5.43	31.03	1.34	73.03
16-1	0	325.4	203	5.43	31.03	1.34	71.73
16-2	0	324.7	187.9	5.43	31.34	1.35	85.81
16-3	0	Not Testable	Not Testable	5.43	30.09	1.30	Not Testable
16-4	0	164.8	56.9	5.43	30.71	1.32	57.56
17-1	0	161.3	98.4	5.43	29.46	1.27	13.87
17-2	0	166.5	108.9	5.43	29.77	1.28	8.24
17-3	0	163.9	98.7	5.43	30.09	1.30	15.52
17-4	0	165.5	104.7	5.43	30.40	1.31	10.79
18-1	0	164.3	81.8	5.43	31.34	1.35	31.51
18-2	0	159.1	87.3	5.43	30.71	1.32	21.46
18-3	0	165.4	99.1	5.43	29.46	1.27	17.27

Specimen - Strand Number	Predicted Void (cc)	Water (g) Before	Water (g) After	End Cap Vol. (cc)	Strand Vol. (cc)	Strand Space (cc)	Measured Void (cc)
18-4	0	163.5	85.2	5.43	31.34	1.35	27.31
19-1	0	162.5	96.8	5.43	29.46	1.27	16.67
19-2	0	165.5	102.5	5.43	29.46	1.27	13.97
19-3	0	163.1	100.1	5.43	29.15	1.26	14.30
19-4	0	163.7	101.5	5.43	28.21	1.22	14.48
20-1	0	163.8	92.8	5.43	33.22	1.43	18.05
20-2	0	164.6	96.2	5.43	32.59	1.41	16.10
20-3	0	164	97	5.43	33.22	1.43	14.05
20-4	0	164.9	101.7	5.43	33.22	1.43	10.25
21-1	0	161.5	98.9	5.43	31.97	1.38	10.95
21-2	0	163.9	98.2	5.43	32.28	1.39	13.73
21-3	0	166.5	99.6	5.43	33.22	1.43	13.95
21-4	0	166.6	97.9	5.43	32.59	1.41	16.40
22-1	0	166.4	101.7	5.43	32.59	1.41	12.40
22-2	0	163.7	101.6	5.43	32.28	1.39	10.13
22-3	0	162.8	95.1	5.43	32.91	1.42	15.07
22-4	0	163.8	105	5.43	32.91	1.42	6.17
23-1	0	165.6	109	5.43	33.85	1.46	2.99
23-2	0	165.1	95.3	5.43	33.53	1.45	16.52
23-3	0	165.3	94.4	5.43	33.22	1.43	17.95
23-4	0	164.4	97.3	5.43	33.22	1.43	14.15
24-1	0	162.3	102.6	5.43	30.71	1.32	9.36
24-2	0	162.7	103.7	5.43	30.71	1.32	8.66
24-3	0	163.1	99.5	5.43	31.34	1.35	12.61

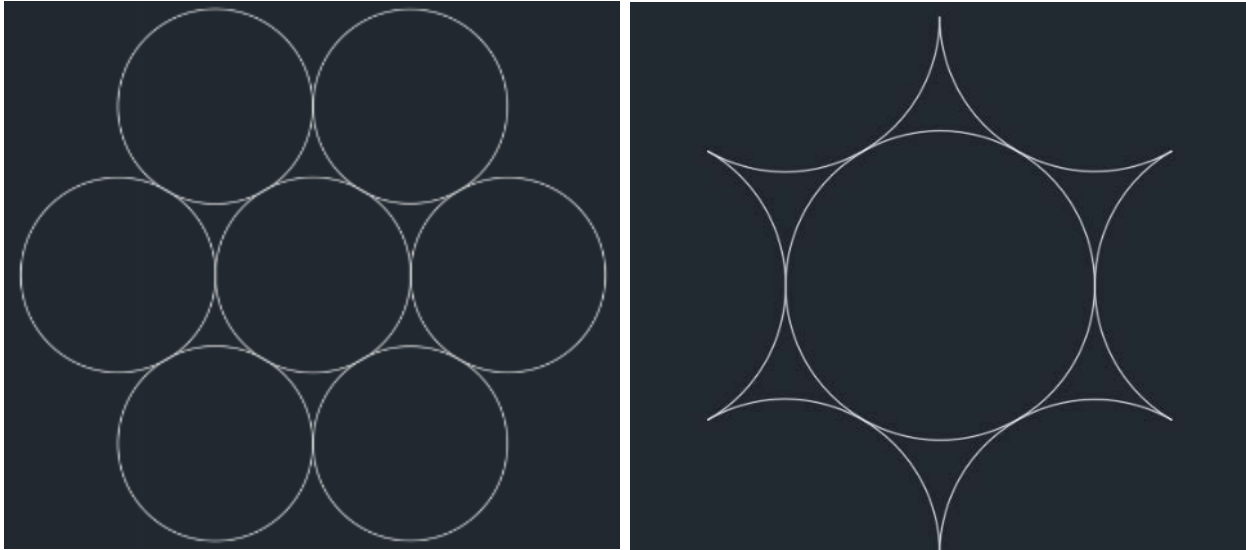


Figure 4-45: Full 1/2-in strand (left); trimmed version of the 1/2-in strand to calculate the interstitial spaces (right).

The time required for the impregnation material to flow through the 12-in nominal length of bonded strand was recorded for each of the last ten samples that were equipped with clear extension tubing. Only these specimens could be visibly scrutinized. Two extremes were noted: instantaneous outflow noted by a 00:00 min:sec reading or an extended amount of time that exceeded 30:00 min:sec. In all but one case out of 39 specimens, the penetrant was found to have migrated through the 12-in bonded region. Table 4-13 and Table 4-14 show the time to show penetrant exiting the strand for the WD-40 and PB Blaster impregnation materials. PB Blaster times were generally less than WD-40.

Table 4-13: Concrete specimens 15–19 oiled with WD-40 at 10 psi.

Specimen - Strand Number	First Appearance (min:sec)	Total Elapsed Time (min:sec)	Left under pressure?	Showed oil after 24-hrs.
15-4	00:13	00:13	Yes	Yes
15-1	05:25	05:38	Yes	Yes
15-2	02:40	08:17	Yes	Yes
15-3	30:00	30:00	Yes	Yes
16-1	00:00	00:00	No	Yes
16-2	00:00	00:00	Yes	Yes
16-3	00:00	00:00	Yes	Yes
16-4	00:00	00:00	Yes	Yes
17-4	00:42	00:42	Yes	Yes
17-2	01:22	02:04	Yes	Yes
17-1	30:00	30:00	Yes	Yes

Specimen - Strand Number	First Appearance (min:sec)	Total Elapsed Time (min:sec)	Left under pressure?	Showed oil after 24-hrs.
17-3	30:00	30:00	Yes	Yes
18-2	06:27	06:27	Yes	Yes
18-1	30:00	30:00	Yes	Yes
18-3	30:00	30:00	Yes	Yes
18-4	30:00	30:00	Yes	No
19-1	00:13	00:13	Yes	Yes
19-2	30:00	30:00	Yes	Yes
19-3	30:00	30:00	Yes	Yes
19-4	30:00	30:00	Yes	Yes

Table 4-14: Concrete specimens 20–24 oiled with PB Blaster at 10 psi.

Specimen - Strand Number	First Appearance (min:sec)	Total Elapsed Time (min:sec)	Left under pressure?	Showed oil after 24-hrs.
20-4	00:13	00:13	Yes	Yes
20-1	30:00	30:00	Yes	Yes
20-2	30:00	30:00	Yes	Yes
20-3	30:00	30:00	Yes	Yes
21-2	00:14	00:14	No	Yes
21-3	00:13	00:27	Yes	Yes
21-1	02:37	03:04	Yes	Yes
21-4	10:10	13:14	Yes	Yes
22-1	00:00	00:00	Yes	Yes
22-2	00:00	00:00	No	Yes
22-3	00:00	00:00	Yes	Yes
22-4	00:00	00:00	Yes	Yes
23-1	00:00	00:00	Yes	Yes
23-2	00:00	00:00	Yes	Yes
23-3	00:00	00:00	Yes	Yes
23-4	00:00	00:00	No	Yes
24-1	00:00	00:00	Yes	Yes
24-2	00:00	00:00	Yes	Yes
24-3	00:00	00:00	Yes	Yes

4.1.3 FINDINGS AND IMPLICATIONS

This study focused on determining the bond developed between high strength seven-wire post-tensioning strands and grout (or the surround grout to concrete). The motivation stemmed from the advent of a new corrosion-inhibiting scheme whereby low-viscosity, oil-based penetrants are pressure-injected into existing post-tensioning tendons. This program was designed to scrutinize the effect of the penetrant on the strand-concrete bond often necessary for proper structural performance.

In the design of the test program, a methodology to introduce flaws (voids) in the grout in the simulated post-tensioning ducts was deemed necessary. However, routine grouting without intentionally producing flaws was shown to periodically produce unintentional flaws even in laboratory settings. This difficulty ultimately became an interesting variable that can be easily equated to routine construction workmanship. Most importantly, the study investigated the effect of oil-based penetrants pressurized into the post-tensioning ducts on bond, the effect of voids (wittingly or unwittingly produced) on bond, and the flow rate of two different penetrants through the tiny interstitial spaces (totaling 0.006 in² per strand) between the six outer wires and the center wire of a standard seven-wire strand.

The average pullout capacity for the concrete samples not purposely injected with water voids was similar for all three conditions (WD-40, PB Blaster, and no penetrant impregnation) as shown in Table 4-15. Values for water-injected specimens with purpose-built voids were inexplicably slightly higher than no-void conditions for the no-penetrant condition and lower for the WD-40 penetrant, but these values are not representative of ideal conditions, and the standard deviation and coefficient of variation values were notably higher.

Table 4-15: Variations in average capacity for different grouting and impregnation conditions.

Penetrant and void injection	Average Normalized Pullout Force (lbs)	Standard Deviation	Coef. of Variation	Number of Specimens
None	12168	4364	0.36	19
None (water)	13402	6731	0.50	7
WD-40	13346	5524	0.41	23
WD-40 (water)	8897	4327	0.49	7
PB Blaster	12587	2213	0.18	19

In short, there appeared to be no adverse effect from the penetrants.

The first five concrete pile segments were prepared both with and without water injected voids which constituted 20 of the 95 pullout strand specimens. All other specimens (75) were cast/grouted with the intention of producing no voids. However, difficulties associated with maintaining grout fluidity quickly revealed that air pockets could still have been introduced inadvertently. The as-built grout volume was therefore determined via post pullout testing evaluations where the volume of the grout and the strand were compared to the total remaining volume of the vacated core hole. The difference was always positive meaning there was some void volume around the strand for all tests. This value ranged from 0.5 to 102-cc (0.03 to 6.2-in³). While 17 of the first 20 grouted strands had intentional voids, the presence of voids was just

as prevalent in all other specimens as well which were intended to have no voids. Figure 4-46 shows the effect of void volume on the pullout capacity. Open markers indicate intentional voids where water was injected; solid markers indicate no water was injected to create a void. Purpose built / intentional voids were restricted to samples with WD-40 and with no impregnating penetrant (none).

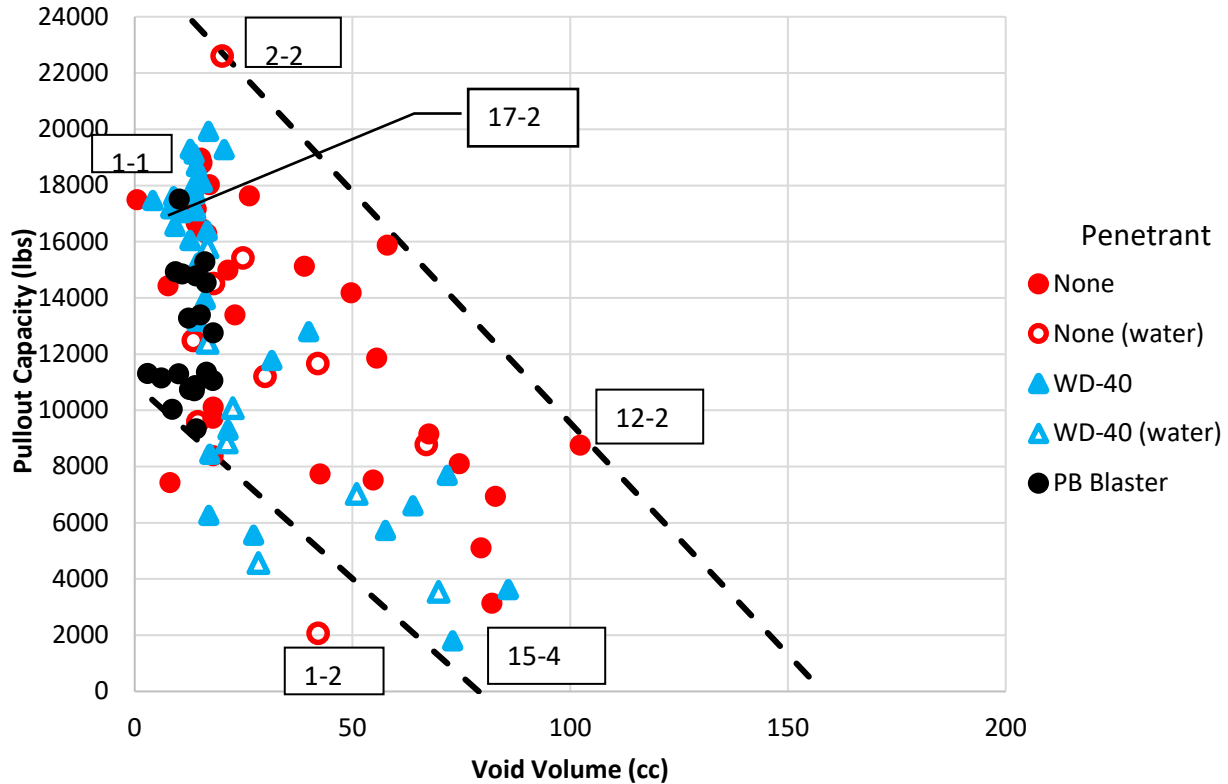


Figure 4-46: Results from pullout capacity (lbs) vs. void volume (cc)

Whether purpose built or not, the presence of voids shows a general trend of decreased capacity with increased void volume (Figure 4-46). This is not unexpected as the magnitude of void volume represents the presence or absence of material capable of bonding the strand to the concrete structure. For reference, the volume of the empty cored hole was approximately 189 cc and the volume of the strand in the 12-in nominal bond length was 31 cc leaving 158 cc of potential void volume around an ungrouted strand. This is denoted by the upper dashed line that indicates zero capacity at 158 cc of void volume and assumes a linear relationship between bonded length and void volume. Figure 4-47 shows this as point 1 and further notes three other points defining the boundaries encompassing 95% of the entire data set. The upper and lower dashed lines represent the highest and lowest grout strength measured over the duration of the test program, respectively, which ranged from 3,000 to 7,000 psi. Point 2 represents half the empty void volume but where the grout was ineffectively distributed only touching the bottom edge of the strand (still zero capacity). Points 3 and 4 represent the lowest and highest predicted bond strength / pullout capacity, respectively, where full bound (zero void volume) would have been provided. The predicted capacities used the simplistic transfer length equation to compute the required development length at 270-psi ultimate strand capacity and then

prorates the full strand capacity on the basis of the bonded length to development length ratio (e.g., 12 in/(270/f'c × 0.5-in) × 270 × (0.153)strand area). The predicted capacities from all cube breaks are shown as full bond (zero void) conditions and lie on the y-axis (Figure 4-47).

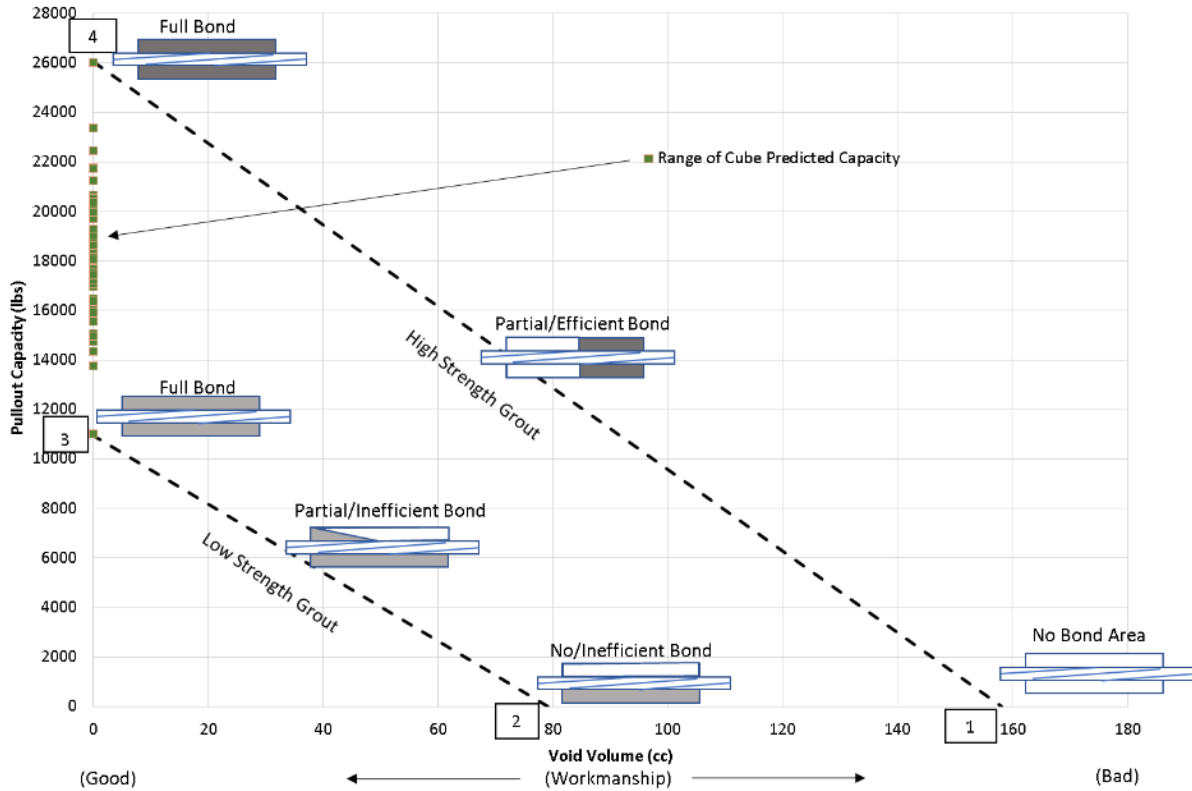


Figure 4-47: Explanation of data scatter shown by the effects of void volume (workmanship).

Depending on the shape of the void, the volume of remaining grout may either fully surround the strand and bond to the concrete over the entire remaining annulus volume or fill the annulus around the strand only on one side (Figure 4-47). This in part explains the wide range of capacity noted for a given void volume. Hence, the shape of the grout volume and how it touches the concrete and strand affects the pullout capacity. Figure 4-48 – Figure 4-53 show borescope images from pullout specimen grouted holes after the strands were removed. These show both full annulus grouting (Figure 4-48, Figure 4-50 and Figure 4-52) as well as incomplete grout coverage (Figure 4-49, Figure 4-51, and Figure 4-53). These images correspond to one of the 6 data points called out in Figure 4-46 (i.e. 1-1, 1-2, 2-1, 12-2, 17-2, and 15-4).



Figure 4-48: Sample 1-1 (none) lowest void perfect grout distribution.



Figure 4-49: Sample 1-2 (none) 40-cc grout on only one side 2,061-lb pullout capacity.



Figure 4-50: Sample 2-2 fully bonded strand, highest pullout load, 20-cc void volume.



Figure 4-51: Sample 12-2 highest void volume, partial bond near bottom, 8,729-lb pullout capacity.



Figure 4-52: Sample 17-2 (WD-40) full bond where strand slipped free.



Figure 4-53: Sample 15-4 (WD-40) lowest bond 73-cc void volume, partial bond near bottom.

The net effect is that voids can form in many shapes which in turn affect the bond performance. Good quality grouting techniques reduce void volumes, increase pullout bond resistance, and reduce the potential for corrosion prone regions.

The premise of the impregnation concept is that a given penetrant can be pressurized to travel long distances (hundreds of feet) within the interstitial spaces of the 7 wire strands. This then assumes that these pathways are present and have not been blocked by corrosion products or other common grout by-products. The 24 specimens used in this study were only 12-in long and were pressurized for up to 24-hrs to promote full penetration into and around the strands thereby creating a worst-case scenario for the bond line between the grout and strands. In one case, penetrant was not found to have traveled the 12-in distance after the prolonged exposure. All other specimens did but in some cases very slowly. Figure 4-54 shows the time taken to see penetrant pass through the grouted strand (simulated mono strand ducts).

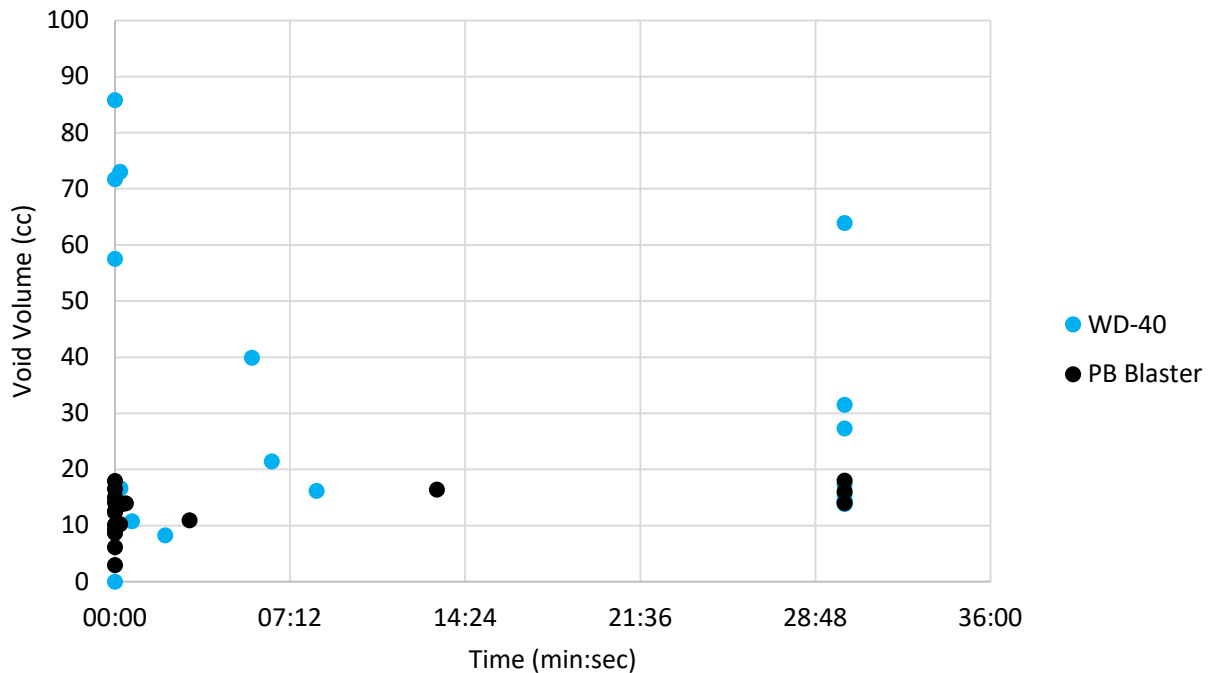


Figure 4-54: Penetration rates for the two penetrants (time /12 in).

In general, flow was either immediate or the time exceeded the 30 minute wait time allocated before sealing of the discharge (exposed strand) side for overnight pressurization. Fourteen of 20 specimens (70%) showed penetrant discharge within 15 seconds when using the PB Blaster; 6 of 20 (30%) when using the WD-40 (again within 15 sec). The data does not support a conclusion as to whether or not the fluid could be pumped over extended distances typical of field conditions.

4.2 VECTOR PROPRIETARY FLUID

This section presents the results of bond strength test on concrete piles similar to those presented in Section A but focused exclusively on the Vector Corrosion impregnation fluid. Where the first phase pullout specimens were cut from a single length of 14-in square prestressed pile (12-in-long pieces), the concrete specimens for these experiments were purpose-cast for the testing program. Twelve-inch segments of precast pile segments were cast at a commercial casting yard in a 14-in square pile bed where pile header plates were used to separate the bed into individual segments. The eight ½-in Grade 270 native pile strands were cut flush with the ends upon removal from the bed and were not used other than to provide reinforcement to the concrete; these strands along with the spiral reinforcement prevented splitting or other concrete failures during pullout testing as in the original specimens cut from longer lengths.

All segments were again cored with a 1 in diameter (O.D.) water flushing core barrel drill in the same fashion as the originally tested specimens previous described. Four core holes were made in each pile segment. Pipe flanges (with ¾-in NPTF threads) were fastened to both ends of the piles with rubber gaskets and four TAPCON screws thereby extending each duct out each end. Barbed hose fittings were threaded into each pipe flange to provide a water-tight connection to 12-in-long, high-pressure hoses. These hoses were used to connect the specimens together making one long concrete segment from eight 12-in long pile segments (Figure 4-55).



Figure 4-55: Pile segments complete with pipe flanges, barbed hose fittings, and high-pressure hoses to simulate a longer length duct.

At the end of each 15ft duct a looped hose was used to connect duct 1 with duct 2 which passed back the entire length of the assembly and where duct 2 was looped back to duct 3 and then which passed back the full length of the assembly thereby terminating an 80 foot long continuous duct (Figure 4-56).

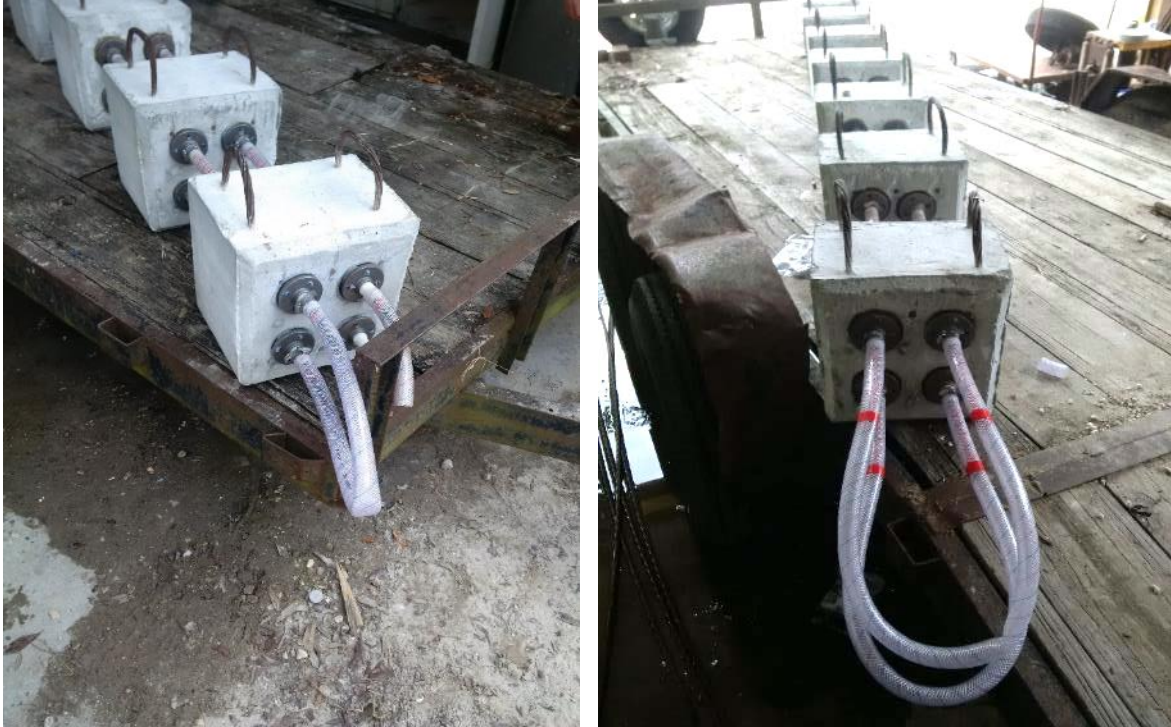


Figure 4-56: Grouting to be performed on all four duct assemblies at once via looped grout hoses on each end.

This unique setup was assembled on a flatbed trailer that could be transported anywhere in the southeastern U.S. to facilitate coordination with the Vector Corrosion team's schedule. This also minimized the number of connections Vector would be required to make while preparing/injecting 32 laboratory specimens.

With 16ft long strands inserted into each of the four ducts, grouting was conducted with a commercial ChemGrout high shear grout mixer and pump where all four ducts were grouted at once (Figure 4-57).



Figure 4-57: Grouting: grout plant (top left); grout hose connected to bottom duct, strand 3 (top right); grout in bottom two ducts but not yet in top two (bottom left); grout exiting four-duct system (bottom right).

Once the grout cured, the end hoses were all removed and new hoses were installed with shut off valves so the ends of the strands were exposed and Vector could inject the protective fluid, close off a ducts to prevent leakage, and ensure the fluid would stay in contact with the grout-to-strand interfaces. Figure 4-58 shows the process of preparing the grouted pile segments for impregnation.



Figure 4-58: Removal of hoses (top); breaking grout off the strands (bottom) before installing new hoses and valves on both ends of the entire 8 specimen assembly.

The specimens were taken to the Vector Corrosion Tampa Office to perform the impregnation of on September 9, 2019. The details of the procedure are provided in Appendix 1 which includes a report written by Vector. Specimens were left until March 11, 2020 when the connecting hoses were cut off exposing residual fluid around the grout with a waxy texture (Figure 4-59).



Figure 4-59: Connecting hoses removed showing residual impregnation product.

The strands on the last specimen on the trailer had been extended 12in to provide a connection for pullout testing (Figure 4-60). At the backside of the specimen, the connecting strands between specimens were flush cut with the flange leaving 12in of strand at one side of each specimen.



Figure 4-60: Strands extending from specimens (left); flush cut on backside (right).

Using a 1/2in strand coupler, the pullout strands were extended to pass through a thick-walled square tube section (housing the strand coupler), a hollow-core hydraulic jack, load cell, bearing plate, and a prestressing chuck with spring loaded wedges. Pullout tests were continued until a minimum of two inches of pullout displacement was achieved (Figure 4-61). Note: the fasteners holding the flanges to the concrete were removed before testing. The inner dimensions of the square tube section were sufficiently large to allow the flange clearance from binding or adding to the pullout resistance.



Figure 4-61: Pullout testing (left); flange displaced upward 2 in (right)

4.2.1 RESULTS AND DISCUSSION

Figure 4-62 shows the pullout resistance as a function of pullout displacement for 16 strands in four concrete specimens. One full length duct / strand was not impregnated making one strand in each specimen that could serve as a control. In all cases, the impregnated strands showed markedly reduced pullout resistance. Table 4-16 shows the individual peak pullout resistance for each strand and the percent reduction in resistance compared to the control. Average loss of pullout capacity was 47% ranging from 21 to 78%.

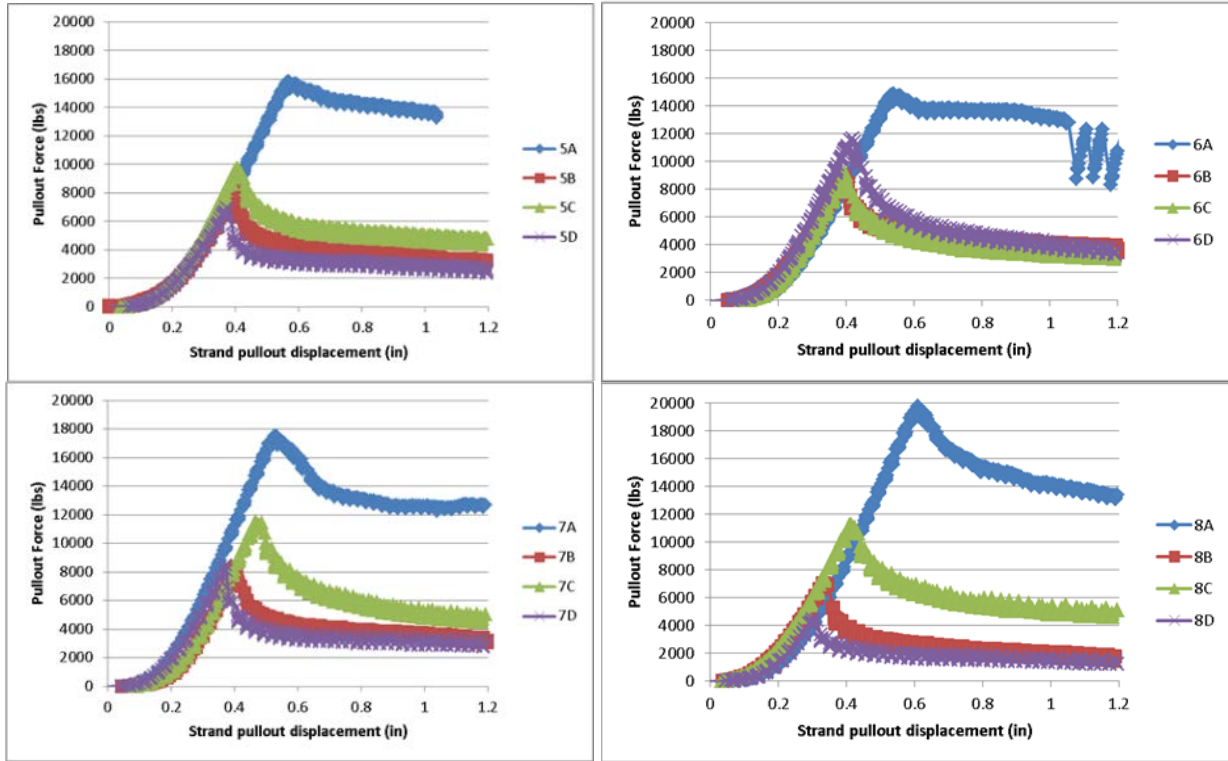


Figure 4-62: Pullout resistance for concrete specimen 5 (upper left), 6 (upper right), 7 (lower left), and 8 (lower right).

Table 4-16: Peak pullout force and the percent reduction compared to the control.

Specimen	Peak Force	Percent Reduction	Specimen Avg
5A	15802	Control	47.56%
5B	8215	48.01%	
5C	9727	38.44%	
5D	6917	56.22%	
6A	14811	Control	32.97%
6B	8978	39.39%	
6C	9152	38.21%	
6D	11654	21.32%	
7A	17501	Control	45.85%

Specimen	Peak Force	Percent Reduction	Specimen Avg
7B	8376	52.14%	
7C	11560	33.94%	
7D	8496	51.45%	
8A	19709	Control	61.67%
8B	7051	64.22%	
8C	11199	43.18%	
8D	4415	77.60%	

4.2.2 SUMMARY

In the process of evaluating the effect of pressurized penetrants on strand to grout bond, numerous specimens were prepared using ½-in Grade 270, 7-wire strands grouted into cored concrete ducts in prestressed concrete pile segments. The bonded length (12-in) was selected to ensure bond failure and not strand breakage. Pullout test results of both impregnated and un-impregnated specimens were conducted. Tendon samples impregnated with the Vector proprietary fluid showed marked reductions in pullout capacity. While this has less effect on unbonded externally post-tensioned tendon applications, it may have dire consequences for bonded tendon applications (internally post-tensioned).

CHAPTER 5 POSSIBLE LIMITATIONS AND SERVICE LIFE FORECASTING

Since the service period for the alternative fluid was found to be much less than that of the VPF, further analysis was focused on the VPF solely. Laboratory experiments were performed to identify the corrosion inhibition mechanism of the VPF and to identify any limitations in its use. Additionally, autopsies of treated and control 1ft and 3ft mock tendons were performed to quantify the corrosion damage and provide input parameters to failure forecasting models. This chapter is presented in 3 separate sections which comprise results of electrochemical testing of VPF coated wires in different immersion solutions, autopsy results for corrosion damage quantification, and tendon damage forecasting to facilitate cost analysis of the impregnation method.

5.1 DEGRADATION MECHANISMS

Experiments were designed to gain a better understanding of the inhibition mechanisms of the impregnation fluid. King wires of the 7 wire steel strands were cut in 5-inch lengths to be used for electrochemical testing. One end of each strand was epoxied to minimize any current distribution effects in the electrochemical tests. A set of wires were dip-coated in impregnation fluid and allowed to dry for 24 hours to allow any volatile components to evaporate resulting in a thin film inhibitor coating on the surface as shown in Figure 2-24. This process was repeated twice for another set of wires resulting in a 3-layer film coating. Coated wires and bare wires were immersed in various solutions that simulated different levels of corrosivity. The solution compositions are reported in Table 3-20 for each test group of wires including the noncoated (group 1), the 1 layer coated (Group 2), and the 3- layer coated (group 3). The saturated calcium hydroxide solution represented normal grout with a high pH of ~12.5. The saturated calcium hydroxide solution containing chlorides was used to represent a case where chlorides were either present in the mix water or inadvertently contained in the grout mixture and correspond to the group of tendons with admixed chlorides. The 0.6 M sodium chloride (~3.5 wt% representative of the world's average seawater salinity) solution was the most aggressive case and was designed to test the ability of the coating to hold up in the case of a voided grout region in the tendon in which seawater infiltrates.

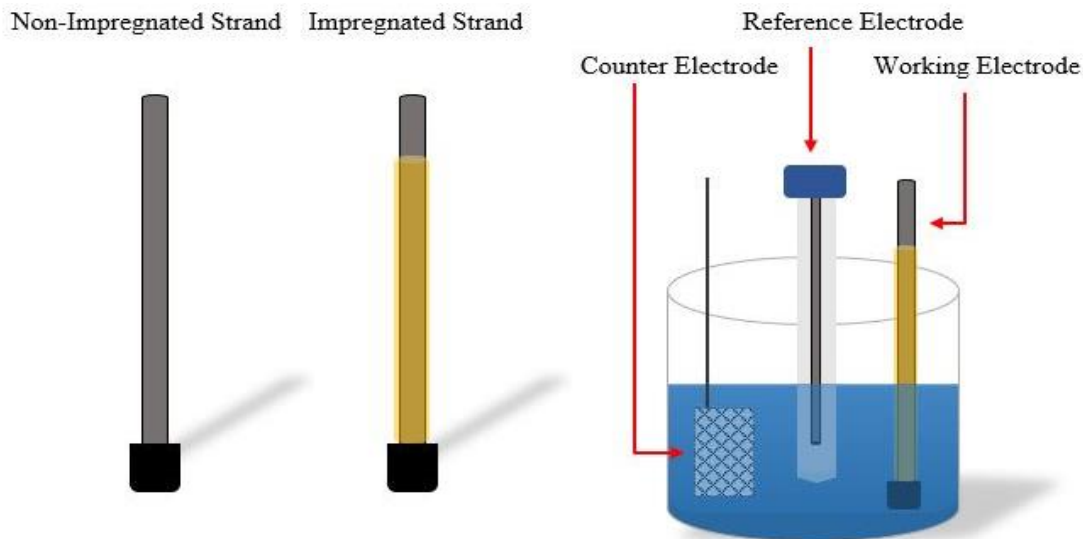


Figure 5-1: A schematic of the experiment for EIS testing on king strands.

Table 5-1: The grouping of the king strands for testing

Test Groups	Solutions
Group 1	0.6 M NaCl
Group 1	Sat. CaOH
Group 1	0.6 M NaCl & Sat. CaOH (1:1 vol ratio)
Group 2	0.6 M NaCl
Group 2	Sat. CaOH
Group 2	0.6 M NaCl & Sat. CaOH (1:1 vol ratio)
Group 3	.6 M NaCl
Group 3	Sat. CaOH
Group 3	.6 M NaCl & Sat. CaOH (1:1 vol ratio)

The coated and bare wires were immersed in an electrochemical cell containing the specified solution for a period of 24 to 48 hours depending on the corrosion performance. Electrochemical impedance measurements were taken throughout the immersion period to observe any changes in the impedance over time and also to monitor corrosion rate. Additionally, potentiodynamic polarization scans were performed to understand the influence of the coating on the anodic and cathodic kinetics in the simulated pore solutions with and without chlorides.

5.1.1 RESULTS AND DISCUSSION

Electrochemical impedance data obtained from measurements of 3-layer coated steel wires is shown in Figure 5-2. The negative component of the imaginary part of the impedance is expressed as a function of the real part for a range of frequencies. The imaginary component of the impedance is associated with capacitive or inductive features of the interface resulting from dielectric properties of materials while the real part of the impedance is associated with electrically and ionically resistive properties of the interface such as a reaction in which electrons are transfer or the ionic resistance of the solution.

Figure 5-2.a shows impedance data in Nyquist format of a wire immersed in saturated calcium hydroxide solution with time as a parameter. At high frequencies, there is a capacitive loop present that is associated with the impedance of the inhibitor coating. The width of this loop can be representative of the film resistance. At lower frequencies, the beginning of a second time constant is shown that over time becomes steeper such that the angle formed between it and the real impedance axis is ~ 45 deg indicating a possible diffusion process likely the result of ionic species entering the coating. Over a period of ~ 2 days the overall magnitude of the impedance actually increases meaning that the film remains intact and protects the steel.

In contrast, the impedance of the coated wire immersed in the solution containing chlorides shown in Figure 5-2.b, decreased substantially over a period of 20 hours. The high frequency time constant associated with the coating impedance reduced by an order of magnitude in size indicating that it was not adequately protecting the steel. The corrosion rates obtained from the impedance measurements for a bare wire, a one-layer and a three-layer coated wire are shown in Figure 5-3.a in log-scale as a function of time. The corrosion rate of the bare wire decreased from 10 to 1 $\mu\text{m}/\text{yr}$ over the first 5 hours likely due to the formation of a passive film, then suddenly increased to $>100 \mu\text{m}/\text{yr}$ indicating that the chlorides present in solution caused the passive film of the steel to breakdown. The corrosion rates of the 1 layer and 3-layer coated wires were similar and slowly increased from 10 to almost 100 $\mu\text{m}/\text{yr}$ over a 24-hour period. Images were obtained of the wires after immersion and are shown in Figure 5-3.b. The wire on the left was not coated and shows a uniform layer of corrosion products up to the level of immersion. The wire in the middle was coated with 1 layer and only shows small pits on the surface just below the level of immersion. The wire on the right was coated with 3 layers and shows what seems to be a mixture of excess coating and corrosion products. Results from replicate experiments show similar trends.

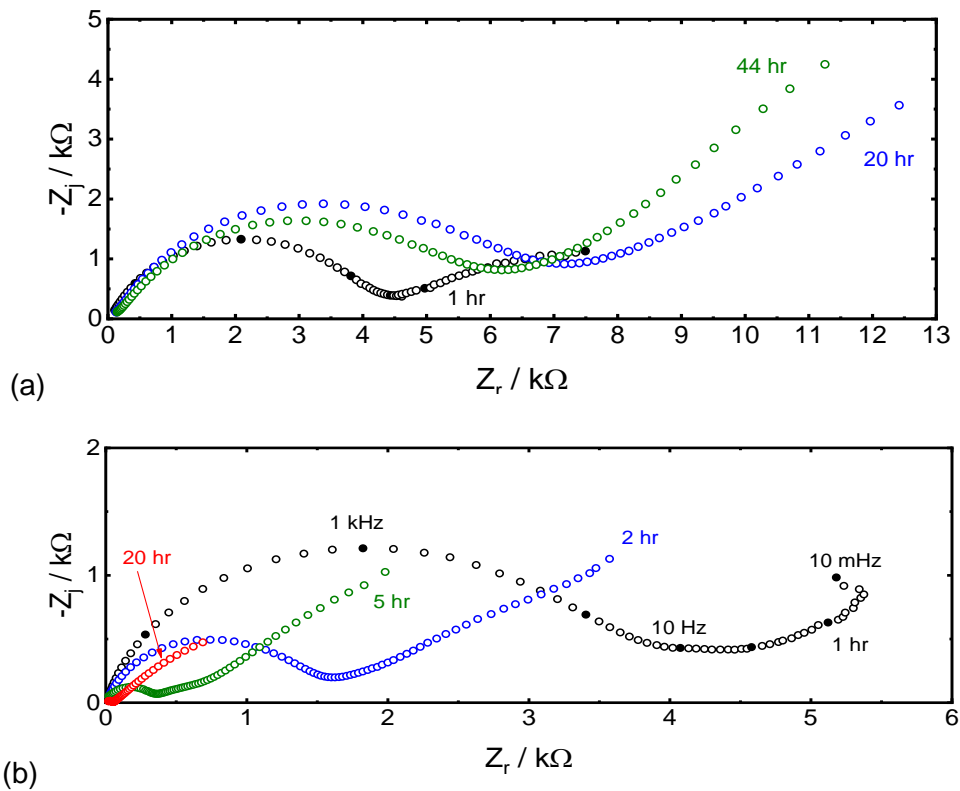


Figure 5-2: Electrochemical impedance in Nyquist format of king wire coated in three layers of the impregnation fluid: (a) saturated calcium hydroxide, pH ~12.5; (b) Calcium hydroxide with chlorides, pH~12.3.

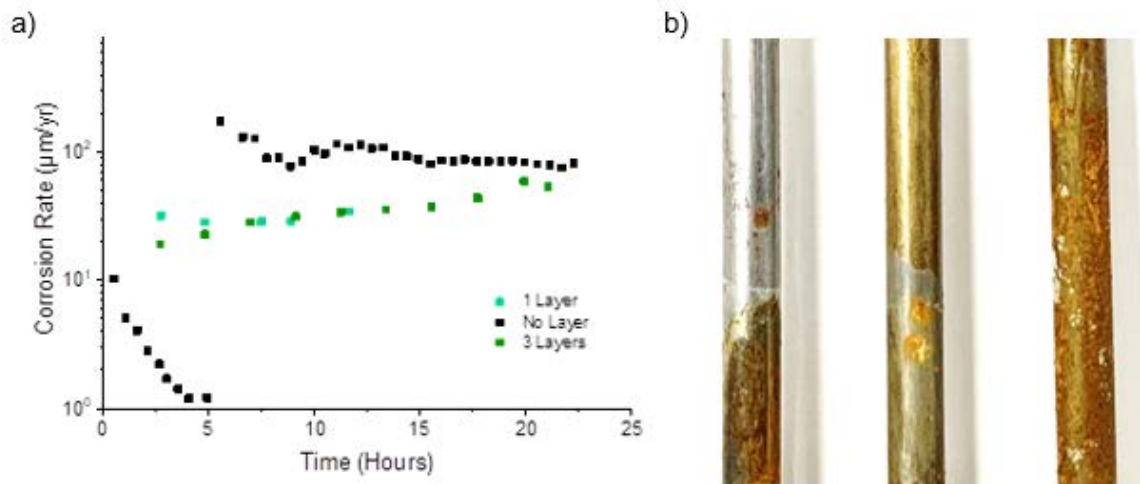


Figure 5-3: (a) Corrosion rate data calculated for the king wire with no impregnation material, one-layer of impregnation material, and three-layers of impregnation material immersed in sat. $\text{Ca}(\text{OH})_2$ and 0.6M NaCl in equal volumetric amounts; (b) king wire immersed in sat. $\text{Ca}(\text{OH})_2$ and NaCl. The non-impregnated king wire is on the left, the one-layer coated wire is in the middle, and the three-layer coated wire is on the right.

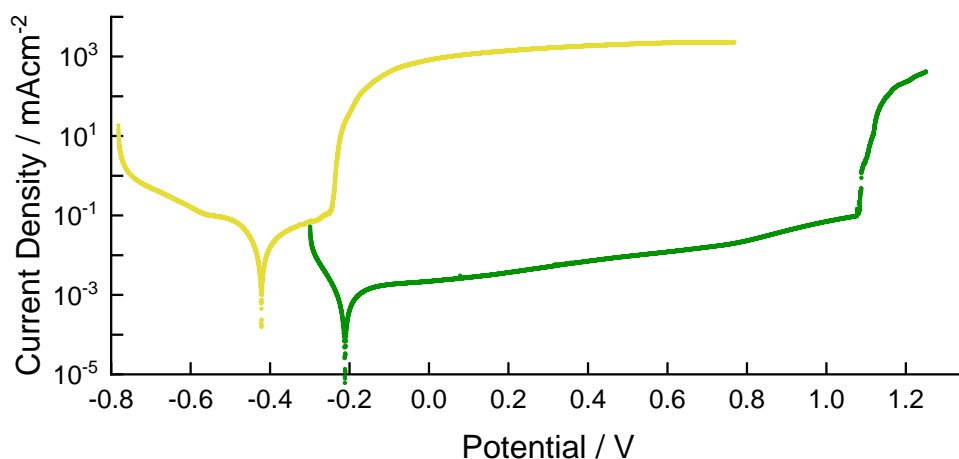


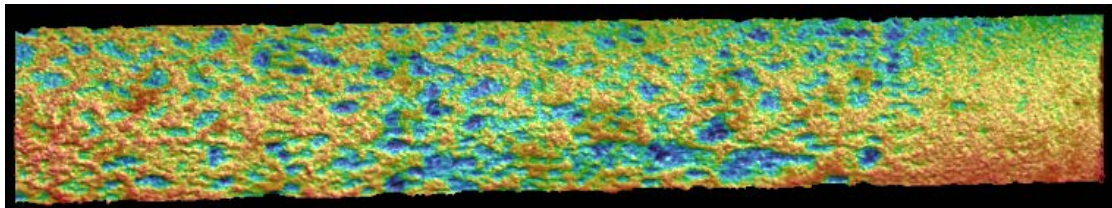
Figure 5-4: Potentiodynamic scan obtained at a scan rate of 0.167 mV/s of three-layer coated wire (green) and a bare wire (yellow) immersed in a saturated calcium hydroxide and NaCl solution.

In addition to impedance measurements, potentiodynamic polarization scans were obtained to show the influence of the inhibitor on the anodic and cathodic kinetics. The results are shown in Figure 5-4 for the three-layer coated wire in the calcium hydroxide solution with chlorides. The data obtained on the bare steel is shown in yellow while the coated steel results are shown in green. The impregnation fluid causes a significant drop in the rates of both the anodic and cathodic kinetics, indicating that the coating acts as a mixed inhibitor that likely

prevents corrosion by forming a barrier on the steel surface. In contrast, some inhibitors are designed to specifically block anodic reactions or specifically reduce the rate of oxygen reduction. Additionally, the inhibitor causes an increase in the pitting potential of almost 1V again indicating that the coating forms some form of a barrier layer. Therefore, the increase in corrosion rates shown from the impedance measurements could be due to a reaction between the coating and the metal during the formation of the barrier. However, further characterization would be required to definitively conclude this.

Surface topography images of wires immersed in a 0.6M NaCl solution are shown in Figure 5-5 without impregnation fluid (a) and with it (b). There is clear corrosion damage on the wire that was bare while the impregnation fluid prevented corrosion along most of the surface of the three-layer coated wire. However, the presence of small pits could indicate that even when the coating is evenly distributed across the surface of the steel, in highly aggressive conditions, there is still the possibility that corrosion could occur. While such conditions should not be present within post-tensioned tendons, there have been cases reported of high chloride content. The impregnation fluid prevented the onset of corrosion along most of the surface area except for the instances of microcell pitting corrosion. The level of corrosion performance exhibited by the impregnation fluid is also noted by the increased amount of immersion time. The king strand with three layers of impregnation fluid was immersed in the electrolyte for 45 hours, 21 hours more than the non-impregnated king strand.

(a)



(b)

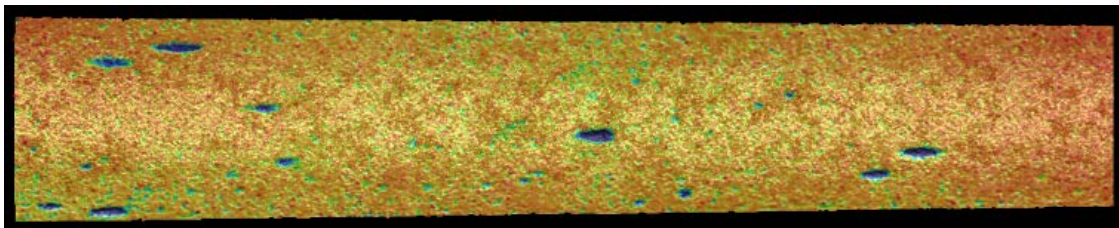


Figure 5-5: The surface topography of steel after immersion in a 0.6M NaCl solution: (a) bare wire for 24 hours; (b) three-layer coated wire for 48 hours.

5.1.2 FINDINGS AND IMPLICATIONS

1. The impregnation fluid caused a significant drop in the rates of both the anodic and cathodic kinetics indicating that the coating acts as a mixed inhibitor that likely prevents corrosion by forming a barrier on the steel surface. An increase in the pitting potential of almost 1 V was observed for the coated king wire, which further supports the corrosion-inhibiting mechanism of the impregnation material to be barrier formation.

2. The overall magnitude of the impedance increased for the impregnated king strand immersed in a simulated pore solution which indicates that the film remained intact protecting the steel over a 2-day testing period.
3. The impedance of the coated wire immersed in the saturated calcium hydroxide solution containing chlorides decreased substantially over a period of 20 hours. The coating impedance reduced by an order of magnitude in size indicating that it was not adequately protecting the steel. This could be indicative of diffusion of chlorides into the coating layer.
4. Surface topography images of wires immersed in the 0.6 M sodium chloride solution show clear corrosion damage on the bare wire that was immersed in a sodium chloride solution, while the impregnation fluid coating prevented corrosion along most of the surface of the 3-layer coated wire. However, the presence of small pits could indicate that even when the coating is evenly distributed across the surface of the steel, in a highly aggressive condition, there is still the possibility that corrosion could occur, which was also indicated by the increase in corrosion rates observed for coated king wires in simulated pore solution containing chlorides.

5.2 AUTOPSY AND FAILURE FORECAST

The corrosion rates obtained in the long-term corrosion performance tests are calculated from impedance data which provides a surface averaged quantity. Therefore, the measurements do not provide information on corrosion damage morphology. The corrosion damage is obtained from an autopsy of the tendon, thus aiding in the understanding of the ability of the impregnation material to arrest the propagation of corrosion at all corroding regions. In this section, average penetration and maximum penetration of corrosion will be measured from the surface topography measurements obtained by a 3D surface profiler. One impregnated and one control tendon was randomly selected from the 1-ft and 3-ft chloride-contaminated groups for autopsy. Additionally, an impregnated and a control tendon without chloride-contamination were autopsied for comparison.

The polymer duct of the tendons was cut longitudinally on two sides using an angle grinder. Removal of the ducts revealed in some cases impregnation fluid deposits on the grout surface as shown in Figure 5-6 by the areas emphasized in red containing yellowish/white material for a 3ft chloride free tendon. This amount of impregnation material was not seen in the 1ft impregnated tendons. Additionally, deposits were also visible in large voids contained within the grout shown in Figure 5-7. The voids contain some impregnation fluid but are not completely filled. The assessment of these relatively empty voids indicates that either the voids were unable to be saturated during impregnation or the voids became unsaturated over time. A possible reason for this is the seepage of impregnation fluid out of the tendons through the space between the polymer duct and the grout. Voids at the steel and grout interface, however, may have a greater likelihood of becoming completely filled by the impregnation fluid.

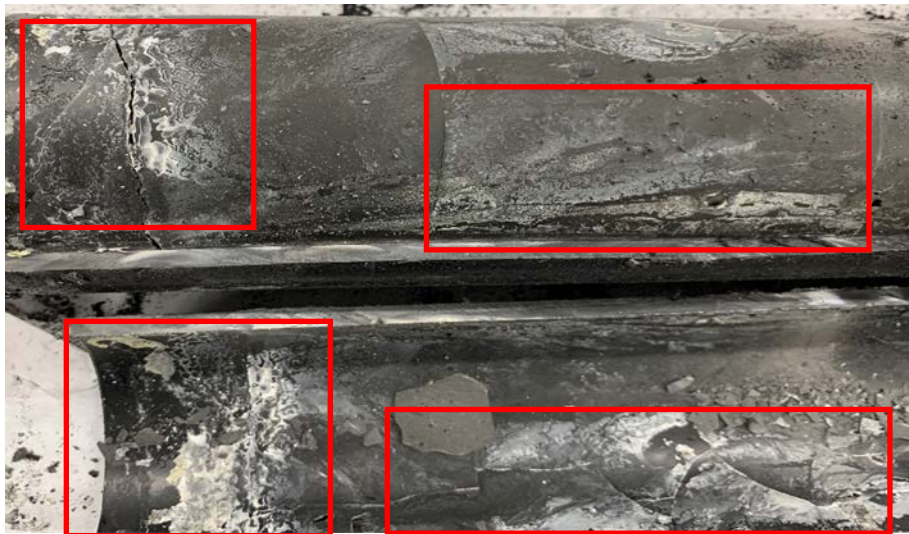


Figure 5-6: The autopsy of the 3-ft normal tendon showing the grout surface after impregnation.

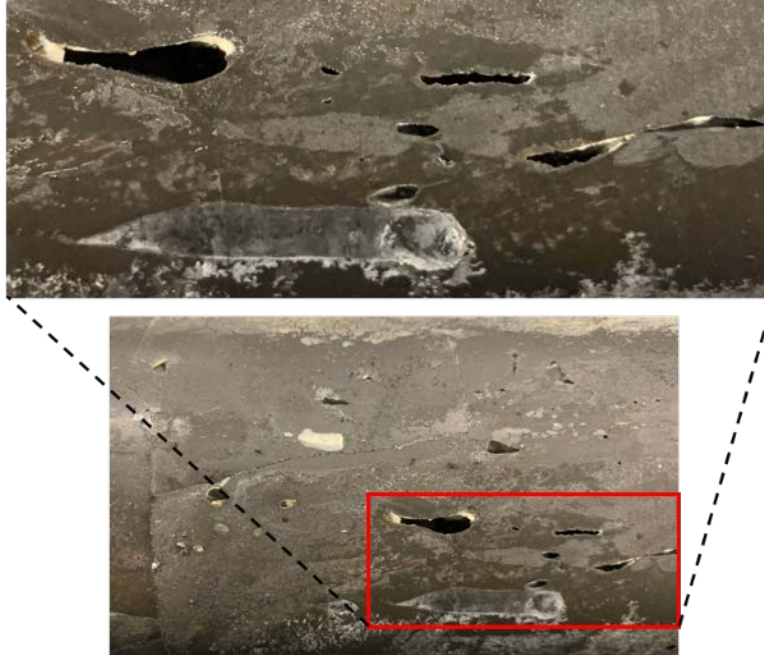


Figure 5-7: The outer surface of the impregnated grout showing the presence of impregnation material that has not completely filled disconnected voids.

After the ducts were removed from the surface of the grout, the tendons were placed under a load press and were carefully compressed to crack the grout and expose the steel strands. Images of the rebar trace along the grout are shown in Figure 5-8. In these images, there are instances of fluid filled pores, partially-filled pores, and empty pores with no impregnation material. The upper right image in Figure 5-8 contains a region outlined in red that shows a portion of the grout that was in contact with the reinforcement but does not show the presence of corrosion product, only the presence of impregnation material. Moreover, areas where reinforcement was in contact with the grout without the presence of impregnation material, there seems to be a large amount of corrosion products. This is illustrated in the region outlined in red in the bottom image of Figure 5-8. This indicates that the impregnation material was not evenly distributed upon impregnation likely due to pre-existing corrosion products. The impact this has on corrosion mitigation will be determined by corrosion damage quantification.



Figure 5-8: Images of the interior pores and voids contained in the 3-ft chloride-contaminated grout with impregnation material.

An image of the strands removed from an impregnated and a non-impregnated chloride free grout is shown in Figure 5-9. The bottom strand, removed from an impregnated tendon, seems to be evenly coated as noted by the slightly darker appearance. This would suggest that the impregnation fluid is better suited for application shortly following construction and prior to corrosion products forming. Upon removal of the strands from chloride contaminated grout shown in Figure 5-10, it is evident that both of the carbon steel reinforcements contain corrosion products but by visual inspection, the reinforcement extracted from the impregnated tendon appears to contain less corrosion product with respect to the non-impregnated tendon. Similar results were observed for the 3ft strands as well.



Figure 5-9: The reinforcement extracted from the 1-ft normal tendons. The reinforcement on the top is from the control group and the reinforcement on the bottom is from the impregnated group.



Figure 5-10: An image of the reinforcement extracted for the 1-ft chloride-contaminated tendons. The top image is the control tendon and the bottom image is the impregnated tendon.

The strands were glass bead blasted to remove any grout residue and corrosion products while ensuring the base metal remained intact. Surface topography images were obtained of the strands at 98mm increments along the surface. The glass bead blasted strands extracted from 1 ft chloride contaminated tendon with and without impregnation are shown in Figure 5-11a and Figure 5-11b, respectively. Visually it is difficult to see any difference in the amount of corrosion damage between the strand extracted from the impregnated and the one from the non-impregnated tendon. However, it does seem that there are regions on the impregnated strand, indicated by red rectangles, that have minimal amounts of corrosion damage that could have been the result of the presence of the impregnation fluid at that location. There is a much more marked difference in the corrosion damage of the 3ft strands between those extracted from the control and the impregnated tendon, shown in Figure 5-12. There is significantly less corrosion damage on the strand from the impregnated tendon which could be the result of the level of fluid observed throughout the grout compared to the minimal amount observed in the 1ft tendons.



Figure 5-11: Steel strands after corrosion product removal extracted from 1-ft tendons: (a) not impregnated; (b) impregnated.



Figure 5-12: Steel strands after corrosion product removal extracted from 3-ft tendons: (a) not impregnated; (b) impregnated.

5.2.1 RESULTS AND DISCUSSION

The following image, Figure 5-13, contains an example measurement for the maximum penetration of the autopsied 3ft tendon without impregnation. The image containing the maximum corrosion penetration is accompanied by a diagram showing the topography of the

area where maximum penetration was found. To the right of the topography image is an image of the reinforcement containing a line indicating the location of the depth measurement.

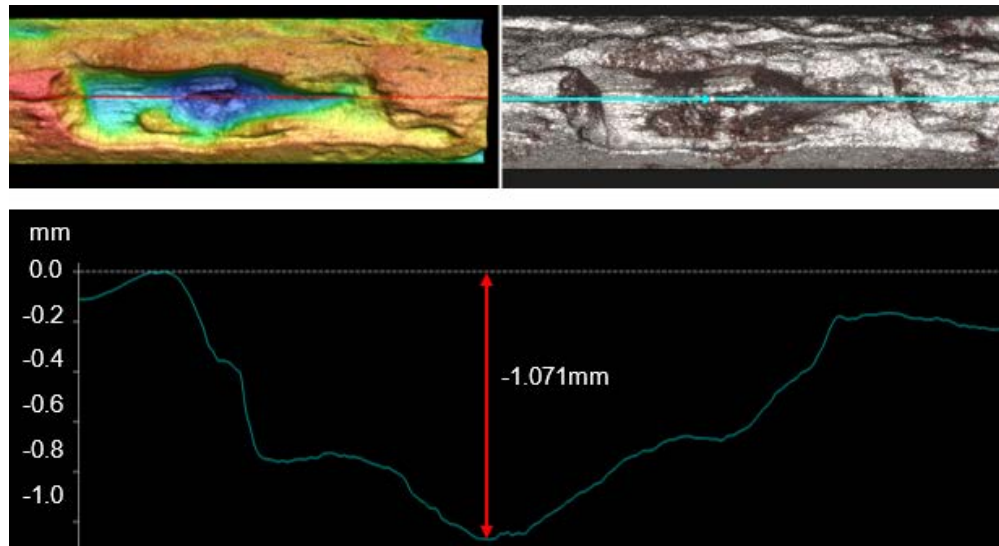


Figure 5-13: The maximum penetration calculation performed on a strand extracted from the 3-ft chloride-contaminated tendon without impregnation material. The image at the top left is the surface topography, the image at the top right contains a blue line which represent the cross-section where depth was calculated, and the bottom image contains the maximum penetration.

Additionally, a non-corroded strand was analyzed to obtain the pre-corroded surface topography. The volume of space between the strand surface and a reference plane was calculated for the uncorroded and corroded strands. By comparing the surface topography of the uncorroded strand and the autopsied strands, the total volume loss due to corrosion was obtained. To calculate volume loss, 16 pictures were obtained from the center of the reinforcement. A section 33mm in length and 8mm in width (approximately 264mm in surface area) was used for calculating the volume. The average corrosion penetration was obtained by dividing the total corroded volume by the surface area. The rate of corrosion penetration was used to calculate a time averaged corrosion rate by considering the total time since the specimens were cast. Similarly, the maximum corrosion rate was obtained by considering the maximum depth of corrosion.

The average (green) and maximum (yellow) corrosion rates are provided in Figure 5-14 for 1 ft and 3ft chloride contaminated tendons with and without impregnation fluid. In both the 1ft and 3ft tendons, the average and maximum values of the corrosion rates are greater for the strands extracted from tendons that were not impregnated. For the 1ft tendons, the average corrosion rate for the impregnated tendon is ~20% less than the tendon that was not impregnated. The 3 ft tendons showed a much greater difference of ~60%. Again, this is likely due to the fact that the 3ft tendon was more efficiently impregnated. Probably the most important result is the decrease in the maximum corrosion rate as this is what would determine the time to the first wire failure. Impregnation of the tendons caused a decrease of ~35% in the maximum corrosion rate for the 1ft tendon and ~70% for the 3ft tendon. This information will be used to develop a distribution of corrosion rates that will determine the influence impregnation has on strand failure rates.

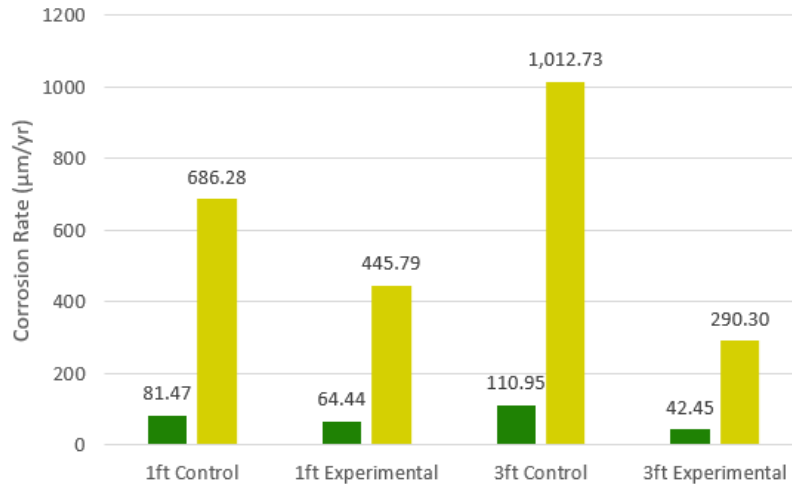


Figure 5-14: Average and maximum corrosion rates of strands extracted from 1-ft and 3-ft chloride-contaminated tendons with and without impregnation.

5.2.2 FINDING AND IMPLICATIONS

Electrochemical testing was performed on VPF coated wires immersed in different simulating solutions representing various levels of corrosivity to determine the protection mechanism and identify any possible limitations. The results showed that the VPF forms a protective coating on the steel surface that limits both cathodic and anodic activity. When coated wires were immersed in an alkaline solution simulating the grout pore solution, the impedance showed that the coating resistance actually increased initially possibly indicating a barrier formation reaction of the coating that would increase its protective qualities. However, when immersed in an alkaline solution with chlorides, the impedance decreased substantially over time. While it is not often expected that chlorides should be present within the tendons, as stated in the literature review there have been cases in which chlorides have infiltrated the tendon duct by water intrusion. The surface topography of a 3-layer VPF coated wire immersed in a chloride solution showed small distinctly separated pits. This may indicate that even if the VPF is able to uniformly coat the steel surface, aggressive water intrusion may still cause corrosion. While it may be unlikely that seawater will directly infiltrate the tendon and fill a voided region, this result helps provide insight on a possible mode of coating degradation.

The VPF fluid was also tested for its ability to fill the grout pore space and to evenly coat the steel strands and arrest corrosion. Upon autopsy, it was clear that the VPF was only able to partially fill the grout pore space in both 1ft tendons with 1 strand and 3 ft tendons with 3 strands. However, there was much more VPF present in the 3ft tendons likely the result of greater inter-wire space provided by the bundled strand configuration. The VPF was observed to preferentially coat less corroded regions of the steel surface indicating that pre-existing corrosion products may impede impregnation. However, even though pre-existing corrosion products may have prevented uniform fluid application, there was a substantial reduction in both the surface averaged and maximum corrosion penetration of the 3ft tendon with 3 bundled strands in comparison to only moderate reductions observed in the single strand 1ft tendons. A significant reduction in maximum corrosion penetration may indicate that the VPF is capable of

arresting corrosion in regions where layers of pre-existing corrosion are present. Overall the results suggest that impregnation is more effective if the strands are grouped together in a bundled configuration which increases inter-wire space and allows for adequate application of the impregnation fluid. Otherwise, in cases where the inter-wire space may be plugged by corrosion products, the VPF may not be as effective.

5.3 FAILURE FORECASTING

The corrosion damage morphology quantified in terms of mean and maximum corrosion penetration are now used to forecast tendon failures based on treated and untreated cases. The results may be used to facilitate life cycle cost estimates. Hartt et al. showed that as corrosion pits on tendon strands grow, they form flat planes that can be simulated to propagate without changing shape into the strand wires⁹¹. The corrosion damage cross sectional area shown in Figure 5-15 as the blue shaded region may be calculated as

$$\text{Equation 5-1} \quad A_c = 0.5r^2 (a - \sin a)$$

where r is the radius of the wire and a is the sector angle formed by the cord length, c , associated with the width of the plane. Therefore, the residual wire cross sectional area, A_r , may be expressed as the difference between initial cross-sectional area and the corroded area. Provided a time-averaged corrosion rate, $\frac{dh}{dt}$, the depth of corrosion penetration, h , as a function of time may be expressed as

$$\text{Equation 5-2} \quad h(t) = \frac{dh}{dt} t$$

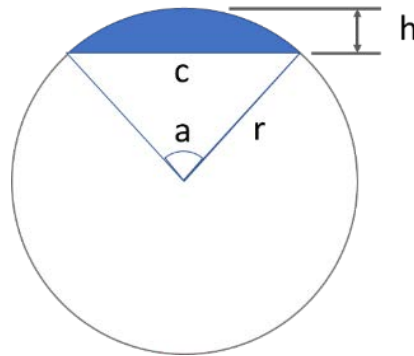


Figure 5-15: Steel strand wire cross-section showing corrosion damage morphology.

The steel strands used in post-tensioned tendon construction are specified to a guaranteed ultimate tensile strength (GUTS) of 1850 MPa. During construction the strands are stressed to 80% GUTS and due to relaxation over time end up at approximately 63% GUTS (1172 MPa). Corrosion damage of the wires results in a loss of cross-sectional area which in turn reduces the tensile strength of the wire. Hartt et al showed that the residual strength of these high strength steel wires due to corrosion damage follows a linear relationship expressed as

$$\text{Equation 5-3} \quad S_r = 1969 A_r/A_0 - 107.2$$

where A_r/A_0 represents ratio of residual area and initial area. According to this equation, when there is no corrosion damage, the strength is equal to the specified GUTS. When the cross-sectional area reduction results in a residual strength that is below the relaxed stress applied to the steel strands, the wire is assumed to fail.

A statistical distribution of corrosion rates was obtained from the corrosion morphology analysis presented in Section 0 of the autopsied tendons. The surface averaged penetration and the time since casting was used to obtain a temporal and spatially averaged corrosion rate. The maximum corrosion penetration from each specimen was used to specify the maximum possible corrosion rate. Assuming a Weibull statistical distribution based on the mean corrosion rate and a standard deviation expressed as the quotient of the maximum value and 3.5, a distribution of corrosion rates is obtained. An example distribution of corrosion rates based on a sample size of 21,384 wires with a mean and standard deviation corrosion rate of 110.95 and 128.88, respectively is shown in Figure 5-16.

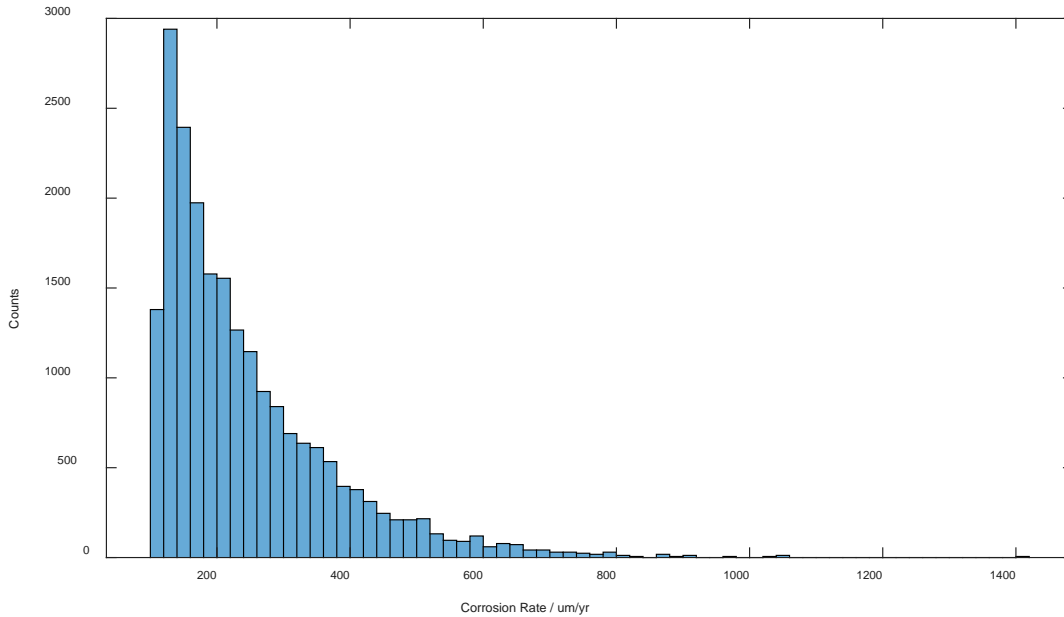


Figure 5-16: Corrosion rate distribution example based upon a sample size of 21,384 with a mean of 110.95 and standard deviation of 128.8. Values correspond to the 3-ft tendon without impregnation

The corrosion rate distributions are used to forecast the accumulation of wire failures over time using Equation 5-3 with 63% GUTS as the failure criteria. When 3 wires within a strand have failed, the strand is assumed to fail.

The failure percentage of wires for the 1ft and 3ft tendons is shown in Figure 5-17. The impregnation fluid is shown to extend the time until 20 % of the wires have failed from 18 to 60 years for the 3ft tendon and from 26 to 38 for the 1ft tendon.

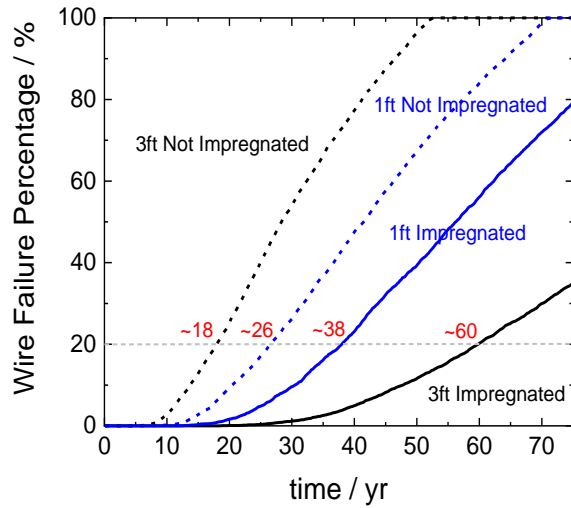


Figure 5-17: Wire failure percentage as a function of time obtained from corrosion data presented in Figure 5-14. Values shown in red correspond to time in which 20% of the wires have failed.

The failure percentage of strands for the 1ft and 3ft tendons is shown in Figure 5-18. The impregnation fluid is shown to extend the time until the first strand failure from 13 to 36 years for the 3ft tendon and from 14 to 18 for the 1ft tendon.

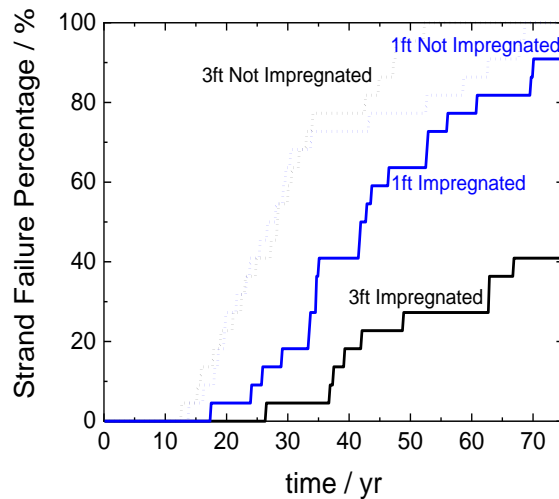


Figure 5-18: Strand failure percentage as a function of time obtained from corrosion data presented in Figure 5-14.

5.3.1 SUMMARY

Impregnation of the tendons caused a decrease of ~35% in the maximum corrosion rate for the 1ft tendon and ~70% for the 3ft tendon. While the results are based only on autopsy of 1/3 of the specimens, the corrosion damage distribution obtained represents a statistically significant sample size of data considering point by point pit depths. Based on the corrosion damage values, a failure forecast model was used to show that impregnation has the ability to substantially extend the time until tendon failure if the fluid is adequately applied as indicated by exiting fluid at the end-point of the targeted application.

CHAPTER 6 CONCLUSIONS AND RECOMMENDATIONS

Testing was performed on mock-up PTT with intentional grout deficiencies to test the ability of the impregnation method to prevent and arrest corrosion. Experimental pile sections were designed to test the influence of the impregnation fluid on the strand to grout and grout to concrete bond strength. A list of detailed conclusions and recommendations are presented below.

6.1 ALTERNATIVE FLUID PERFORMANCE

1. Experiments with mock-up specimens, with grout deficiencies in the form of a void temporarily filled with 3 wt.% NaCl solution, yielded good prognosis for successful corrosion abatement by impregnating PTT specimens with a alternative impregnation material delivered via the inter-wire channels.
2. Potentiodynamic polarization and electrochemical impedance spectroscopy tests indicated an estimated reduction in corrosion rate, upon impregnation, of about one or more orders of magnitude.
3. The experimental results suggested that once impregnation was initiated, corrosion mitigation was initially under cathodic activation control. Anodic polarization was indicated as well as time proceeded. The mitigation mechanism appears to be related to the formation or deposition of a film on the steel surface. Increased grout resistivity as well as decreased oxygen transport did not show signs of being dominant factors in mitigating corrosion.
4. While initial results showed promise in the ability of the alternative fluid to arrest corrosion, the effectiveness was found to only last a few months, indicating that the alternative fluid tested should not be considered for use without multiple impregnation events or some form of modification to extend the useful service period.
5. Pullout test results of both impregnated and un-impregnated specimens indicated no discernible effect from the presence or use of two different alternative penetrant materials when compared to normal un-impregnated samples.

6.2 VECTOR PROPRIETARY FLUID PERFORMANCE

1. The Vector proprietary fluid was effective in arresting corrosion noted by the steady decrease in corrosion rate upon impregnation of chloride-contaminated specimens for a period of at least six months.
2. Upon impregnation of the 3ft chloride free tendons, there was a significantly larger decrease in corrosion rate relative to that of the 1ft chloride free tendons, a likely result of better fluid application and distribution which may have been facilitated by greater inter wire space provided by bundled strand configuration.
3. Autopsy of selected tendons revealed that the VPF is able to penetrate the grout but may not fill small or large voids that may be disconnected from the strand's inter-wire space.

4. Autopsy also confirmed the results of the electrochemical test showing that the VPF effectively mitigated corrosion on pre-corroded 3ft tendons with a bundled strand configuration despite visual observation of nonuniform fluid distribution at the steel and grout interface.
5. Chloride intrusion was identified as a possible mechanism that may compromise the VPF's corrosion mitigating abilities.
6. Tendon samples impregnated with the VPF showed marked reductions in pullout capacity. While this has less effect on externally post-tensioned tendon applications, it may have dire consequences for grouted internal tendon applications.

6.3 INFLUENCE OF PARAMETERS ON CORROSION RATES

1. Modeling identified a potentially adverse effect of impregnation, consisting of enhancing the corrosion rates of remaining anodes, if the impregnation caused mainly an activation polarization increase on the anodic reaction but not covering the entire metal surface.
2. Modeling also projected that for an ideal condition where oxygen was not allowed to be replenished inside the duct, supplemental protective measures such as impregnation would be of limited need. However, for more realistic conditions of no-airtight ducts, or when oxygen might flow through strand's interstitial sites, the model projections supported the need for implementation of protection and or prevention practices. Further details of the work here were also presented in a NACE conference paper⁹².

6.4 RECOMMENDATIONS

1. VPF fluid should only be used in tendons where bond strength is not required such as some external post-tensioned tendons.
2. Adequate application of the VPF should be ensured. If pressure injection seems to be difficult, as was the case for the pre-corroded 1ft mock-up PTT, then other intermediate injection ports should be used. Otherwise, impregnation will likely not be as effective in mitigating corrosion.
3. Once impregnated, water-intrusion should be prevented as much as possible and periodic corrosion monitoring should be implemented.

REFERENCES

1. Martin, L. D., and Perry, C.J, PCI design handbook: precast and prestressed concrete. MNL-120. 6th ed. Chicago, IL: PCI, 2004.
2. Feld, J., Carper, K. L., Construction Failure, Vol. 78, John Wiley & Sons, 1997.
3. Powers, R. G., Sagüés, A.A., Virmani, Y.P., "Corrosion of Post-Tensioned Tendons In Florida Bridges", Proceedings, 17th. U.S.-Japan Bridge Engineering Workshop, Nov. 12-14, 2001, Public Works Research Institute, Japan, Technical Memorandum of PWRI No. 3843, Hiroshi Sato, Ed. pp. 579-594, PWRI, 2002.
4. Corven, J., Mid Bay Bridge Post-Tensioning Evaluation, Final Report, Corven Engineering, Inc., Tallahassee, October 2001.
5. Wang, H., Sagüés, A.A., Powers, R.G., Corrosion of the Strand-Anchorage System in Post-Tensioned Grouted Assemblies. Paper No 05266, Corrosion 2005, NACE International, Houston, 2005.
6. Sagüés, A. A., Powers, R. G., Wang, H., Mechanism of Corrosion of Steel Strands in Post Tensioned Grouted Assemblies. Paper No. 03312, Corrosion 2003, NACE International, Houston, 2003.
7. Venugopalan, S., Hartt, W. H., Powers, R. G., Corrosion Evaluation of Post-Tensioned Tendons on the Mid Bay Bridge in Destin, Florida. Final Report, Florida Atlantic University, Boca Raton, FL, 2002.
8. Schokker, A. J., West, JS, Breen, JE, and Kreger, ME, Interim Conclusions, Recommendations, and Design Guidelines for Durability of Post-Tensioned Bridge Substructures. Report No. FHWA/TX-04/0-1405-9. Center for Transportation Research, Austin- Texas, 1999.
9. Salas, R. M., Schokker, A. J., West, J. S., Breen, J. E., Kreger, M. E., Conclusions, recommendations, and design guidelines for corrosion protection of posttensioned bridges." University of Texas at Austin, Center for Transportation Research; National Technical Information Service, Austin, TX; Springfield, Va., 100. 2004.
10. Sprinkel, M., Napier, C. S., VDOT experience with grouts and grouted port-tensioned tendons in Varina-Enon precast segmental post-tensioned bridge. Virginia Concrete Conference 2008., PTI Journal August 2015, 51-61, 2015
11. Moreno, E. I., Sagüés, A. A., Carbonation-induced corrosion of blended-cement concrete mix designs for highway structures. Paper No. 636, Corrosion 1998, NACE International, Houston, 1998.
12. Taveira, L. V., Sagüés, A. A., Lopez-Sabando, J., Detection of Corrosion of Post- Tensioned Strands in Grouted Assemblies. Paper No. 08398, Corrosion 2008, NACE International, Houston, 2008.

13. Chen, Y.-M., Orazem, M. E., Impedance analysis of ASTM A416 tendon steel corrosion in alkaline simulated pore solutions. *Corrosion Science* 2016, 104, 26-35.
14. Corven, J., Moreton, A., Post-tensioning tendon installation and grouting manual. Manual No. FHWA-NHI-13-026. Federal Highway Administration, Washington, D.C. 2004.
15. Lau, K., Rafols, J., Lasa, I., Paredes, M., Laboratory Corrosion Assessment of Post-Tensioned Tendons Repaired with Dissimilar Grout. Paper No. 2602, Corrosion 2013, NACE International, Houston, TX, 2013.
16. Rafols, J. C., Lau, K., Lasa, I., Paredes, M., ElSafty, A., Approach to Determine Corrosion Propensity in Post-Tensioned Tendons with Deficient Grout, *Open Journal of Civil Engineering* 3.03 (2013): 182.
17. Permech, S., Lau, K., Lasa Ivan, Mario, P., Material and Corrosion Evaluation of Deficient PT Grout with Enhanced Sulfate Concentrations. Paper No. 5828, Corrosion 2015, NACE International, Houston, 2015.
18. Lau, K., Powers, R., Paredes, M., Corrosion Evaluation of Repair-Grouted Post-Tensioned Tendons in Presence of Bleed Water. Paper No. 2604, Corrosion 2013, NACE International, Houston, 2013.
19. Vallier, R. W., Flexible Filler Material for Post-Tensioned Systems. FDOT, 2014 Design Training Expo. Presentation at 2014 Design Training Expo, Florida Department of Transportation, Tallahassee, FL, June 11, 2014.
20. Lee, S.-K., Zielske, J., An FHWA Special Study: Post-Tensioning Tendon Grout Chloride Thresholds, Publication No. FHWA-HRT-14-039, Federal Highway Administration, McLean, VA, 2014.
21. Hartt, W. H., Vincent, J. F., Ivanov, V. I., Wire/Strand Slippage in Anchorages – A Potential Failure Mode for Corroding Post-Tensioning Tendons, Paper No 5461 Corrosion 2015, NACE International, Houston, 2015.
22. Hartt, W. H., Lee, S.-K., Projecting Corrosion-Induced Bridge Tendon Failure Resulting from Deficient Grout: Part I—Model Development and Example Results. *Corrosion* 2016, 72 (8), 991-998.
23. Vector Corrosion Technologies, Post-Tech® PTI Impregnation System Corrosion Protection System for Bonded Post-Tension Tendons, Manitoba, Canada, 2014.
24. Rahim, A.; Jansen, D.; Abo-Shadi, N., Concrete Bridge Deck Crack Sealing: An Overview of Research, Final Report No. F05IR345 , Cal Poly State University, San Luis Obispo, 2007.
25. Žemajtis, J.; Weyers, R., Concrete bridge service life extension using sealers in chloride-laden environments. *Journal of the Transportation Research Board*, 1561, 1-5, 1996.
26. Soriano, A., Alternative sealants for bridge decks. Final Report No. SD2001-04-D, South Dakota Department of Transportation, Pierre, 2002.

27. Sprinkel, M. M.; DeMars, M., Gravity-fill polymer crack sealers. Transportation Research Board, 1490, 43-53, 1995.
28. Frank, K.; Breen, E., Evaluation of agents for lubrication and temporary corrosion protection of post-tension tendons, Center for Transportation Research, The University of Texas at Austin, Report No. FHWA/TX-94+1264-1 for Texas Department of Transportation, August, 1993.
29. Sagüés, A. A.; Karins, F. C.; Lau, K., Corrosion Characteristics of Post-Tensioning Strands in UngROUTED Ducts, Final Report to Florida Dept. of Transportation. May 16, 2011.
30. PTI, Post-Tensioning Institute. Specification for Grouting of Post-Tensioned Structures. PTI Guide Specification, 2nd. Ed, PTI, Phoenix, Arizona, April. 2003.
31. ASBI, Temporary tendon protection against corrosion. ASBI Newsletter Segments, 46, Spring. 2005.
32. Cortec Corporation, MCI® Coating for Rebar, 2011, St. Paul, MN.
33. Lüthi, T.; Diephuis, J. R.; Icaza A, J. J.; Breen, J. E.; Kreger, M. E., Effects of Duct Types and Emulsifiable Oils on Bond and Friction Losses in Posttensioned Concrete. Journal of Bridge Engineering 2008, 13 (1), 100-109.
34. Marti, P.; Ullner, R.; Faller, M.; Czaderski, C.; Motavalli, M., Temporary corrosion protection and bond of prestressing steel. ACI Structural Journal 2008, 105 (1), 51.
35. Isecke, B.; Mahicke, W.; Mietz, J.; Rueckert, J., Temporary corrosion protection of prestressing steels with film forming coatings. Materials and Corrosion 1997, 48 (9), 613-623.
36. Isecke, B.; Mietz, J.; Schütt, K., Temporary corrosion protection of prestressing steels in non-injected ducts. Materials and Corrosion 2003, 54 (6), 413-418.
37. Borzovič, V.; Laco, J., Bond Stress-slip behaviour of prestressing units coated with corrosion protection. In Transactions of the VŠB – Technical University of Ostrava, Civil Engineering Series, 2013; Vol. 13, p 13.
38. Laco, J.; Borzovic, V., Experimental Investigation of Prestressing Strand Bond on Behavior of Concrete Members. ACI Structural Journal 2017, 114 (1), 15.
39. Vander Velde, H., Patent. Corrosion condition evaluation and corrosion protection of unbonded post-tension cables in concrete structures. Patent number 5,460,033. 1995.
40. Banks, L.; Hosgood, H. D., Patent. Inhibiting corrosion in reinforced concrete. Publication No. WO/1987/006958. 1992.
41. Cailleux, E.; Pollet, V.; Dubois, P.; Michaux, D., A new corrosion treatment for prestressed rebars: the direct injection of a corrosion inhibitor by an ultrasonic pump. Proceedings for Structural Fault and Repair, Edinburgh (2008).

42. Schupack, M, 1974, p. 28-39, PRECAST/PRESTRESSED CONCRETE INSTITUTE. JOURNAL, Volume: 19, Issue Number: 6
43. Whitmore, D.; Lasa, I. In Cable Impregnation for Post-Tension Grouting Problems, Transportation 2014: Past, Present, Future-2014 Conference and Exhibition of the Transportation Association of Canada//Transport 2014: Du passé vers l'avenir-2014 Congrès et Exposition de l'Association des transports du Canada, 2014.
44. Whitmore, D.; Beaudette, M., Impregnation of Post-Tensioning Tendons, A solution for post-tensioning steel corrosion. Aspire ASPIRE, 36-37 2016, Winter 2016.
45. Whitmore, D., Corrosion protection of cables in a concrete structure, Patent, publication No. EP2885452 A4. 2016.
46. Whitmore, D.; Arnesen, T.; Pales, B., Investigating and Resolving Bridge Grouted PT-Strand Corrosion Problems. Structures Congress, Denver, Colorado, 2017.
47. Whitmore, D.; Fallis, G.; Liao, H.; Strombeck, S.; Lasa, I., Tendon Impregnation Technology Mitigates Corrosion and Protects Post-Tensioned Tendons. PTI Journal, 17-21 2014, August 2014.
48. Whitmore, D.; Lasa, I.; Haixue, L., Impregnation technique provides corrosion protection to grouted post-tensioning tendons. In Multi-Span Large Bridges, CRC Press: 2015; pp 1065-1072.
49. Sprinkel, M. Presentation, "Performance of Posttensioned Bridges"; Virginia Transportation Research Council: 2017.
50. Bergum, K.; Risher, T. Presentation, "Evaluation of a Silicon Based Polymer Corrosion Inhibitor for Post-Tensioned Tendons"; State Materials Office-Florida Department of Transportation-Corrosion/Durability Laboratory: 2017, 2017.
51. Wittmann, F. H.; Wittmann, A. D. A.; Wang, P. G., Capillary Absorption of Integral Water Repellent and Surface Impregnated Concrete. In Restoration of Buildings and Monuments, 2014; Vol. 20, p 281.
52. Lipiec, J.; Hajnos, M.; Świeboda, R., Estimating effects of compaction on pore size distribution of soil aggregates by mercury porosimeter. Geoderma 2012, 179, 20-27.
53. Zhang, P.; Wittmann, F.; Zhao, T., Capillary Suction of and Chloride Penetration into Integral Water Repellent Concrete/Kapillare Saugfähigkeit und Eindringen von Chloriden in integral hydrophobierten Beton. Restoration of Buildings and Monuments 2009, 15 (3), 187-194.
54. Dai, J.-G.; Akira, Y.; Wittmann, F. H.; Yokota, H.; Zhang, P., Water repellent surface impregnation for extension of service life of reinforced concrete structures in marine environments: The role of cracks. Cement and Concrete Composites 2010, 32 (2), 101-109.
55. Zhan, H.; Wittmann, F., Relation between the Silicon Resin Profiles in Water Repellent Treated Concrete and the Effectiveness as a Chloride Barrier/Zusammenhang zwischen

dem Tiefenprofil des Silikonharzes und der Wirksamkeit einer Hydrophobierung als Chloridschranke. *Restoration of Buildings and Monuments* 2005, 11 (1), 35-46.

56. Johansson, A. Impregnation of concrete structures: transportation and fixation of moisture in water repellent treated concrete, TRITA-BKN. Bulletin 84,2006.
57. Wang, P.; Wittmann, F. H.; Zhao, T.; Lu, W.; Yao, X. Chloride Penetration into Integral Water Repellent Concrete Produced with Linseed Oil, Proc. 7th Int. Conf. on Water Repellent Treatment of Building Materials, Hydrophobe VII, Aedificatio Publishers, Germany, 2014; pp 39- 45.
58. Zhu, Y.-G.; Kou, S.-C.; Poon, C.-S.; Dai, J.-G.; Li, Q.-Y., Influence of silane-based water repellent on the durability properties of recycled aggregate concrete. *Cement and Concrete Composites* 2013, 35 (1), 32-38.
59. Basheer, P. A. M.; Basheer, L.; Cleland, D. J.; Long, A. E., Surface treatments for concrete: assessment methods and reported performance. *Construction and Building Materials* 1997, 11 (7), 413-429.
60. Thompson, J. L.; Silsbee, M. R.; Gill, P. M.; Scheetz, B. E., Characterization of silicate sealers on concrete. *Cement and Concrete Research* 1997, 27 (10), 1561-1567.
61. Delucchi, M.; Barbucci, A.; Cerisola, G., Study of the physico-chemical properties of organic coatings for concrete degradation control. *Construction and Building Materials* 1997, 11 (7), 365-371.
62. Ibrahim, M.; Al-Gahtani, A. S.; Maslehuddin, M.; Almusallam, A. A., Effectiveness of concrete surface treatment materials in reducing chloride-induced reinforcement corrosion. *Construction and Building Materials* 1997, 11 (7), 443-451.
63. Asthana, K. K.; Aggarwal, L. K.; Lakhani, R., A novel interpenetrating polymer network coating for the protection of steel reinforcement in concrete. *Cement and Concrete Research* 1999, 29 (10), 1541-1548.
64. Seneviratne, A. M. G.; Sergi, G.; Page, C. L., Performance characteristics of surface coatings applied to concrete for control of reinforcement corrosion. *Construction and Building Materials* 2000, 14 (1), 55-59.
65. Moon, H. Y.; Shin, D. G.; Choi, D. S., Evaluation of the durability of mortar and concrete applied with inorganic coating material and surface treatment system. *Construction and Building Materials* 2007, 21 (2), 362-369.
66. Medeiros, M. H. F.; Helene, P., Surface treatment of reinforced concrete in marine environment: Influence on chloride diffusion coefficient and capillary water absorption. *Construction and Building Materials* 2009, 23 (3), 1476-1484.
67. Suter, S. P.; Skalak, R., The history of Poiseuille's law. *Annual Review of Fluid Mechanics* 1993, 25 (1), 1-20.

68. Munson, B. R.; Young, D. F.; Okiishi, T. H., *Fundamentals of fluid mechanics*. New York 1990.
69. Chandrasekar, M.; Suresh, S.; Chandra Bose, A., Experimental studies on heat transfer and friction factor characteristics of Al₂O₃/water nanofluid in a circular pipe under laminar flow with wire coil inserts. *Experimental Thermal and Fluid Science* 2010, 34 (2), 122-130.
70. Pak, B. C.; Cho, Y. I., Hydrodynamic and heat transfer study of dispersed fluids with submicron metallic oxide particles. *Experimental Heat Transfer an International Journal* 1998, 11 (2), 151-170.
71. Walsh, M. T.; Sagüés, A. A., Steel Corrosion in Submerged Concrete Structures—Part 2: Modeling of Corrosion Evolution and Control. *Corrosion* 2016, 72 (5), 665-678.
72. Walsh, M. T., Sagüés, A.A, Steel Corrosion in Submerged Concrete Structures—Part 1: Field Observations and Corrosion Distribution Modeling. *Corrosion* 2016, 72 (4), 518-533.
73. Whitmore, D.; Lasa, I. In *Cable Impregnation for Post-Tension Grouting Problems*, Transportation 2014: Past, Present, Future-2014 Conference and Exhibition of the Transportation Association of Canada//Transport 2014: Du passé vers l'avenir-2014 Congrès et Exposition de l'Association des transports du Canada, 2014.
74. Whitmore, D.; Fallis, G.; Liao, H.; Strombeck, S.; Lasa, I., Tendon Impregnation Technology Mitigates Corrosion and Protects Post-Tensioned Tendons. *PTI Journal*, 17-21 **2014**, August 2014.
75. Kestin, J.; Sokolov, M.; Wakeham, W. A., Viscosity of liquid water in the range- 8 C to 150 C. *Journal of Physical and Chemical Reference Data* **1978**, 7 (3), 941-948.
76. Morris, W.; Moreno, E. I.; Sagüés, A. A., Practical evaluation of resistivity of concrete in test cylinders using a Wenner array probe. *Cement and Concrete Research* **1996**, 26 (12), 1779-1787.
77. Azarsa, P.; Gupta, R., Electrical resistivity of concrete for durability evaluation: a review. *Advances in Materials Science and Engineering* **2017**, 2017.
78. Sagüés, A. A.; Wang, H.; Powers, R. G., Mechanism of Corrosion of Steel Strands in Post Tensioned Grouted Assemblies. Paper No. 03312, Corrosion 2003, NACE International, Houston, 2003.
79. Sagüés, A. A.; Pech-Canul, M. A.; Shahid Al-Mansur, A. K. M., Corrosion macrocell behavior of reinforcing steel in partially submerged concrete columns. *Corrosion Science* **2003**, 45 (1), 7-32.
80. Li, L.; Sagüés, A. A., Chloride Corrosion Threshold of Reinforcing Steel in Alkaline Solutions—Open-Circuit Immersion Tests. *CORROSION* **2001**, 57 (1), 19-28.
81. ASTM G102-89(2015)e1, Standard Practice for Calculation of Corrosion Rates and Related Information from Electrochemical Measurements, ASTM International, West Conshohocken, PA, 2015, www.astm.org.

82. McCafferty, E., Validation of corrosion rates measured by the Tafel extrapolation method. *Corrosion Science* **2005**, 47 (12), 3202-3215.
83. Kranc, S. C.; Sagüés, A. A., Detailed modeling of corrosion macrocells on steel reinforcing in concrete. *Corrosion Science* **2001**, 43 (7), 1355-1372.
84. Weiss, R. F., The solubility of nitrogen, oxygen and argon in water and seawater. *Deep Sea Research and Oceanographic Abstracts* **1970**, 17 (4), 721-735.
85. Kranc, S. C.; Sagüés, A. A., Computation of Reinforcing Steel Corrosion Distribution in Concrete Marine Bridge Substructures. *CORROSION* **1994**, 50 (1), 50-61.
86. Walsh, M. T.; Sagüés, A. A., Steel Corrosion in Submerged Concrete Structures—Part 1: Field Observations and Corrosion Distribution Modeling. *CORROSION* **2016**, 72 (4), 518-533.
87. Chyżewski, E.; Evans, U. R., The Classification of Anodic and Cathodic Inhibitors. *Transactions of The Electrochemical Society* **1939**, 76 (1), 215-230.
88. Fontana, M. G., *Corrosion Engineering*. McGraw-Hill, New York, 1986.
89. Whitmore, D.; Fallis, G.; Liao, H.; Strombeck, S.; Lasa, I. (2014). "Tendon Impregnation Technology Mitigates Corrosion and Protects Post-Tensioned Tendons," PTI Journal, V. 10, pp. 17-21.
90. Whitmore, D.; Lasa, I.; Haixue, L. (2015). "Impregnation technique provides corrosion protection to grouted post-tensioning tendons," Multi -Span Large Bridges - Pacheco and Magalhaes, Eds., Taylor and Francis Group, London, pp. 1065-1072.
91. Hartt, William H., and Seung-Kyoung Lee. "Projecting corrosion-induced bridge tendon failure resulting from deficient grout: Part I—Model development and example results." *Corrosion* 72, no. 8 (2016): 991-998.
92. Mraied, H.; Mullins, G.; Sagüés, A. A.; & Lasa, I., Mechanism of Corrosion Mitigation of Post-Tensioned Tendons by Impregnation. Paper No. 13449, Corrosion 2019, NACE International, Houston, 2019.

APPENDIX



VECTOR CORROSION TECHNOLOGIES LTD.

474B Dovercourt Drive, Winnipeg, MB R3Y 1G4

Main: 204-489-9611 | Fax: 204-489-9633

Info@Vector-Corrosion.com

Evaluation of Corrosion Inhibiting Materials Applied by Impregnation Methods to Prevent Corrosion of Post-Tensioned Tendons

USF Research Project 21041265

Post-tech PTI Impregnation Report

September 2019

Introduction

The research project, funded and awarded by the Florida Department of Transportation (FDOT), has a stated object to evaluate commercially available material used for impregnation of tendons. The research team from the University of South Florida (USF) has been working toward that objective and created a number of samples for testing.

Vector Corrosion Technologies (VCT) brought this corrosion protection option to market in recent years and has worked closely with FDOT and others to extensively to prove its value and effectiveness at protecting steel strands in post-tensioned concrete structures. For this project Vector Corrosion Technologies was subcontracted by the University of South Florida to impregnate the samples created by the USF research team. Impregnation work was completed during the week of August 26-30, 2019.

The Post-Tech Post-Tension Impregnation (PTI) system, utilizes a hydrocarbon and silicon-based material that has the ability to impregnate and saturate the post-tension tendon and the surrounding grout within a duct. Once the tendon is impregnated, the impregnation material forms a protective film around the tendon that stops or slows present and future corrosion.

Three types of test specimens were treated. The first type consisted of eight (8) interconnected concrete blocks with four (4) grouted single tendons. Three of the tendons were impregnated with Post-Tech PTI material. The second type of specimens consisted of eight (8) one-foot (1') long samples of a single tendon grouted in a four inch (4") diameter duct. The third type of specimens consisted of nine (9) three-foot (3') long samples of three (3) tendons in the same 4" diameter duct.

We Save Structures™

The Post-Tech PTI material was impregnated into the provided specimens with the following observations:

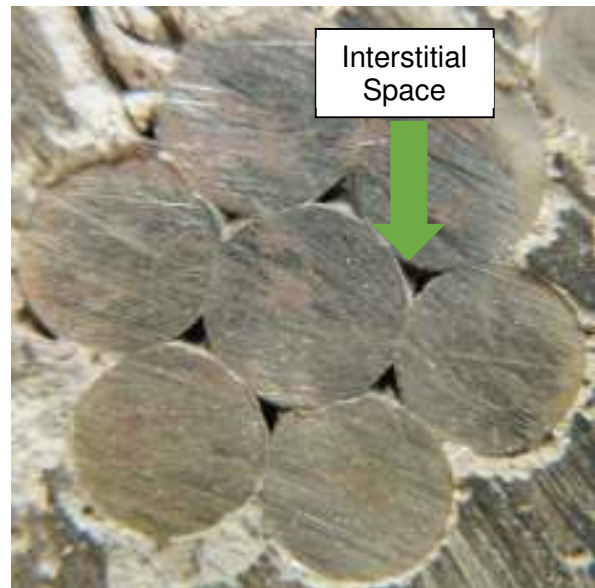
1. The Post-Tech PTI system impregnated the full length of the three individual tendons in the 8 interconnected concrete blocks when completed from one end of the tendons.
2. The Post-Tech PTI system transmitted through 3 of the 8 – 1' samples.
3. The Post-Tech PTI material impregnated the full length of the 9 – 3' samples.

Background

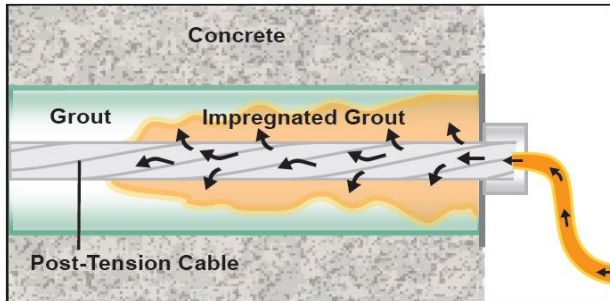
Various problems have been identified in bonded post tensioned structures. These include:

1. Bleed water voids and a layer of chalky grout. This is a common problem in structures that utilized site mixed cement/water grout.
2. Segregated grout with different physical, chemical, and electrochemical properties at different locations.
3. The presence of soft, plastic grout that has not cured or hardened properly.
4. The presence of chloride contaminated grout which was manufactured using materials with elevated chloride levels.

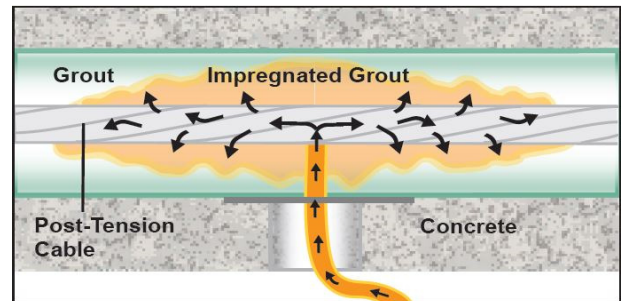
The Post-Tech PTI system has been developed to mitigate corrosion caused by these problems. This system utilizes the interstitial spaces between the wires to deliver a unique corrosion mitigating material along the length of the cable which is then available to impregnate the surrounding grout or concrete. In doing so, the initiation of corrosion activity is reduced or prevented by impregnating the grout around the cables while also creating a protective film on exposed steel surfaces.



A single strand from a tendon showing the interstitial spaces between the wires



Impregnation from end of exposed tendon



Impregnation from midpoint location

Procedure

Interconnected Blocks Specimens:

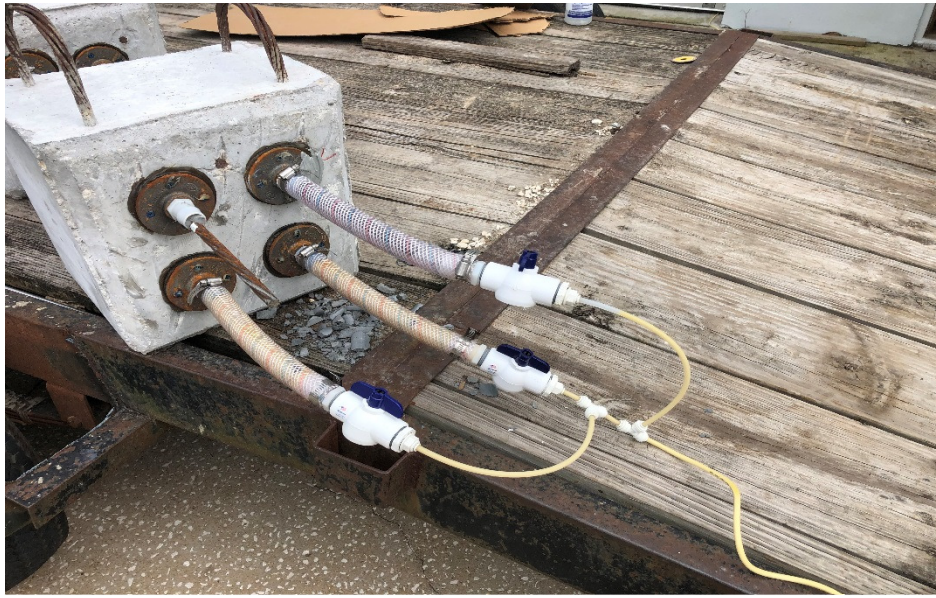
The first set of specimens that were impregnated were the interconnected concrete blocks.

In preparation, valves were installed at either end of the hoses that encapsulated the tendon ends that were exposed at the start and end of the line of 8 blocks. At the one end, the valves were fitted with pumping ports to which the impregnation pump could be connected.

The tendons were then tested with compressed air to determine the location of any leaks. Locations where air was leaking were identified and then sealed with a two-part epoxy paste. Confirmation testing with compressed air was then re-performed prior to the impregnation.



Interconnected concrete blocks



Impregnation end of tendons – photo shows bottom two tendons' valves opened and filled with impregnation material and top one closed. Top joint also shows a location of a sealed leak.

The impregnation of these specimens commenced on August 27th in the afternoon. Impregnation material was observed exiting the down-stream valves of the two right tendons minutes after initiating treatment. These valves were then closed. Impregnation material was observed exiting the down-stream valve of the single left tendon a number of hours after initiating treatment. It was also closed at that time.

The impregnation system remained connected to the specimens for 48hrs. During this time the system was held to a pressure between 30 and 40psi. After 48hrs, the system was halted, and the specimens were disconnected from the impregnation pump.



Down-stream end of tendons – photo shows two right tendons' valves closed after appearance of impregnation material. Bottom joint also shows a location of a sealed leak.

One-Foot-Long Specimens:

The second set of specimens that were impregnated were the one-foot-long single tendon in a grouted duct.

In preparation, the caps and collars that were on the samples were removed and the exposed ends were cleaned and prepared for sealing. Valves were installed at either end of the specimens on the grouted nipples that surrounded the tendon at either exposed end. At the one end, the valves were fitted with pumping ports to which the impregnation pump could be connected.



Preparation of 1ft Specimens

The ends of the ducts were capped and sealed with two-part epoxy then tested with compressed air to determine the location of any leaks. Locations where air was leaking were identified and then sealed. This procedure repeated until no leaks were evident.

The impregnation of these specimens commenced on August 28th in the afternoon. Impregnation material was observed exiting the down-stream valves several minutes after initiating treatment on the three samples marked as “Normal”. These valves were then closed. Impregnation material was not observed exiting the down-stream valves of the samples marked as “NaCl” or as “MF” during the treatment time. These valves remained open.

The impregnation system remained connected to the specimens for 48hrs. During this time the system was held to a pressure between 30 and 40psi. After 48hrs, the system was halted, and the specimens were disconnected from the impregnation pump. Material did not exit the samples noted above where impregnation material was not observed to exit during the initial phase.

Pressure was limited to 30 to 40 psi on these samples to minimize leaks and to avoid

blowouts and failure of the epoxy paste seal as these samples exhibited many leaks and a significant quantity of seal material was required to seal them compared to typical field installations. Impregnation pressures used on field structures are often 100 to 150 psi.

Three-Foot-Long Specimens:

The final set of specimens that were impregnated were the three-foot-long, three-tendon samples in a grouted duct.

In preparation, the caps and collars that were on the samples were removed and the exposed ends were cleaned and prepared for sealing. Valves were installed at either end of the specimens on the grouted nipples that surrounded the tendons at either exposed end. At the one end, the valves were fitted with pumping ports to which the impregnation pump could be connected.

The ends of the ducts were capped and sealed with two-part epoxy then tested with compressed air to determine the location of any leaks. Locations where air leaked were identified and then sealed. This procedure was repeated until no leaks were evident.

The impregnation of these specimens commenced between the afternoon of August 29th and the afternoon of August 30th. Impregnation material was observed exiting the down-stream valves anywhere between several minutes and several hours after initiating treatment on all samples. Once material was observed at the down-stream valve, the valves were subsequently closed.

The impregnation system remained connected



Preparation of 3ft Specimens



Air testing 3ft Specimen – photo shows bubbles formed by air exiting the interstitial spaces in the tendons.

to the specimens for 48hrs. During this time the system was held to a pressure between 30 and 40psi. After 48hrs, the system was halted, and the specimens were disconnected from the impregnation pump.

Summary

The research team from the University of South Florida created a number of specimens for testing. Vector Corrosion Technologies was subcontracted by the University of South Florida to impregnate their specimens. Impregnation work was completed during the week of August 26-30, 2019.

Three types of test specimens were treated. The first type consisted of eight (8) interconnected concrete blocks with four (4) grouted single tendons. The Post-Tech PTI system impregnated the full length of the three individual tendons in the interconnected concrete blocks which were to be impregnated. This work was completed from one end of the tendons.

The second set of specimens consisted of eight (8) one-foot (1') long samples of a single tendon grouted in a four inch (4") diameter duct. The Post-Tech PTI system transmitted through 3 of the 8 – 1' samples.

The third set of specimens consisted of nine (9) three-foot (3') long samples of three (3) tendons in the same 4" diameter duct. The Post-Tech PTI material impregnated the full length of the 9 – 3' samples.

